ROLE OF MACROPHAGE OSR1 IN LIVER INFLAMMATION AND NONALCOHOLIC STEATOHEPATITIS (NASH)

A Dissertation

by

LIN LIU

Submitted to the Graduate and Professional School of
Texas A&M University
in partial fulfillment of the requirements for the degree of

DOCTOR OF PHILOSOPHY

Chair of Committee,	Linglin Xie
Committee Members,	Chaodong Wu
	Junyuan Ji
	Ke Zhang
Head of Department,	David Threadgill

August 2021

Major Subject: Nutrition

ABSTRACT

One third of non-alcoholic fatty liver disease (NAFLD) progresses to its inflammatory subtype called non-alcoholic steatohepatitis (NASH). Liver macrophage-mediated inflammation contributes to the pathogenesis of NASH. However, their associated pathophysiology and the molecular mechanisms remain unclear. Osr1 is a transcription factor containing four C2H2-type zinc finger motifs. Our previous data described that Osr1 could regulate hepatic inflammation and cell survival in the progression of NAFLD in a pre-cancer model. And Osr1 is strongly expressed in hepatic macrophages during NAFLD pathogenesis. In this study, we investigated the physiological function and possible hepatoprotection role of Osr1 in macrophages on NAFLD development in high-fat diet (HFD) and Methionine/Choline deficient diet (MCD) diet treated mice.

Specifically deleting Osr1 in myeloid cells promoted NASH development, evidenced by severer liver inflammation and steatosis, suggesting a protective effect of Osr1 against NASH. Deleting Osr1 in macrophages induced more inflammation both *in vivo* and *in vitro*, associated with phenotype switch towards inflammatory, suggesting Osr1 might maintain macrophages toward alternative M2 like profile. Our RNA sequencing of the wild type and Osr1 myeloid knockout mice liver showed *Osr1*-dependent expression of genes and signaling pathways involved in macrophage polarization. In cultured bone marrow derived macrophages (BMDMs) for in vitro polarization study, Osr1 expression was found positively correlated with the M2 marker

genes such as PPAR-γ in macrophage phenotype switch (M0/M1/M2), confirmed the role of Osr1 in maintaining macrophage M2 polarization. We also investigated the role of Osr1 in the macrophage metabolic reprogramming. Deleting Osr1 shift the macrophages to a glycolysis dependent ATP production profile. Further experiment also indicated that Osr1 is highly involved in the palmitate oxidation. Additionally, PPAR-γ was identified as the downstream targets of Osr1 by CHIP-qPCR and luciferase reporter assays. While compound heterozygotes of macrophage PPAR-γ and Osr1 promoted NASH progression, PPAR-γ agonist treatment inhibited the NASH progression, suggesting the functional Osr1-PPAR-γ axis in the liver macrophages for NASH progression. Upon establishing the role of Osr1 in macrophage alternative polarization, we performed the macrophage-hepatocytes coculture experiment and confirmed the effect of Osr1-null macrophages in inducing the hepatocytes inflammation and fat deposition.

In summary, we demonstrated that macrophage Osr1 plays an important role in hepatic inflammation and NASH progression via mediating macrophage activation.

ACKNOWLEDGEMENTS

First and foremost, I would like to thank my committee chair Dr. Linglin Xie for making me not only a better scientist, but also a better person in the past several years. Her knowledge her encouragement of independent thinking has allowed me to search for and pursue my scientific interests. Her patience and understanding made a profound impact on me and will continue to be a positive source throughout my career. I am also grateful to my committee, Dr. Chaodong Wu for his guidance and motivation. He has paved the road for me to the liver metabolism research world and kindly provided me the transgenic mouse lines to establish my animal model. I also would like to thank Dr. Kurt Zhang for his advice and continued support throughout my graduate career. Without his guidance about bioinformatics analysis, I would not have any directions to conduct my project. I would like to thank Dr. Jun-yuan Ji for his encouragement on taking proactive attitude towards problem-solving and guided my transition from a clinical doctor to a real research scientist. He has benefited my career tremendously and his insight on my dissertation is greatly appreciated.

I would like to recognize my colleagues who have offered me guidance in my research. I would like to thank Yi Zhou, Jiangyuan Li, Guannan Gao, Zhimin Liu, and Xian Wang for their contribution to this study. I am grateful to Leya He, Zehuan Ding, Ernest Lynch, and Zhen Li for sharing their knowledge and their experience, and Yushu Qin, Naomi McCauley, and Lauren Lawless for their assistance in the lab. I am fortunate to have worked with such diverse and supportive teammates.

I would like to express my sincere gratitude to the faculty and graduate students of the Department of Nutrition for all the scientific discussions and debates, which made graduate school an intellectually rewarding experience. I would also like to thank the staff for the core facility trainings, animal maintenance and assistance with administrative work.

Finally, I would like to thank my family and friends especially to my wife Xiaoyu for her patience, love, support, and encouragements.

CONTRIBUTORS AND FUNDING SOURCES

Contributors

This work was supervised by Professor Linglin Xie and a dissertation committee consisted of Professor Linglin Xie(Chair), Chaodong Wu of the Department of Nutrition, Professor Ke Zhang of the Institute of Biosciences and Technology and Professor Jun-yuan Ji from the Department of Molecular & Cellular Medicine, TAMU/ Department of Biochemistry and Molecular Biology, Tulane University.

The experiments and other thesis related works were performed by the student.

Special appreciation goes towards members and visiting scholars of the Xie lab and Zhang lab consisting of Jiangyuan Li, Guannan Gao, Yi Zhou, Zhimin Liu, Ernest Lynch and Xian Wang for their contribution to this study. Their determination and effort for the project were not only essential to the completion of my program but also motivated me to give my best.

Funding Sources

This project is supported by an NIH R01 grant (1R01DK112368-01, PI: Linglin Xie).

NOMENCLATURE

NAFLD	Non-Alcoholic Fatty Liver Disease
NASH	Nonalcoholic Steatohepatitis
HCC	Hepatocellular carcinoma
BMDM	Bone Marrow-Derived Monocytes
CD	Chow Diet
HFD	High-fat Diet
MCD	Methionine/Choline Deficient
LPS	Lipopolysaccharide
ChIP	Chromatin Immunoprecipitation
IPGTT	Intraperitoneal Glucose Tolerance Test
IPITT	Intraperitoneal Insulin Tolerance Test
DEG	Differentially Expressed Gene
qPCR	Quantitative Polymerase Chain Reaction
RNA-seq	RNA sequencing
GO	Gene Ontology
FACS	Fluorescence-activated Cell Sorting
ECM	Extracellular Matrix
PPAR- γ	Peroxisome proliferator-activated receptor- γ
DEN	Diethylnitrosamine
ALT	Alanine aminotransferase

AST	Aspartate aminotransferase
TC	Total Cholesterol
LDL-c	Low-density Lipoproteins cholesterol
HDL-c	High-density Lipoprotein cholesterol
TBA	Total Bile Acid
FAO	Fatty Acid Oxidation
OXPHOS	Oxidative phosphorylation
LCFA	Long Chain Fatty Acid
IR	Insulin Resistance
DNL	*de novo* Lipogenesis
IDH	Isocitrate dehydrogenase
SDH	Succinate dehydrogenase
IC	Immune Complex
TLR	Toll-like Receptor
ATM	Adipose Tissue Macrophage
TZD	Thiazolidinedione
VEGF	Vascular Endothelial Growth Factor
MAPK	Mitogen-activated Protein Kinase
JNK	c-Jun N-terminal Kinase
ERK	Extracellular signal-regulated Kinase
PAMP	Pathogen Associated Molecular Pattern
DAMP	Damage Associated Molecular Patterns

HSP	Heat Shock Protein
PRR	Pattern-recognition Receptor
NLR	Nucleotide-binding and oligomerization domain –like Receptor
EGTA	Ethylene Glycol Tetra-acetic Acid
RLR	RIG-I like Receptor
CLR	C-type Lectin Receptor
NR	Hormone Receptor
ETC	Electron Transport Chain
PM	Peritoneal Macrophages
EMT	Epithelial-Mesenchymal Transition
NPC	Non-parenchymal Cells
DMSO	Dimethyl sulfoxide
ANOVA	Analysis of variance

TABLE OF CONTENTS

Page

ABSTRACT ii

ACKNOWLEDGEMENTS iv

CONTRIBUTORS AND FUNDING SOURCES vi

NOMENCLATURE vii

TABLE OF CONTENTS x

LIST OF FIGURES xiii

LIST OF TABLES xv

CHAPTER I INTRODUCTION 1

1.1 The Mechanistic Basis of Non-alcoholic Fatty Liver Disease (NAFLD) 1
1.1.1 The prevalence of NAFLD 1
1.1.2 The "two-hit" and "multiple-hit" hypothesis of NAFLD 1
1.1.3 Innate inflammation and NASH 3
1.1.4 Cellular and molecular mechanisms in the pathogenesis of NASH 4
1.2 Macrophage polarization and the associated metabolic change 8
1.2.1 Macrophage polarization and related mechanisms 8
1.2.2 The role of metabolic change in macrophage reprogramming 11
1.3 Targeting macrophage dysregulation as a therapeutic strategy in NASH 13
1.4 The role of macrophage PPARγ in obesity and NAFLD and emerging pharmaceutical strategies to target PPARγ in the treatment of NAFLD 16
1.5 The protective role of Osr1 in the development of NAFLD 19
1.5.1 Overview of Osr1 in the embryonic development 19
1.5.2 Osr1 acts as a tumor suppressor in cancer 20
1.5.3 Osr1 in the pathogenesis of NASH- a "pre-HCC" model 20
(adapted from Yi Zhou et al., 2020) 21
1.5.4 Osr1 in hepatic steatosis and inflammation under HFD treatment. 22

CHAPTER II METHODS 24

CHAPTER III MACROPHAGE OSR1 PREVENTED NUTRITIONAL STEATOHEPATITIS IN MICE UNDER HFD AND MCD DIET TREATMENT 35

3.1 More fat deposition in Osr1$^{\Delta mac}$ mouse liver under long term normal chow diet feeding. 35
3.2 Osr1 is expressed in human liver macrophages and its expression is increased in mouse models of NASH 37
3.3 Macrophage-specific Osr1 played an important role in protecing NASH pathogenesis 39
3.3.1 Study model: HFD induced NAFLD and MCD diet induced NASH models 39
3.3.2 Macrophage Osr1 protected HFD-induced hepatic steatosis and inflammation response in mice 40
3.3.3 Macrophage Osr1 protected MCD diet-induced hepatic steatosis and inflammation response in mice 44
3.3.4 Macrophage Osr1 inhibit liver fibrosis under a long-term MCD diet treatment. 47

CHAPTER IV DELETING OSR1 IN MYELOID CELLS LED TO THE ABNORMAL BILE ACID SYNTHESIS AND CHOLESTEROL TRAP IN LIVER UPON MCD TREATMENT 48

CHAPTER V DELETING OSR1 IN MYELOID CELLS INDUCED HEPATIC PRO-INFLAMMATORY RESPONSE BY REGULATING MACROPHAGE M2 ALTERNATIVE POLARIZATION 53

5.1 Deleting Osr1 in myeloid cells induced hepatic pro-inflammatory response 53
5.1.1 Deleting Osr1 in myeloid cells induced more hepatic pro-inflammatory cytokine production *in vivo* 53
5.1.2 RNA sequencing and macrophage population analysis identified that Osr1 was required for macrophage alternative M2 polarization *in vivo* 53
5.2 Macrophage specific Osr1 expression increased during macrophage M2 induction *in vitro*, while its deficiency blunted macrophage alternative polarization 56
5.3 PPAR-γ and c-Myc are direct targets of Osr1 for regulating macrophage alternative M2 polarization 58

CHAPTER VI OSR1 IN MACROPHAGES METABOLIC PROGRAMMING 63

6.1 Osr1 deletion shifted the macrophage towards the glycolysis dependent ATP production profile 63
6.2 Osr1 is required for the palmitate oxidation during macrophage alternative polarization 64
6.3 The impairment of palmitate oxidation in Osr1 knockout macrophages is independent of the IL-4 and AKT signaling 68

CHAPTER VII DELETING MACROPHAGE OSR1 AGGRAVATED THE INFLAMMATION AND FAT DEPOSITION IN HEPATOCYTES 70

7.1 Osr1 deletion aggravates macrophage proinflammatory activation. 70
7.2 Macrophage Osr1 deletion induces lipid accumulation and pro-inflammatory cytokine production in hepatocytes *in vitro* by cytokine production 74
7.2.1 Macrophage Osr1 deletion induces more pro-inflammatory response in hepatocytes 74
7.2.2 Macrophage Osr1 deletion shifts macrophages to M1 polarization and hepatocyte steatohepatitic changes through the induction of cytokines 76

CHAPTER VIII PHARMACOLOGICAL PPAR- Γ AGONIST ROSIGLITAZONE PREVENT HFD INDUCED STEATOHEPATITIS IN OSR1$^{\Delta MAC}$ MICE 78

CHAPTER IX DISCUSSION 84

REFERENCES 93

APPENDIX 106

LIST OF FIGURES

Page

Figure 1. Schematic summary of macrophage polarization 10

Figure 2. Metabolic signature of proinflammatory M1 and anti-inflammatory M2 macrophages 13

Figure 3. Osr1 is expressed in hepatocytes and macrophages in the liver 21

Figure 4. Osr1+/− mice displayed worsen liver injury and inflammation than WT upon HFD and DEN treatment 22

Figure 5. Osr1+/- mice exhibited more liver steatosis and inflammation upon HFD treatment 23

Figure 6.Gating strategy of macrophages separated from liver tissue 33

Figure 7. More fat deposition in Osr1$^{\Delta mac}$ mouse liver under long term chow diet treatment 36

Figure 8. OSR1 was upregulated in liver macrophages of human NASH and murine steatohepatitis 38

Figure 9. Special diet treatment study design 39

Figure 10. Deletion of macrophage Osr1 aggravated high fat diet (HFD)-induced hepatic steatosis and inflammation response 42

Figure 11. Deletion of macrophage Osr1 aggravated MCD diet-induced hepatic steatosis, early fibrosis and inflammation response 45

Figure 12. Osr1$^{\Delta mac}$ mice were induced more liver fibrosis under longer MCD diet treatment 47

Figure 13. Deleting Osr1 leads to the disruption of bile acid synthesis and cholesterol trap in the liver upon MCD diet treatment 51

Figure 14. Osr1 was required for macrophage alternative M2 polarization *in vivo* 55

Figure 15. Inhibition of Osr1 expression blocks the induction of Osr1 dependent M2 markers 57

Figure 16. PPAR-γ and c-Myc are directly regulated by Osr1 in macrophages 60

Figure 17. The PPARγ ligand, rosiglitazone, rescued the downregulated M2 markers in Osr1Δmac macrophages during M2 induction 62

Figure 18. Osr1 deletion shift the macrophage to a glycolysis like metabolism profile and disrupt the mitochondrial palmitate oxidation during M2 polarization 66

Figure 19. Schematic diagram of Osr1 in macrophage polarization and cell metabolic change 67

Figure 20. STAT6 and AKT activity are normal in $Osr1^{\Delta mac}$ macrophages and not involved in the macrophage metabolic profile change 69

Figure 21. Osr1 disruption aggravates macrophage pro-inflammatory activation..... 72

Figure 22. Osr1 disruption aggravate the effects of macrophages on increasing hepatocyte inflammation signaling through cytokine excretion..... 75

Figure 23. Osr1 disruption aggravate the effects of macrophages on increasing hepatocyte fat deposition and inflammation related gene expression through cytokine excretion..... 77

Figure 24. Pharmacological PPAR-γ agonist rosiglitazone prevent HFD induced liver injury in $Osr1^{\Delta mac}$ mice 79

Figure 25. Rosiglitazone improves insulin sensitivity and glucose tolerance in $Osr1^{\Delta mac}$ mice under HFD treatment 81

Figure 26. Pharmacological PPARγ agonist rosiglitazone prevents HFD-induced liver inflammation in $Osr1^{\Delta mac}$ mice 83

LIST OF TABLES

Page

Table 1 Primers used for RT-qPCR……106

Table 2 Primers used for ChIP-qPCR……107

CHAPTER I

INTRODUCTION

1.1 The Mechanistic Basis of Non-alcoholic Fatty Liver Disease (NAFLD)

1.1.1 The prevalence of NAFLD

NAFLD is a detrimental condition associated with metabolic syndrome, diabetes, obesity, hyperlipidemia, hyperinsulinemia, and hypertension. In recent years, NAFLD has become one of the most common chronic liver disease, affecting around 25% of the global population(*1*). With the prevalence and severity of obesity increasing at an alarming rate, the prevalence of all classifications of NAFLD is in a rising trend(*2*) .Among which, one third of NAFLD develops into a more inflammatory subtype, Non-alcoholic steatohepatitis (NASH), and approximately a quarter of NASH with cirrhosis eventually develops hepatocellular carcinoma (HCC) (*3*). NASH is characterized by hepatic inflammation, steatosis, with or without fibrosis(*4*). Comparing to patients with simple fatty liver, those with NASH have an impaired survival due to the liver or cardiovascular causes(*5*). In United States, it has become the third leading cause of HCC and the second leading indication for liver transplantation (*6*).

1.1.2 The "two-hit" and "multiple-hit" hypothesis of NAFLD

Despite the high prevalence of NAFLD, only a small proportion of patients develop to NASH(*7*). To understand the underlying mechanisms for the development of NASH, various theories have been formulated. Among which, the "two hits " hypothesis has been accepted as the NASH pathogenesis model initially. According to this theory, the first hit refers to the sedentary lifestyle, dietary factors such as high fat diet, obesity, and

insulin resistance, leading to hepatic accumulation of lipids. Followed up by the 'second hit', which activates inflammatory and fibrogenesis responses(*8*). However, this view becomes too simplistic to explain the complexity of NAFLD considering multiple factors acting synergistically in the development and progression of NAFLD(*9*). Consequently, a "multiple-hit hypothesis" which incorporate dietary habits, environmental and genetic factors, obesity, insulin resistance, and changes in the intestinal microbiome has more widely accepted to explain the etiology of NAFLD(*8, 9*).

Firstly, dietary or metabolic factors contribute to the pathogenesis of NAFLD. Specifically, the dietary patterns with high calorie intake leads to obesity and insulin resistance (IR). Both high calorie intake and IR result in the excess fatty acid storage capacity of adipose tissue, impaired inhibition of adipose tissue lipolysis, with consequent increased flux of fatty acids to the liver. Meanwhile, IR alters the production and secretion of adipokines and inflammatory cytokines, which also contribute to the development of NAFLD. The fat accumulation and increased lipotoxicity from high levels of free fatty acids, free cholesterol and other lipid metabolites induces the mitochondrial dysfunction and endoplasmic reticulum (ER) stress with oxidative stresses and the production of reactive oxygen species (ROS).

Additionally, the altered gut flora increased the fatty acid absorption and circulating inflammatory cytokines, which contribute to the activation of inflammatory pathways in the liver, aggravating the pathogenesis of NAFLD(*10*).

Genetic factors have been identified to play important roles in modulating the NAFLD occurrence, severity, and long-term prognosis. In terms of the “multiple-hit hypothesis”, genetic factors or epigenetic modifications could affect hepatocyte fat content and liver inflammatory environment. In which, the immunological facets involving macrophages have become one of the central mechanisms in the initiation and progression of NAFLD. A state of chronic hepatic inflammation would induce heterogeneous hepatocellular damage pathways, with progression to hepatocellular death and deposition of fibrous matrix(*11*).

1.1.3 Innate inflammation and NASH

The liver is the largest visceral tissue mass and with unique blood supply distinct from other organs. The hepatic artery brings oxygenated blood to the hepatic tissues and account for only 20% -25% of the total blood entering the liver. While the portal vein account for the remaining 75%-80%, collecting the deoxygenated blood from the gastrointestinal tract (GI tract), filtering it to eliminate toxins and process the nutrients during absorption. Thus, the liver is constantly exposed to antigenic loads from GI tract. Hence, the innate immune system is the first line of defense against invading pathogens that is critical for not just the liver but the overall survival of the host. Innate immune cells (such as monocytes, macrophages, dendritic cells, mast cells, neutrophils and natural killer (NK) cells) could recognize pathogen associated molecular patterns (PAMPs) released by microorganisms (such as lipopolysaccharide (LPS), flagellin, lipoproteins, external RNA or DNA) and endogenous ligands (such as heat shock proteins (HSPs) released by damaged cells) via their pattern-recognition receptors

(PRRs). Several PRRs have been recognized including Toll-like receptors (TLRs), nucleotide-binding and oligomerization domain (NOD)-like receptors (NLRs), RIG-I like receptors (RLRs), C-type lectin receptors (CLRs), and other non-specific sensors.(*12-14*)

1.1.4 Cellular and molecular mechanisms in the pathogenesis of NASH

The population of macrophages in the liver is highly heterogeneous containing the resident macrophages, Kupffer cells (KCs) and the recruited bone marrow derived macrophages (BMDMs). During infectious or other insults in the liver, the resident Kupffer cells are the first immune cells to detect the presence of invading pathogens. Upon activation, Kupffer cells release cytokines such as TNFα, IL-1, and IL-6 as well as chemokines including CXCL 1–3, CXCL-8, CCL-2–4 that initiate the inflammation response. At the same time, the activation of TLRs and NLRs by PAMPs and DAMPs in Kupffer cells as well as in HSCs leads to the secretion of pro- inflammatory cytokines to provoke the progression of NASH. Proinflammatory cytokines released from activated Kupffer cells coordinate with the upregulated adhesion molecules from LSECs (such as VCAM-1, ICAM1, MAdCAM etc.) to further stimulate the recruitment of circulating blood monocytes and neutrophils to the liver. B cells and T cells also accumulate during NASH and produce TNFα and IL-6 or IFN-γ and IL-17. Following the recruitment, the circulating monocytes derived from bone marrow undergo differentiation into tissue macrophages (Mφ), which release TNFα, IL-1β, G-CSF, and GM-CSF factors that crosstalk with neutrophils and lymphocytes to sustain their survival at the site of inflammation to perform the pathogen clearance(*15-17*).

During the late phase, for the inflammation to be resolved, the apoptotic neutrophils and the cytokines released by other cells are recognized by the receptors on macrophages. This process initiate macrophage phagocytosis and the transcriptional profile modification, which further increase the production of cytokines including IL-10 and TGF-b for resolving inflammation and tissue repair (*16*).

Dysregulation of liver inflammation is a hallmark of NASH development, which is mediated by multiple overlapping pathways during the pathogenesis of NASH. Persistent activation of innate immune pathways, in response to MAMPs or DAMPs released due to excess consumption fat and tissue damage, leads to the pathological liver inflammation. The nuclear factor-kappa B (NF-κB) and MAPK signaling pathways (including c-Jun N-terminal kinase (JNK) as well as P38 MAPK pathways) are among the key pro-inflammatory signaling pathways in NASH (*18, 19*).

NF-κB signaling

NF-κB is a nuclear transcription factor widely expressed in varied cells and is closely related with inflammation. In addition, NF-κB regulates a variety of cytokines expression involved in inflammation, cell adhesion and protease gene transcription both *in vitro* and *in vivo*. NF-κB activation promotes the expression of inflammatory cytokines, which further enhance the pro-inflammatory activity of NF-κB. Cytokines (TNF-α, IL-6, IL-1, etc.), bacteria products (LPS, etc.), growth factors (such as insulin), stress response (oxygenation, etc.), and other factors could induce NF-κB activation, initiating transcription of many genes such as TNF-α, IL-1, IL-6, IL-8. (*12, 19, 20*)These cytokines regulated by NF-κB are involved in the liver inflammation, liver fibrosis, liver

regeneration, apoptosis and insulin resistance (IR)(*20, 21*). Therefore, the NF-κB signaling pathway are highly involved in the pathogenesis of NAFLD(*22*).

JNK signaling

Mitogen-activated protein kinase (MAPK) is a class of serine/threonine protein kinase widely existed in a variety of cells and mediates signal conduction from the cell surface to the cell nuclei. The MAPK family has three members, extracellular signal-regulated kinases (ERKs), c-Jun N-terminal kinase (JNK) and p38 MAPK. The ERKs play a major role in the cellular response, and JNK and p38 are mainly related with stress and inflammation(*19*). The fat accumulation and cell injury in hepatocytes could activate the JNK(*23*). JNK is also activated in the adipocytes, macrophages, and striated muscle of HFD-fed mice(*24*). JNK is associated with the decreased whole-body insulin sensitivity due to its inhibitory role in insulin- stimulated Akt activation(*25, 26*). It has been established that inflammatory cytokines such as TNF-α, free fatty acids (FFAs), oxidative stress could lead to IR which is closely mediated by JNK signaling. A feedforward self-sustaining signaling pathway has been elucidated in liver models as the JNK amplification loop (P-JNK → Sab → Intramitochondrial pathway → ↑ ROS → ↑ P-ASK1 → ↑ P-MKK4 → ↑ P-JNK)(*24*).In normal liver, the activation of JNK is minimal or transient. Upon activation, the phosphorylated JNK translocates to mitochondria and binds with mitochondrial outer membrane protein Sab. This further leads to inhibition of mitochondrial respiration and electron transport, leading to ROS release from mitochondria and activation of MAP3K/MAP2K pathway sustaining JNK activation. In the liver, JNK is an important effector MAPK which catalyzes the

phosphorylation of nuclear AP1 transcription factors (c-Jun, etc) as well as other protein kinases and phosphatases such as scaffold proteins, and other functional proteins (*27*). JNK activation and substrate phosphorylation has two major direct consequences: regulation of gene expression through AP1 transcription factors and direct activation or inhibition of protein targets. The main effects about JNK activation include inflammation, hepatocyte apoptosis and mitochondria dysfunction, which contributes to the liver injury, NAFLD/NASH, obesity and insulin resistance were developed(*24*).

P38 MAPK signaling

The p38 MAPK family is comprised of four isoforms encoded by Mapk14 (p38α) Mapk11 (p38β), Mapk12 (p38γ) and Mapk13 (p38δ)(*28*). The most extensively studied and expressed are p38α and p38β MAPKs (*29*). In the liver, the predominately expressed isoform is p38α. The p38 MAPK was activated by the phosphorylation of MAPK kinases or autophosphorylation at pT180/pY182(*30*). Previous studies have demonstrated a role for p38αMAPK in the energy expenditure, glucose homeostasis and lipid metabolism. p38a expression was reported to be increased in livers of human patients with NAFLD and was implicated in many inflammatory related diseases including inflammatory bowel diseases (*31*, *32*). p38 MAPK signaling pathway is also highly involved in the cell inflammatory response and apoptosis process under stress conditions and related with the release of a variety of inflammatory cytokines (such as IL-1, TNF-α and IL-6, etc.) after activation(*33*). In conclusion, obesity and the associated inflammation activate the stress-responsive MAPKs, such as the p38 MAPKs

and JNKs, making it a promising working hypothesis that these MAPKs drive hepatic metabolic dysfunction in the development of NAFLD.

1.2 Macrophage polarization and the associated metabolic change

1.2.1 Macrophage polarization and related mechanisms

Macrophage is a highly heterogeneous cell population that respond and adapt to a variety of micro-environmental signals (*34*). As mentioned before, tissue infiltration by inflammatory macrophages is a major contributor to inflammation, insulin resistance and NASH development (*35*). The skewed macrophage differentiation status may have an important role in the pathogenesis of NASH.

Macrophage activation and functions are profoundly affected by cytokines and microbial products within the microenvironment. In general, macrophages are classified into classically activated (pro-inflammatory or M1 macrophages), and alternatively activated (anti-inflammatory, or M2 macrophages) (*36*). Upon pro-inflammatory stimuli (i.e., LPS or IFN-γ), transcription of the transcription factors including NF-κB, STAT1，STAT3，AP1 or HIF-1a are induced to drive a series of cell surface markers (i.e., CD80/86, MHCII) and cytokine (i.e., TNF-α，IL-6，IL-1β，IL-12) expression. However, for the M2 polarization, the anti-inflammatory cytokines, IL-4 or IL-13, are always the drivers to induce the expression of transcription factors such as STAT6, SOCS1, PPARγ or GATA3,

which drive expression of a distinct series of cell surface markers (i.e., CD206, CD36, CD163) and cytokines (i.e., TGF-β, IL-10) expression.

M2 macrophages can be sub divided into M2a, M2b, M2c, and M2d(*37*). M2a macrophages are activated by IL-4 or IL-13, leading to the increased expression of IL-10, TGF-β, CCL17, CCL18, and CCL22. The M2a macrophages enhance the endocytic activity, promote cell growth and tissue repair. Activated by immune complex(IC), Toll-like receptor (TLR) ligands and IL-1β , M2b macrophages release both pro- and anti-inflammatory cytokines, such as IL-1β, IL-6, IL-10 and TNF-α. Based on the expression profiles of cytokines and chemokines, M2b macrophages regulate the breadth and depth of immune responses and inflammatory reactions which decided the overall inflammation degrees(*38*). M2c macrophages are considered as inactivated macrophages and can be induced by glucocorticoids, IL-10 and TGF-β. These cells secrete IL-10, TGF-β, CCL16, and CCL18 and play crucial roles in the phagocytosis of apoptotic cells (*39*). M2d macrophages are activated by TLR antagonists and are related with the release of IL-10 and vascular endothelial growth factors (VEGF) to promote angiogenesis and tumor progression(*36, 37*). (Fig.1)

	M1	M2
Polarization stimuli	LPS, IFN γ, LPS+IFN γ	IL-4, IL-13, IL-10, TGF-b
In vitro Morphology	Round/oval	Elongated, fibroblast-like
Released cytokines and markers	TNF-a, IL-1b, CXCL10, CD80, CD86, MHCII	IL-10, TGF-b, CCL12, CD206, CD36, CD163
Metabolic enzyme	iNOS, PFKFB3, PKM2, ACOD1	ARG1, CARKL, IDO
Phagocytic activity/ Antigen presentation	High/high	Low/low
Transcription factors	NF-kB(p65), STAT1, STAT3, HIF1a, AP1, IRF3	STAT6, SOCS1, PPARγ, GATA3
Functions	Bacterial killing, tumor resistance, pro-inflammation	Tissue remodeling, wound healing, anti-inflammation, immunoregulation, angiogenesis

Figure 1. Schematic summary of macrophage polarization.(*40*) (*41*)

Both classically activated and alternatively activated macrophages undergo a complex activation status during obesity where classifying macrophages to M1 or M2 is oversimplified. Indeed, several studies have described a ‘mixed’ M1/M2 phenotype for

macrophages in adipose tissue in obese mice and humans, suggesting that macrophages adopt more complex states *in vivo(42)* . Mario Kratz *et al* reported a "metabolically-activated" phenotype in macrophages that is distinct from classical activation by treating macrophages with glucose, insulin, and palmitate- conditions characteristic of the metabolic syndrome(*43*). Further analysis identified that the markers of metabolic activation are expressed by pro-inflammatory adipose tissue macrophages (ATMs) in obese humans/mice and are positively correlated with adiposity. They also stated that metabolic activation is driven by pro- and anti-inflammatory pathways distinct from the classical M1/M2 signaling. These data provide insights about the metabolic disease-specific phenotype of macrophages. Considering the obesity is a whole-body disease which is the consequence of multiple organ dysregulation, and the recruited macrophages have the same origins (*44*) , it is reasonable to speculate that macrophages in other tissues/organs other than adipose tissue (such as liver or muscles) share same pro- or anti- inflammatory signaling pathway. Nonetheless, the metabolic disease-specific pathways driving macrophages activation during NAFLD need to be further investigated.

1.2.2 The role of metabolic change in macrophage reprogramming

Macrophages can be activated by different metabolic factors and undergo a distinct "metabolically-activated" phenotype. On the other hand, macrophage polarization always companied by the metabolic change itself. The hallmark, and the most detailed metabolic difference between M1/M2 polarization is energy using difference. Briefly, M1 macrophages rely mainly on glycolysis, while M2 cells are more dependent on oxidative

phosphorylation (OXPHOS) and fatty acid oxidation (FAO) for their energy production (*45*). In M1 cells, the TCA cycle is disrupted at two key steps: the accumulation of citrate due to a decrease in isocitrate dehydrogenase (IDH) expression and the accumulation of succinate due to a decrease in Succinate dehydrogenase (SDH) expression. Due to the present of two breaks on the TCA cycle, excess succinate leads to Hypoxia Inducible Factor 1α (HIF1α) stabilization that, in turn, activates the transcription of glycolytic genes. HIF1α is initially induced in hypoxia environment, and it has been shown that HFD could induce the hypoxia environment in the liver and adipose tissue. In macrophages, two main signaling pathways culminate in the regulation of HIF1α transcription independent of oxygen supply: the TLR/NF-κB and AKT/mTOR pathways(*46-49*). The glycolytic M1 metabolic adaptation favors rapid ATP production to sustain their phagocytic function and provides metabolic precursors to feed the pentose phosphate pathway and inflammatory mediators production. However, M2 cells' TCA cycle is intact and provides the substrates for the complexes of the electron transport chain (ETC)(*40*). Thus, they have enhanced fatty acid oxidation (FAO) and OXPHOS.

Although it was initially thought that M1 macrophages solely rely on glycolytic and that FAO and OXPHOS in M2 macrophages, recent findings support the need of glycolysis for M2 macrophages, and FAO has also been found to occur in M1 macrophages. Additionally, it has been established that targeting the metabolism in macrophages could determine the fate of macrophage polarization. Therefore, understanding the metabolic

changes during the polarization of macrophages will make a positive contribution for us to target macrophages to improve human health. (Fig.2)

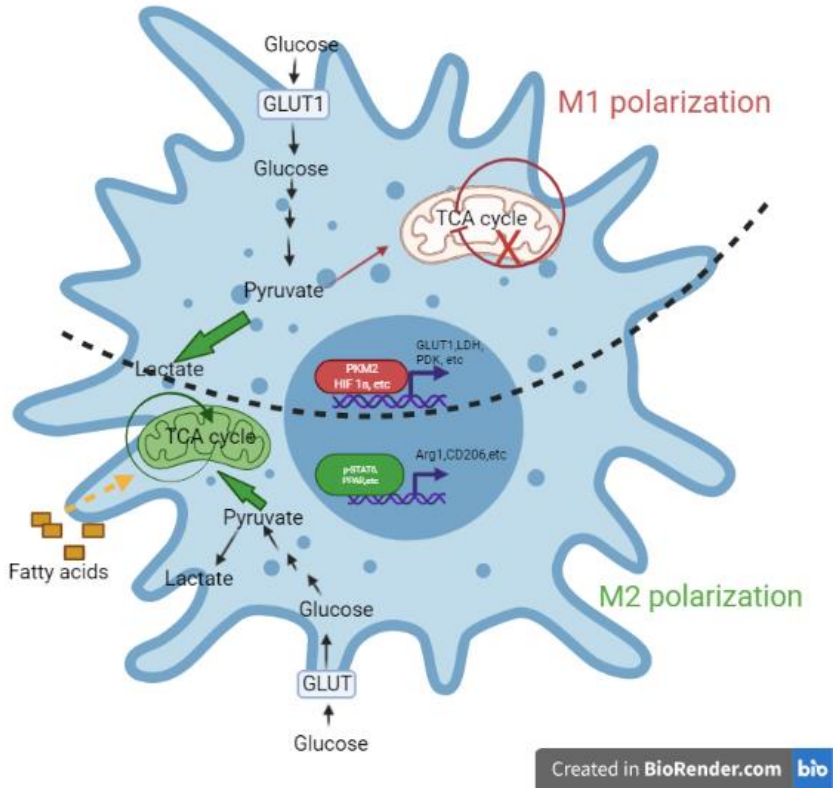

Figure 2. Metabolic signature of proinflammatory M1 and anti-inflammatory M2 macrophages

M1 macrophages rapidly upregulate glycolysis (over oxidative phosphorylation) as a main source of ATP with disrupted TCA cycle. However, the oxidative metabolism in anti-inflammatory M2 macrophages is normal with intact TCA cycle.

1.3 Targeting macrophage dysregulation as a therapeutic strategy in NASH

The liver consists of several cell types that are responsible for the biophysiological functions of metabolism, coagulation, detoxification, and immune responses. Four major

liver cell types—hepatocytes, Kupffer cells (KCs), hepatic stellate cells, and sinusoidal endothelial cells (LSECs)—spatiotemporally cooperate to maintain the liver functions (11). Hepatocytes are primarily engaged in the fundamental functions of the liver, including lipid metabolism, protein production, blood glucose regulation. KCs serve as immune sentinels. During the pathogenesis of NAFLD, many circulating monocytes derived from bone marrow are recruited to liver and help maintain the microenvironment in the liver. A lot of immune-mediated hepatic responses, such as reactive metabolite production, infectious diseases, circulating cytokines, and gut-derived endotoxin inflammation, require interactions among hepatocytes and immune cells (12).

Hepatic macrophages are mainly derived from resident KCs and circulating bone marrow-derived monocytes (BMDMs) (13, 14). KCs regulate liver homeostasis by mediating immunity, leading to pathogen clearance and antigen presentation to lymphocytes present in the sinusoid. BMDMs infiltrate into the liver upon injury and are likely responsible for replenishing the macrophage population in homeostasis(*50*). Nowadays different populations of hepatic macrophages have been identified with distinct phenotypes and discrete functions explained by the classical central dogma of M1 and M2 macrophages. Upon nutrient overloading, KCs recruit additional immune cells including inflammatory blood monocytes, which differentiate towards the classically activated macrophages (M1 type) that have phagocytic activity and secrete pro-inflammatory cytokines and reactive oxygen species (ROS) (*51-57*) . In HFD-fed and MCD-fed mice, macrophage infiltration with a dominant M1 phenotype leads to

increased production of pro-inflammatory cytokines (*58*). The MCD-fed mice have peaked inflammatory cytokine production at 4-week and decrease thereafter, suggesting a phenotypic shift during the progression of NASH (*59*). M2 macrophage is associated with attenuated hepatic injury in NAFLD and improved insulin sensitivity (*60*). Consistently, macrophage polarization towards M2 phenotype is found to partially reverse the hepatic steatosis and apoptosis (*60-62*). Macrophage polarization is often associated with the pro-inflammatory state in liver. An increase of M1 macrophages number or decrease of M2 macrophages number resulted aberrant M1/M2 ratio, which further triggers the production and secretion of various pro-inflammatory signals.

The upregulation of the immune regulatory pathways aims at minimizing excessive tissue damage. However, persistent inflammatory signals, produced by a range of immune cell and non-hematopoietic cell populations may lead to severe liver injury. In these situations, the dysregulated balance between inflammation and immunosuppression within the liver promotes the progression of liver NASH(*63*). In another word, lack of resolution for inflamed liver resulting chronic liver injury may lead to progressive liver fibrosis and permanent liver damage.

Tissue infiltration by pro-inflammatory macrophages (M1) is a major contributor to inflammation and insulin resistance (*35*). It has been reported that depletion of KCs attenuates methionine-choline-deficient (MCD) and HFD-induced steatohepatitis(*12*).However, the molecular mechanisms of liver macrophage activation

and polarization is not fully understood. Thus, the understanding of the role of hepatic macrophages provides more opportunities for understanding NAFLD pathogenesis. In terms of this, finding the directors in regulating macrophage polarization and its associated *in vivo* functions in obesity and NASH/NAFLD is the main aim of this study.

1.4 The role of macrophage PPARγ in obesity and NAFLD and emerging pharmaceutical strategies to target PPARγ in the treatment of NAFLD.

The peroxisome proliferator-activated receptor γ (PPAR γ) has been indicated to play an important role in the development of obesity, insulin resistance and NAFLD(*64*, *65*). PPAR γ is a ligand-activated transcription factor that regulates genes important in cell differentiation, and lipid/glucose homeostasis(*66*). PPARγ represents a nuclear hormone receptor (NR) belonging to the steroid receptor superfamily. PPARγ has been the focus of intense scientific and clinical research because of its role in the treatment of type 2 diabetes mellitus(*64*, *67*). It is a target of the synthetic insulin sensitizers – thiazolidinediones (TZDs) (such as rosiglitazone and pioglitazone). The mechanism relies on that PPARγ plays a central role in adipogenesis and appears to be involved in the regulation of lipid metabolism(*68*). Adipose PPARγ protects non-adipose tissues against excessive lipid overload and maintains normal liver and skeletal muscle functions. Activated PPARγ in adipocytes maintains a balanced and adequate secretion of adipocytokines (such as adiponectin and leptin) so that the insulin sensitivity of the whole body is maintained(*69*).

In hepatocytes, PPARγ is a regulator of genes involved in *de novo* lipogenesis (DNL) and free fatty acid (FFA)import (*70*). In response to a HFD, the induced hyperlipidemia causes the liver to act as a secondary reservoir for the excess lipid, which further induces the expression of PPARγ. In hepatocytes, PPARγ promotes fatty acid binding protein 4 (FABP4) and CD 36-mediated FFA uptake and induces the DNL enzymes Fasn and Acc1, facilitating an increase in hepatic lipid content (*70*). It has been established that hepatocyte-specific knockout of PPARγ mice showed a significant reduction in hepatic lipid vacuoles, as well as down-regulation of proteins involved in lipogenesis, lipid transportation and storage, as well as their modulators and activators such as Srebp1c, Acc1, CD36 and Phosphoenolpyruvate carboxykinase (PEPCK) in response to a HFD treatment(*71*).

PPAR γ is also a ligand-activated nuclear receptor and act as a transcription factor with anti-inflammatory properties that modulates cellular inflammatory response (*72*). PPAR γ is abundantly expressed in macrophages, where its expression is rapidly induced upon differentiation of monocytes into macrophages (*73*). It has been shown that PPARγ is required for polarization of alternatively activated macrophages with anti-inflammatory response by negatively interference with the nuclear factor κB (NF-κB), activating protein 1 (AP-1), and signal transducer and activator of transcription (STAT) signaling pathways (*74*). A switching to oxidative metabolism is an integral component of alternative macrophage polarization(*40*). In IL-4 stimulated PPARγ null macrophages, there was about 70% reduction in the rate of fatty acid oxidation (*75*).

Deletion of PPARγ in myeloid cells impairs alternative macrophage activation, thereby promoting the development of diet-induced obesity and insulin resistance(*75*). Kupffer cell-specific PPARγ deficiency also caused increased hepatic M1 inflammatory cytokines expression and exacerbated liver fibrosis in CCL4-induced liver injury(*76*). A recent study found that macrophage PPARγ interact with NF-κB to modulate the macrophage M2 polarization and plays protective role in the pathogenesis of NAFLD under long-term HFD(*65*). This indicates that loss of macrophage PPARγ induces M1 polarization and enhances liver injury.

In the quest of treatment targets for NAFLD, PPARγ agonists TZD have attracted increasing attention. Rosiglitazone was expected to aggregate steatosis because PPARγ could activate the adipogenic gene expression in hepatocytes. However, clinical trials in NAFLD patients show significant reduction of hepatic steatosis when treated with the PPARγ agonists rosiglitazone or pioglitazone. (*70*). In murine models, it has also been established that PPARγ agonist rosiglitazone could reduce the hepatic inflammation in the lipopolysaccharide (LPS)-treated precision-cut liver slices (PCLS)(*77*). In murine diet induced NAFLD model, researchers have reported that the treatment of rosiglitazone could decrease the number of M1 macrophages in the liver, attenuating the steatosis as well as inflammatory response(*65*) .

1.5 The protective role of Osr1 in the development of NAFLD

1.5.1 Overview of Osr1 in the embryonic development

The *Odd-skipped related 1* (*Osr1*) gene encodes a putative transcription factor containing four C2H2-type zinc finger motifs (*78*). The *Drosophila* homolog, *Odd-skipped* (*Odd*), was initially discovered as a pair-rule gene required for segmentation (*79, 80*).*Odd* also expresses in the *Drosophila* lymph gland, which can give rise to two mature types of hemocytes, plasmatocytes (*Drosophila* macrophages) and crystal cells(*81*). Odd-skipped has been reported to play the role in maintaining the prohemocyte population and blocked differentiation of plasmatocytes, indicating that *Odd* is involved in the gene regulatory model of prohemocyte cell fate choice(*82*). In murine model, Osr1 has multiple functions, and it is essential for the development of the intermediate mesoderm. Osr1 is first reported to regulate the cardiac precursors' proliferation during embryonic heart and urogenital development(*83*). Our group has reported that Osr1 interacts with Tbx5 to regulate posterior second heart field cell cycle progression for cardiac septation(*84*). In addition, Osr1 also serves important roles in tongue development and regulates differentiation of embryonic limb mesenchyme and bone marrow mesenchymal stromal cells(*85*). Its expression is down regulated by Runx2 and Ikzf1 transcription factors(*86*) and can be activated by Bone morphogenetic protein (BMP) , retinoic acid , and 1,25-dihydroxyvitamin D3(*87*).

1.5.2 Osr1 acts as a tumor suppressor in cancer

Osr1 is also reported as a tumor suppressor in some types of cancer. OSR1 expression was significantly downregulated in primary gastric cancer tissues due to the promoter hypermethylation(*88*). During gastric cancer, OSR1 acts as a functional tumor suppressor through the activation of tumor suppressor p53 and repression of TCF/LEF. Overexpression of OSR1 significantly arrests the cell cycle and inhibits cell growth, as well as induces the cell apoptosis in the gastric cancer cell lines. Zhang *et al* demonstrated lower expression of Osr1 in renal cell carcinoma (RCC) cells(*89*). Depletion of OSR1 repressed the expression level of tumor suppressor genes p53 in RCC cells. Recently, OSR1 is reported to be downregulated in breast cancer tissue(*90*). Further cell culture experiments confirmed that OSR1 downregulated the activity of the Wnt signaling pathway and Epithelial-Mesenchymal Transition (EMT), which inhibits the proliferative and invasive abilities of breast cancer(*91*). Despite of the published data regarding to the role of Osr1 in cancer, to dates, the study of underlying mechanism of OSR1 is limited and has not been well characterized.

1.5.3 Osr1 in the pathogenesis of NASH- a "pre-HCC" model

To date, no *in vivo* experiments were performed to investigate the role of Osr1 in cancer. Our group has investigated the potential role of Osr1 in NASH development in a pre-hepatocellular carcinoma (HCC) mouse model(*92*). In the study, NASH was induced in Osr1 heterozygote (*Osr1+/-)* male mice treated with HFD plus diethylnitrosamine (DEN), which is widely used to induce HCC. Upon treatment, *Osr1+/-* mice displayed severer NASH (Fig.4A) with higher serum ALT levels than the WT mice. The data also

shows that knocking down Osr1 promoted hepatic inflammation in the progression of NAFLD/NASH. Overactivation of both JNK and NF-κB signaling, along with enhanced hepatic expression of Il-1b and Il-6 was also observed (Fig.4B and C). The data also indicated that Osr1 was strongly expressed in hepatic macrophages during NASH (Fig.3). This is consistent with the expression pattern of *Odd* in Drosophila prohemocytes, suggesting the developmental conserved function of Osr1 between different species.

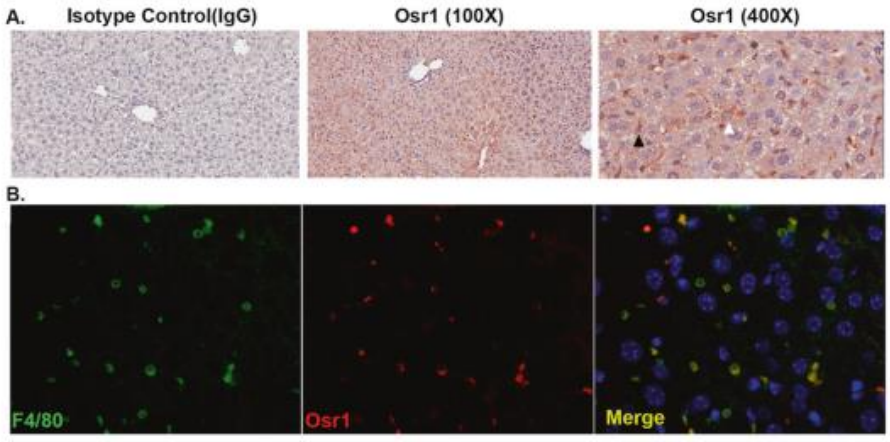

Figure 3. Osr1 is expressed in hepatocytes and macrophages in the liver
(adapted from Yi Zhou et al., 2020)

(A). IHC staining of Osr1 on WT liver tissue. White arrowhead indicates weak Osr1 expression in the hepatocytes. Black arrowhead indicates strong Osr1 expression in liver macrophages. (B). Co-IF staining of Osr1, F4/80 and DAPI on WT liver tissue.

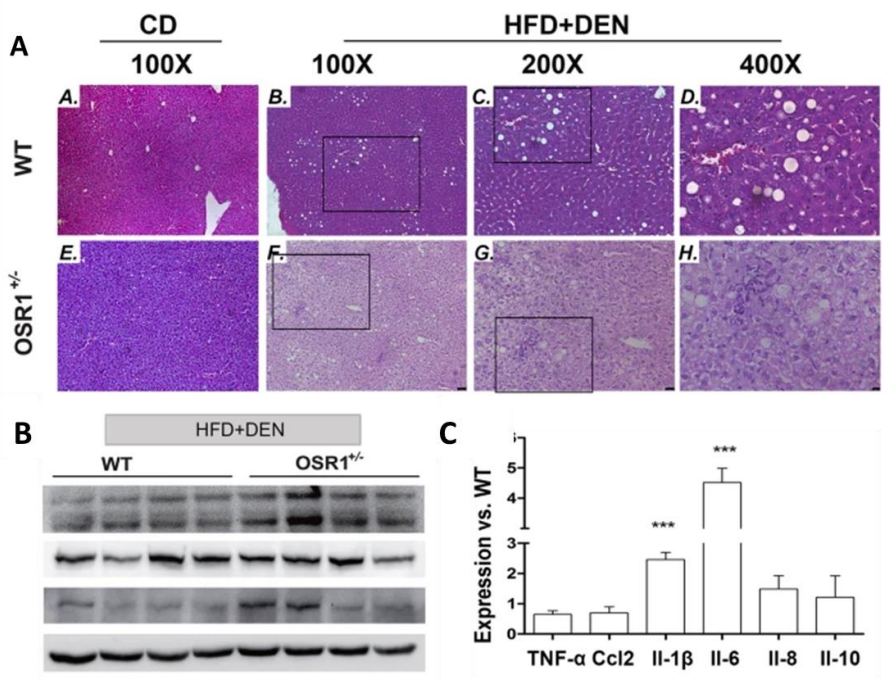

Figure 4. Osr1+/− mice displayed worsen liver injury and inflammation than WT upon HFD and DEN treatment (adapted from Yi Zhou et al., 2020)
(A) Histology of the liver (HE staining) (B) Western blot of p-JNK (46/54) and p-NF-κB showed higher expression in Osr1+/− mice exposed to HFD and DEN.(C) Expression of key genes involved in inflammation was measured by RT-PCR in Osr1+/− and WT livers.

1.5.4 Osr1 in hepatic steatosis and inflammation under HFD treatment.

To investigate the potential role of Osr1 in the pathogenesis of NAFLD, HFD was given to *Osr1*$^{+/-}$ or its littermate control WT mice for 10 weeks. Upon HFD, both the *Osr1*$^{+/-}$ male and female mice had significantly severer steatosis (Fig.5A). In addition, qPCR result showed that *Osr1*$^{+/-}$ mice had increased expression of *Il-1β* and *Tnf-α* in the liver

(Fig. 5B). Moreover, both the male and female Osr1 knockdown group displayed overactivation of JNK signaling, with a statistically significant increase of pJNK and pJNK/JNK ratio. Overactivation of NF-κB signaling was also observed in Osr1 knockdown mice, evidenced by significantly higher ratio of p-NF-κB and p-NF-κB/NF-κB (Fig. 5C). As mentioned before, both NF-κB and JNK pathway are highly related with inflammation. By combining with the qPCR result showing that the pro-inflammatory cytokines are significantly increased in the *Osr1*$^{+/-}$ mice, the data indicated that Osr1 did play protective role in the pathogenesis in NAFLD/NASH. And the main function of Osr1 may rely on its regulation of liver inflammation.

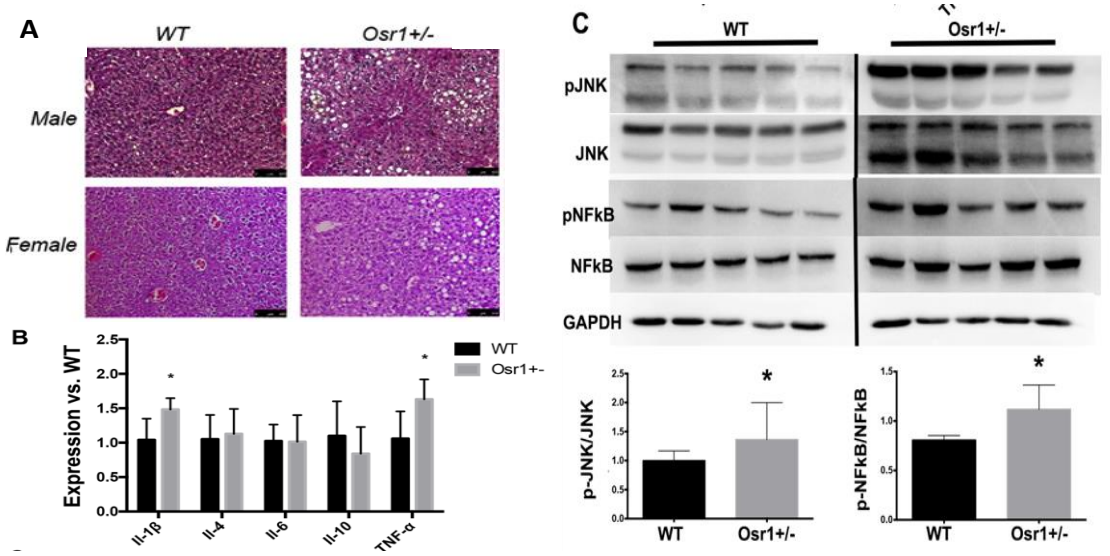

Figure 5. Osr1+/- mice exhibited more liver steatosis and inflammation upon HFD treatment

(A)Knocking down Osr1 induced more steatosis in the liver. (B) Expression of inflammation related cytokine genes by RT-PCR (C) Expression of JNK and NK-κB signaling by Western Blots (N=5, * P<0.05)

CHAPTER II

METHODS

Animal Models

The $Osr1^{fl/+}$ mice are kind gift from Dr. Rulang Jiang (Division of Developmental Biology, Department of Pediatrics, University of Cincinnati, Cincinati, US). The $LysM^{Cre/+}$ mice are from Dr. Chaodong Wu (Department of Nutrition, Texas A&M University, College Station, US).

Mice were maintained in a C57BL/6 background. Crossing the $Osr1^{flox/flox}$ mice with the $LysM^{-Cre}$ transgenic mice resulted in Cre-mediated deletion of the loxP-flanked Exon2 of Osr1 in the Myeloid cells. $Osr1^{fl/+}$ or $Osr1^{fl/fl}$ (labeled as $Osr1^{fl}$) and $LysM^{cre}Osr1^{fl/fl}$ (labeled as $Osr1^{\Delta mac}$) mice were treated with either chow diet (CD), HFD (Research Diets, 60% fat, 20% carbohydrate, and 20% protein) or MCD diet (Research diets) from 8 week of age for 4,8 or 14 weeks. Upon euthanizing and sacrificing, blood and liver samples were collected for later experiment. Mouse experiments were completed according to a protocol reviewed and approved by the Institutional Animal Care and Use Committee of the Texas A&M University in compliance with the US Public Health Service Policy on Humane Care and Use of Laboratory Animals.

Intraperitoneal glucose tolerance test (IPGTT)

For the intraperitoneal glucose tolerance test (IPGTT), mice were fasted overnight by transferring them to clean cages with no food in upper or bottom sections of the cage. Mice were weighed and injected intraperitoneally with 20% glucose solution (2 g/kg

body weight glucose). Blood from the tail vein was obtained at 0, 15, 30, 60, 90 and 120 min after the injection for determining blood glucose level with glucose meter.

Intraperitoneal insulin tolerance test (IPITT)

For the intraperitoneal insulin tolerance test (IPITT), mice were fasted 4h by transferring them to clean cages with no food in upper or bottom sections of the cage. Mice were weighed and injected intraperitoneally with insulin (1 U /kg body weight). Blood from the tail vein was obtained at 0, 15, 30, 45, 60 and 90 min after the injection for determining blood glucose level with glucose meter.

Tissue Dehydration and Sectioning

Liver tissues were fixed in 10% buffered formalin at 4°C overnight. Tissues were washed in PBS for 15 minutes on an orbital shaker, then dehydrated in 50%, 70%, 80%, 95% (×2), and 100% (×2) alcohol (Thermo Scientific) sequentially. Clearing was performed using two rounds of xylene and infiltration was performed using two rounds of paraffin. Tissues were embedded and sectioned serially at 5 μm.

H&E, Sirius Red and Trichrome Masson staining

Tissue sections were deparaffinized using two rounds of xylene and rehydrated in 100% (×2), 90%, 70% alcohol and water. Sections were subjected to hematoxylin-eosin staining for pathological and steatosis evaluation. For Sirius Red staining (Abcam), apply adequate Picro Sirius Red Solution to completely cover the tissue section and incubate for 60 minutes. Rinse slide quickly in 2 changes of Acetic Acid Solution and in absolute alcohol 1 change. Then the slide was dehydrated in 2 changes of absolute alcohol. After clearing, the slide was mounted in Permount Mounting Medium (Fishier

Scientific). For Trichrome Masson staining, the rehydrated sections were performed re-fixation and serial staining according to manufacturer's instructions (Newcomer supply, 9179A). Briefly, the sections were deparaffinized thoroughly in three changes of xylene and rehydrated through series of alcohol to water. Then the sections were fixed again in Bouin Fluid and put in fresh-made hematoxylin for the cell nuclei staining. After that, the sections were further stained in Biebrich Scarlet-Acid, Phosphomolybdic-Phosphotungstic Acid and Aniline Blue. Then the sections were washed in running water and 5% acetic acid and dehydrated and mounted. The Collagens, cytoplasm and nuclei were stained with blue, red, and black color respectively.

Immunofluorescence (IF) and Immunohistochemical (IHC) Staining

Deparaffinize sections if necessary and hydrate in distilled water similar with H&E staining. Antigen retrieval was performed by incubating with Antigen Unmasking Solution (Vector Laboratories) for 20 minutes at above 95°C. After the slides have cooled down to room temperature, endogenous peroxidase activity was quenched by incubating in 3% H_2O_2 for 5 minutes (IF staining does not need). Immunolabeling was performed using the VECTASTAIN ABC Kit (Vector Laboratories) according to manufacturer's instructions. Sections were incubated with F4/80 (Invitrogen, Catalog # MA5-16624) antibody at 1:50 dilution or Osr1 (Santa Cruz Biotechnology, Catalog # sc-376529) antibody at 1:200 dilution overnight. The sections were then washed and incubated in corresponding biotinylated secondary antibodies. After incubating for 30 minutes with prepared VECTASTAIN Elite ABC reagent, sections were washed and incubated with ImmPACT DAB peroxidase substrate (Vector Laboratories) until desired

stain intensity develops. The sections were then counterstained with hematoxylin for 5 seconds, dried and mounted. For IF staining, after the incubation with primary antibody overnight, the sections were washed and performed with secondary antibodies: F (ab')2-Goat anti-Rat IgG-Alexa 594 (Catlog#A11020, 1:800 dilution) and Goat anti-Rabbit IgG-Alexa 488 (Catlog#A31628, 1:800 dilution) from Thermo Fisher Scientific. Nuclei staining used were DAPI (Catlog#F6057) from Sigma-Aldrich (Oakville, ON, Canada).

Frozen section and oil red O staining

Embed the liver tissue in frozen section medium (Leica) in a plastic embedding box. Freeze it at -20 °C for 30 min. Cut it into 10-µm sections and mount the tissue on a slide. Then the sections were placed at room temperature for at least 30 min for air dry. Then the slides were fixed with 10% formalin for 10min. After fixation, the slides were quickly dipped in 60% isopropanol and stained in working Oil Red O solution for 15min. The slides were then dipped in 60% isopropanol and DI water one time quickly and counterstained with hematoxylin for 5 seconds. The slides were washed by dipping the slides in DI water for 10 times quickly and mounted in aqueous mounting gel.

Biochemical analyses

The plasma levels of alanine aminotransferase (ALT), aspartate aminotransferase (AST), total cholesterol (TC), low-density lipoproteins cholesterol (LDL-c), high-density lipoprotein (HDL-c) and total bile acid (TBA)were measured with the biochemical analyzer (DxC 700 AU, Beckman Coulter). Serum and hepatic triglyceride was quantified using a Triglyceride test kit (Abcam). Briefly, the triglyceride was extracted in 5% NP-40/ddH_2O at 80-100 °C. After lipase digestion, in the presence of the mix

provided by the manufacturer, the output was measured on a microplate reader at OD 570 nm for colorimetric assay.

Bile acid extraction and quantification

We obtained the bile acid extraction protocol from Dr. John Y. L. Chiang, Department of Integrative Medical Sciences, Northeast Ohio Medical University. Briefly, approximately 100 mg frozen liver tissue were homogenized in 500ul 95% EtOH, followed by incubating in 60°C water bath for 3 hr or overnight. Centrifuge the samples at 3500 rpm for 10 min and collect the supernatant. Resuspend and vortex the pellet in 80% EtOH, extract by repeating the incubation and centrifuge step and combine the supernatant. Resuspend and vortex pellet in 2:1 (v:v) chloroform:MeOH. Extract by incubating at room temperature for 1 hr or overnight. Centrifuge at 3500 rpm for 10 min and combine supernatant. At last, centrifuge total extract at 3500 rpm for 10 min at room temperature to pellet debris. The concentration of bile acid was quantified using Bile Acid Assay Kit (Colorimetric) (Abcam, CA.# ab239702) by Using 5 µL bile acids for all samples and 80% EtOH as a blank. Briefly, the extracted samples were mixed with the bile acid probe and reaction mix provided by the manufacturer and the absorbance was measured at 405 nm in a kinetic mode at 37°C for 60 min, protected from light.

RNA Extraction

Tissues used for independent validation of gene expression were stored in RNAlater Stabilization Solution (Thermo Fisher) upon collection. Tissues were homogenized on ice and total RNA was extracted using EconoSpin® RNA Mini Spin Columns. Cell RNA was extracted according to the manufacturer's instructions (Quick-RNA™

Miniprep Kit, Zymo Research). Approximately 500ng RNA was used for reverse transcription using iScript reverse transcription supermix (Bio-rad).

Quantitative PCR

Quantitative PCR (qPCR) was performed using SYBR Green supermix (Bio-rad) on the CFX384 real-time system (Bio-Rad). After the cycling program, the melt curve analysis was performed immediately after amplification to confirm primer specificity. 3 or more biological replicates were used for each condition and 2 technical replicates were performed for each sample.

Quantification data was analyzed using methods derived from the comparative CT method (*93*). For gene expression analysis, genes of interest were normalized to *Cyclophilin* and data was expressed as fold change against *Cyclophilin* (± SEM). For ChIP assay analysis, enrichment of a region of interest was determined by interpolating from a standard curve generated with serial dilutions of the input control and data was shown in percentage of input (% input). Student's t-test was performed to determine statistical significance and $p < 0.05$ was considered significant.

RNA Sequencing

RNA from wild type and Osr1 Myeloid knockout mice liver tissues was extracted using Quick-RNA midi prep Kit (ZYMO RESEARCH) and suspended in 15 μl Elution Buffer. RNA quantification was performed on Bioanalyzer (Agilent Technologies). One nanogram (1 ng) was used as input for library preparation using Nextera XT DNA Library Prep Kit (Illumina) and Nextera XT Index Kit (Illumina). Libraries were

quantified, normalized to 4 nM, pooled and further diluted to be sequenced on the NextSeq (Illumina) using 75 bp paired-end sequencing.

Western blot

Proteins were extracted from either the liver tissue or cells. After averaging the concentration of each samples, the proteins were boiled with SDS and loaded to the SDS-PAGE gel. Then the proteins were transferred to membranes and blocked for 2 hours in 5% milk in TBST. Membranes were incubated overnight with 1° antibody overnight (18 hours). The membranes were incubated with the following antibodies: Osr1 antibody (sc-376529X, Santa Cruz Biotechnology), c-Myc (ab32072,Abcam), PPARγ (#2430, Cell Signaling Technology),Cyp7a1(ab65596, Abcam),phosphorylated NF-κB p65 (#3033, Cell Signaling Technology), NF-κB p65 (# 8242, Cell Signaling Technology), phosphorylated JNK (#4668, Cell Signaling Technology), JNK (#3708, Cell Signaling Technology), phosphorylated p38 (#4511, Cell Signaling Technology), p38 (#9212, Cell Signaling Technology), phosphorylated Akt (#9271, Cell Signaling Technology), Akt (#9272, Cell Signaling Technology), phosphorylated STAT6 (#56554, Cell Signaling Technology), STAT6 (#5397, Cell Signaling Technology), and Gapdh (#2118, Cell Signaling Technology).

Primary cell isolation, cell culture and treatment

We follow the protocol previously describes with some modifications. Briefly, the primary hepatocytes were isolated from $Osr1^{fl}$ and $Osr1^{\Delta mac}$ mice. In situ liver perfusion was performed with ethylene glycol tetra acetic acid (EGTA) buffer followed by collagenase II (# 17101015, Thermo Fisher Scientific) digestion. After digestion, the

liver tissue was dissected, placed in a sterile petri dish containing cold Dulbecco's modification of Eagle medium (DMEM), and passed through a 70 µm cell strainer. The cell suspension was then centrifuged at 40 x g for 5 min at 4 °C. The supernatant was kept for macrophage isolation. The hepatocyte pellet was collected and resuspended with 8 ml cold DMEM. The suspended hepatocytes were transferred to a tube with 9 ml cold Percoll (#17089102, GE Healthcare Life Sciences) and 1ml 10 x HBSS and then centrifuged at 1800 rpm for 6 min at 4°C. The supernatant kept before was collected after a further two cycles of centrifuge at 54 x g for 2 min at 4 °C. The supernatant was then transferred to a new collection tube and the cell suspension was centrifuged at 300 x g for 10 min at 4 °C. The liver macrophage pellet was re-suspended and taken for other experiments.

Bone marrow progenitor cells were seeded in 12ml RPMI 1640 containing 50 ng/ml M-CSF, 10% inactivated FBS, and 1x penicillin-streptomycin in polystyrene tissue culture dishes (Corning). After three days of stimulation, 6 ml of new prepared medium was added. At day seven, BMDMs (>99% macrophages based on flow cytometry using parameter F4/80) were collected for the experiments. BMDMs were stimulated with lipopolysaccharide (LPS, 0.1 µg/ml, Sigma-Aldrich) and interferon- (IFN-) γ (20 ng/ml, PeproTech) or with IL-4 (20 ng/ml, PeproTech) to induce polarization towards M1 or M2 phenotypes, respectively.

For co-culture studies, primary hepatocytes from $Osr1^{fl}$ mice and BMDMs from the $Osr1^{fl}$ and $Osr1^{\Delta mac}$ mice were seeded on the co-culture chamber (Corning). Palmitic

Acid was added in the co-cultured system for the last 24 h. Hepatocytes were assayed for hepatocyte fat deposition and inflammatory responses.

Fluorescence activated cell sorting (FACS) analysis

Liver sections were collected, digested with collagenase II and filtered with a 70 μM cell strainer. Cell suspension was prepared after removal of red blood cells by Ammonium-Chloride-Potassium (ACK) lysing buffer. The LIVE/DEAD™ Fixable Aqua Dead Cell Stain Kit (Thermo Fisher Scientific) was first used to determine the viability of cells. Cells were then subsequently stained with fluorochrome-conjugated monoclonal antibodies: Alexa Fluor 700 anti-mouse CD45 (#560510, BD Biosciences), PE anti-mouse F4/80 (#123110, BioLegend), FITC anti-mouse CD11b (#557396, BD Biosciences), PerCP anti-mouse I-A/I-E (MHCII, #562363, BD Biosciences) and APC anti-mouse CD206 (#141708, BioLegend) antibodies. Samples were analyzed using Flow Cytometer (Beckman Coulter). Total macrophages were identified as $CD45^+F4/80^+CD11b^+$, and M1 and M2-like macrophages were identified as $CD45^+F4/80^+CD11b^+MHCII^+$ and $CD45^+F4/80^+CD11b^+CD206^+$, respectively. Subsequent analysis was performed with FlowJo software. (Figure 6)

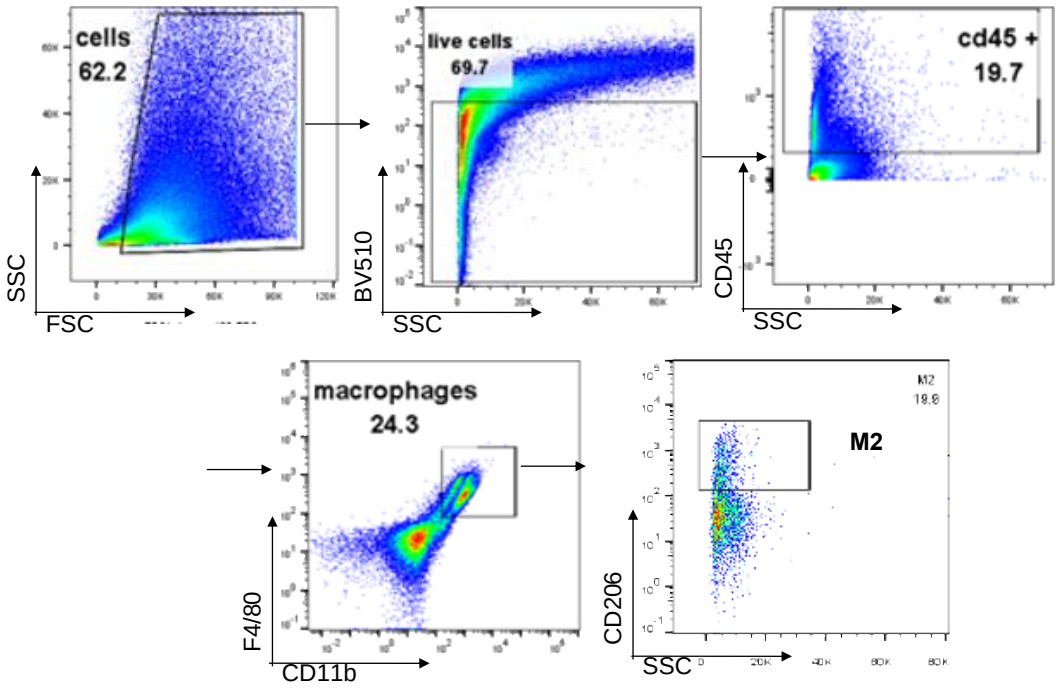

Figure 6.Gating strategy of macrophages separated from liver tissue

Chromatin Immunoprecipitation

BMDMs were collected and pooled in PBS containing Complete Mini EDTA-free Protease Inhibitor Cocktail (Sigma-Aldrich) on ice. Cells were crosslinked in 1% formaldehyde in PBS on the rotator for 10 minutes. Crosslink was quenched by adding glycine to a final concentration of 0.125 M and incubating for 5 minutes. The crosslinked cells were pooled into Sonication Buffer (0.5% SDS, 20 mM Tris, pH 8.0, 2 mM EDTA, 0.5 mM EGTA, with freshly added 0.5 mM PMSF and Protease Inhibitor), homogenized using Grinder and incubated for 30 minutes on ice for cell lysis. Chromatin was sheared and fragmented and then incubated with Osr1 antibody (sc-376529X, Santa Cruz) with rotation at 4°C overnight. Chromatin-antibody complexes

were captured using Dynabeads Protein G (Thermo Fisher Scientific) and washed with Low Salt Buffer, High Salt Buffer, LiCl Buffer and TE Buffer. Chromatin-antibody complexes were then eluted and reverse-crosslinked overnight at 65°C using NaCl. After RNA and proteins digestion with RNAse A and Proteinase K, DNA was then purified using phenol-chloroform followed by ethanol precipitation.

Luciferase Reporter Assay

Regulatory regions were cloned upstream of a firefly luc2 gene in the pGL4.23 reporter vector (Promega). 2×10^4 RAW264.7 cells were plated per well in a 96-well plate containing 100 µl culture media. After 24 h, reporter vectors were transfected into the cells, with Osr1 vectors or control vectors, using FuGENE HD Transfection Reagent (Promega). Cells were then lysed and assayed 24 h after transfection using the Dual-Luciferase Reporter Assay System (Promega). Student's t-test was performed to determine statistical significance and $p < 0.05$ was considered significant.

Statistical analysis

Data are presented as means± SD (standard deviation) or means ± SE (standard error) as indicated in the figures. Statistical significance was assessed by unpaired, two-tailed Student's *t* tests or Analysis of variance (ANOVA). Differences were considered as significant at the two-tailed $P < 0.05$. Statistical difference was indicated as: *, $P < 0.05$; **, $P < 0.01$; ***, $P < 0.001$.

CHAPTER III

MACROPHAGE OSR1 PREVENTED NUTRITIONAL STEATOHEPATITIS IN MICE UNDER HFD AND MCD DIET TREATMENT

3.1 More fat deposition in Osr1$^{\Delta mac}$ mouse liver under long term normal chow diet feeding.

Osr1 is expressed in both hepatocytes and macrophages in the liver, and Osr1+/- mice were reported to have more severe steatosis and inflammation(*92*).Thus we hypothesis that macrophage Osr1 plays important roles in the NASH development. To specifically investigate the role of macrophage Osr1 in the pathogenesis of NASH, we combined the Osr1$^{flox/flox}$ mice with the LysM-Cre transgenic mice to obtain the control (Osr1$^{fl/+}$ or Osr1$^{fl/fl}$ mice, labeled as Osr1^{fl}) as well as myeloid specific knock down (LysM^{cre}Osr1$^{fl/+}$ mice, labeled as Osr1$^{\Delta mac/+}$) or knockout mice (LysM^{cre}Osr1$^{fl/fl}$ mice, labeled as Osr1$^{\Delta mac}$). We first examined liver pathophysiology of Osr1^{fl} and the Osr1$^{\Delta mac}$ mice. The mice were treated with CD for 20 weeks. Surprisingly, even though we did not see the steatosis in either group, we did observe more fat deposited in Osr1$^{\Delta mac}$ mice liver with Oil red O staining (Fig.7A and B), which is the premise of the pathogenesis of NAFLD. The result indicated that macrophage Osr1 may play the important role in protecting fat accumulation in the liver.

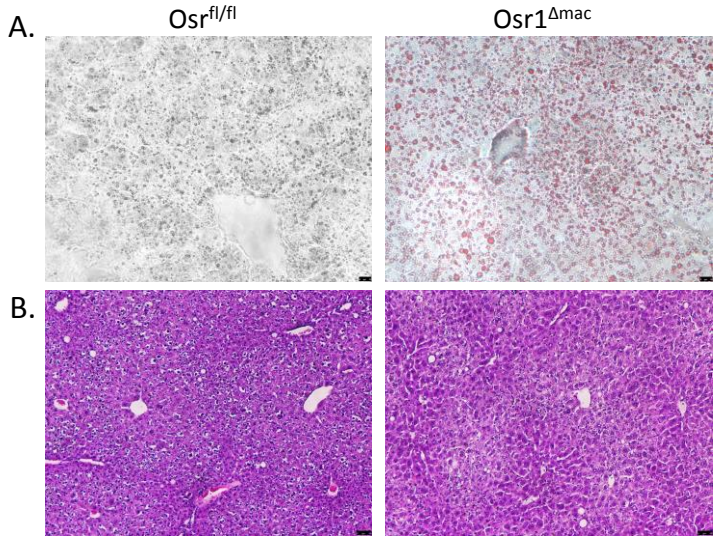

Figure 7. More fat deposition in Osr1$^{\Delta mac}$ mouse liver under long term chow diet treatment

Both the Osr1^{fl} and the Osr1$^{\Delta mac}$ male mice at 8 weeks were treated with CD for 20 weeks. (A) Oil red O staining in frozen sections. (B) HE staining in paraffin embedded sections. n=6

3.2 Osr1 is expressed in human liver macrophages and its expression is increased in mouse models of NASH.

To date, no clinical study has been reported about the role of Osr1 in NAFLD/NASH development. We first examined Osr1 expression in normal liver and the liver tissues of patient with NASH. As shown by IHC staining, Osr1 was widely expressed in hepatocytes and liver non-parenchymal cells, which strongly concentrated around sinusoids from patients with NASH by comparing to control (Fig.8A). To confirm that the Osr1 is still expressed in macrophages during NASH, we did IF staining co-labelled with F4/80 and Osr1. The result indicated that the Osr1 expression still can be found in macrophages (Fig.8B). Interestingly, when treating the mice with MCD diet, the Osr1 expression congregated in the sinusoids by comparing to the CD group (Fig.8C). Then we further analyze the expression pattern of Osr1 in positive hepatic non-parenchymal cells and confirmed that Osr1 was strongly expressed in macrophages/or Kupffer cells by mouse macrophage marker F4/80 and Osr1 IHC staining on serial sections (Fig.8D). The IHC staining also showed the upregulated Osr1 protein level in macrophages in NASH mice liver tissues, which is consistent with observed in NASH patient liver samples (Fig.8D).

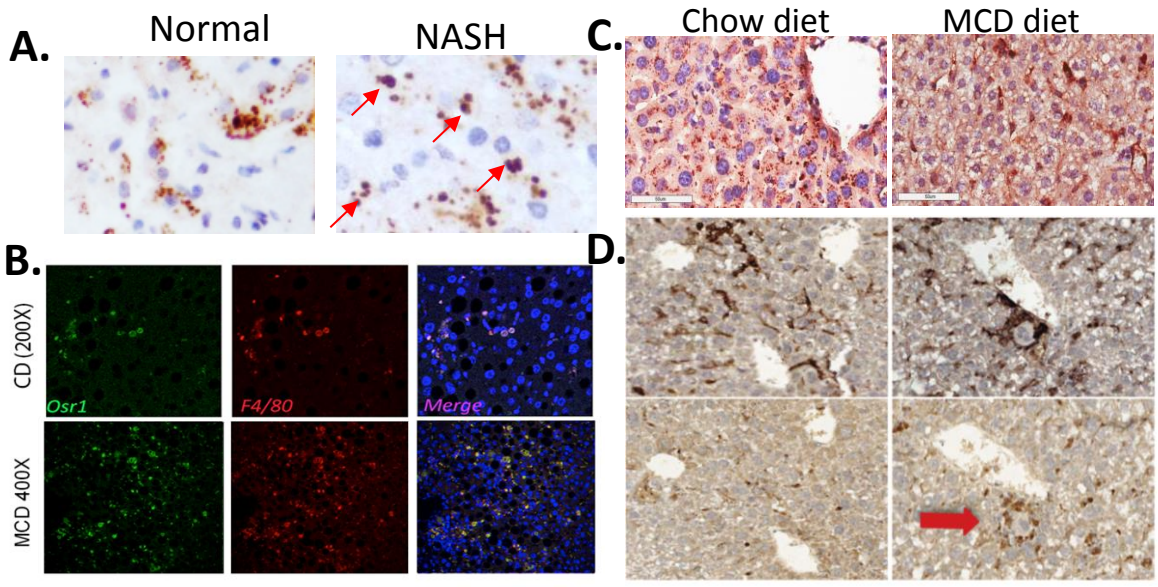

Figure 8. OSR1 was upregulated in liver macrophages of human NASH and murine steatohepatitis

(A) OSR1 can be expressed in human normal and NASH liver macrophages and its expression is up regulated in non-parenchymal cells during NASH (arrowhead). (B) Immufluorescence staining indicates colocalization of Osr1 and F4/80 in murine NASH liver sections. (C) Osr1 expression congregates in liver sinusoid in NASH liver sections. (D) Osr1 expression is increased in mouse liver of NASH (arrowhead).

3.3 Macrophage-specific Osr1 played an important role in protecing NASH pathogenesis

3.3.1 Study model: HFD induced NAFLD and MCD diet induced NASH models

To specifically study and investigate the potential role of Osr1 in F4/80+ macrophages, $Osr1^{fl}$, $Osr1^{\Delta mac/+}$ and $Osr1^{\Delta mac}$ mice were fed with either HFD or MCD diet to induce the progression of NAFLD or NASH, respectively (Fig.9A). Both feeding models are the most common models used in NAFLD/NASH research. To validate the knockout efficiency, we extracted peritoneal macrophages' protein from both control and $Osr1^{\Delta mac}$, the result showed that Osr1 expression was significantly down regulated in knockout macrophages

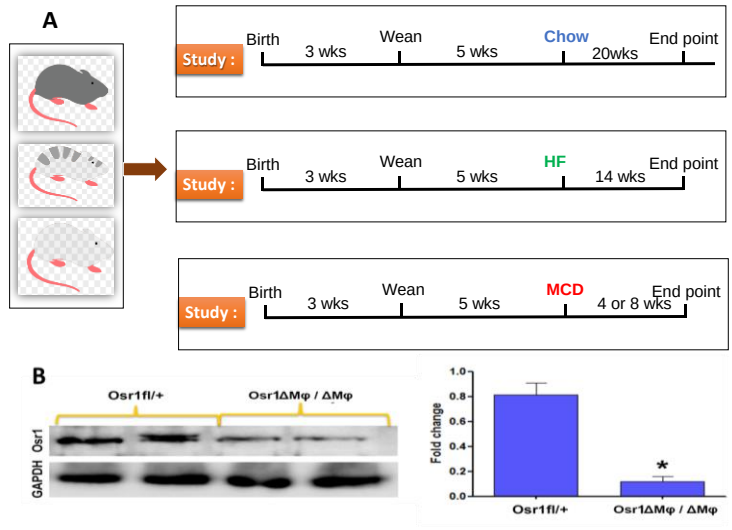

Figure 9. Special diet treatment study design

(A) special diet treatment design. (B) Expression of Osr1 was significantly lower in the isolated macrophages of $Osr1^{\Delta mac}$ mice than the $Osr1^{fl}$ mice.

(Fig.9B).

3.3.2 Macrophage Osr1 protected HFD-induced hepatic steatosis and inflammation response in mice

Under HFD treatment, both the $Osr1^{fl}$ and $Osr1^{\Delta mac}$ mice significantly gained body weight. The $Osr1^{\Delta mac}$ group showed significantly higher body weight comparing to the $Osr1^{fl}$ group. Moreover, the $Osr1^{\Delta mac}$ mice exhibited heavier liver weight (Fig. 10A) and more severe glucose intolerance at 12w of HFD treatment (Fig. 10B) than the $Osr1^{fl}$ mice. The NAFLD phenotype was more advanced in $Osr1^{\Delta mac}$ mice, evidenced by more steatosis (HE and Oil Red O staining) and more collagen deposition (Fig. 10D). Next, we did western blot for the well-established NF-κB(p65) and MAPK(p38) signaling pathway. The results showed significantly increased phosphorylation level of NF-κB(p65) and MAPK(p38) (Fig.10E), suggesting more inflammation in the $Osr1^{\Delta mac}$ liver. We further did F4/80 IHC staining and count the cell number of macrophages in both control and $Osr1^{\Delta mac}$ group and confirmed more macrophages infiltration in Osr1 knockout group (Fig.10F). All of these indicated that Osr1 deletion in macrophages did cause worsen liver injury in mice. The following qPCR results also showed that there was increased lipogenesis in $Osr1^{\Delta mac}$ group evidenced by the upregulation of genes involved in *de novo* lipogenesis comparing to control (Fig.10G). In terms of immune-mediated hepatic responses, we found increased expression level of *Tnf-α* and *Il-1β* ,as well as *Adgre1(F4/80) in* $Osr1^{\Delta mac}$ group(Fig.10G). We also tested the serum level of the parameters commonly used for clinical liver function diagnosis. Consistent with the pronounced steatohepatitis seen on histology, Aspartate Aminotransferase (AST) and low-density lipoproteins (LDLs) were significantly higher in $Osr1^{\Delta mac}$ mice compared to

control. Although serum alanine aminotransferase (ALT) levels and cholesterol levels were not significant different, we still can see the increased trend of them (Fig.10H). Collectively, these results indicate that macrophage Osr1 deletion induced more severe obesity and NASH phenotype and overactivated inflammatory response in the liver during HF diet treatment.

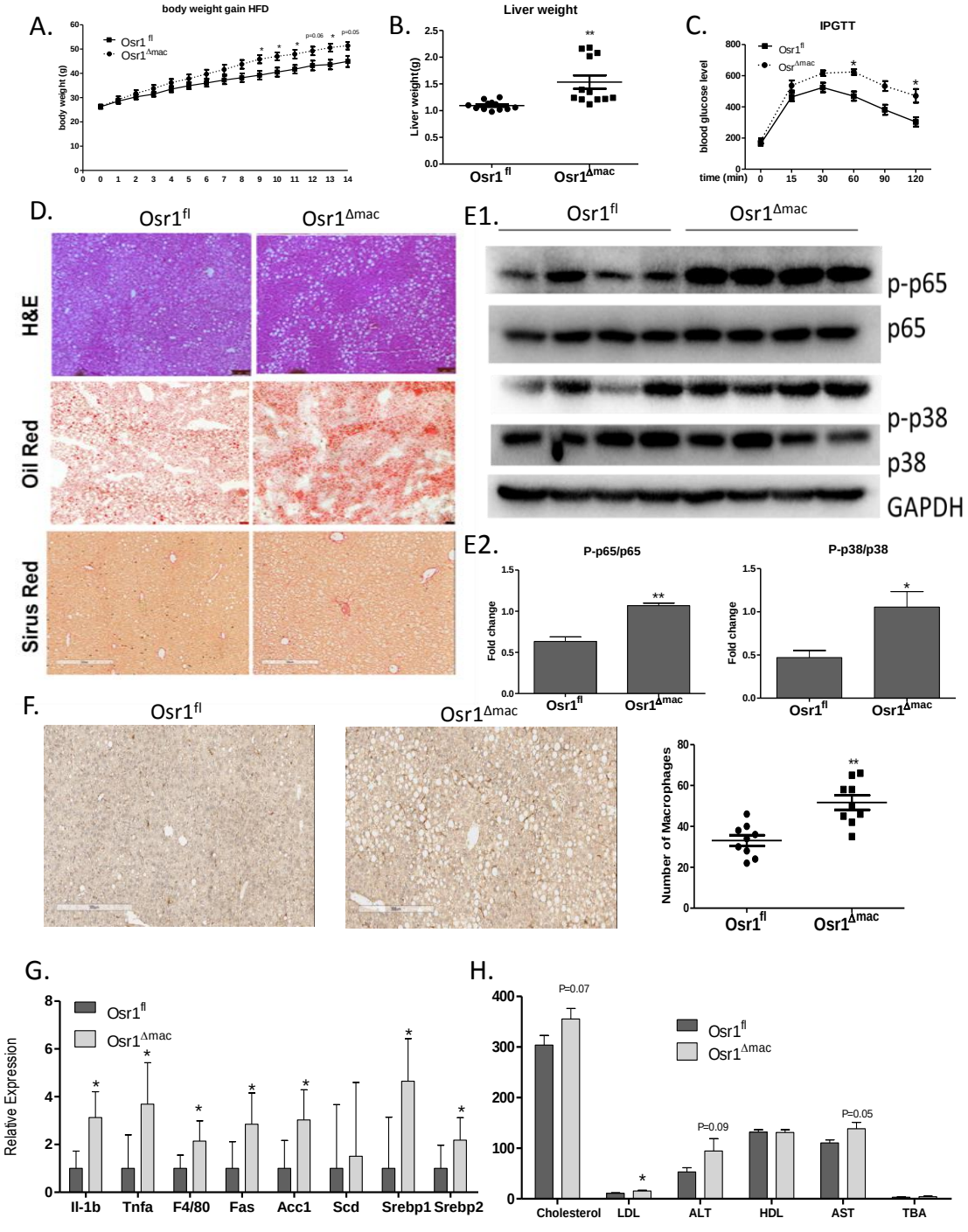

Figure 10. Deletion of macrophage Osr1 aggravated high fat diet (HFD)-induced hepatic steatosis and inflammation response

Male Osr1^{fl} and Osr1$^{\Delta mac}$ mice at 8 weeks of age, were fed with HFD for 14 weeks. (A) Body weight gain upon

HFD feeding. (B) Liver weight (C) Intraperitoneal glucose tolerance test (IPGTT) (D) Representative images of H&E, Oil Red-O and/or Sirius red staining for liver sections. (E) Liver proinflammatory signaling. (F) Representative images of liver F4/80 immunohistochemistry (IHC) staining. (G) Inflammation and *de novo* lipogenesis related genes. (H) Lipid metabolism and hepatocyte damage blood serum markers.

For E, liver lysates were subjected to Western blot analysis. Bar graphs, quantification of blots. For G, gene expression was quantified by quantitative real time PCR (qRT-PCR). For H, serum levels were quantified by the biochemical analyzer (DxC 700 AU, Beckman Coulter). For A – F, numeric data are means ± SE. n = 8 – 12. For G – H, numeric data are means ± SE. n = 6 – 8. Statistical difference between $Osr1^{fl}$ and $Osr1^{\Delta mac}$ mice in A, B, C, E, F, G, H: *, $P < 0.05$ and **, $P < 0.01$.

3.3.3 Macrophage Osr1 protected MCD diet-induced hepatic steatosis and inflammation response in mice

Under MCD diet treatment, the hepatic steatosis was much more severe in the $Osr1^{\Delta mac}$ mouse than the control mice (Fig.11A). There was also more macrovascular steatosis as well as microgranulomas present in the liver of $Osr1^{\Delta mac}$ mouse (Fig.11A), indicating large number of inflammatory cells congregated in the liver. The blood serum analysis indicated that the marker of liver injury, Alanine aminotransferase (ALT) also significantly increased in the $Osr1^{\Delta mac}$ mice (Fig.11B). Further qpcr and F4/80 IHC/IF staining indicated significantly increased macrophage infiltration in $Osr1^{\Delta mac}$mice liver (Fig.11C and D). Consistent with this, increased level of inflammation cytokines (*Tnf-α* and *Il-1β*) expression was also detected in the $Osr1^{\Delta mac}$ mice (Fig.11C). Western blots of the proteins of JNK, NF-κB and P38 signaling pathways were performed to disclosure if these pro-inflammatory signaling pathways were involved in steatohepatitis mediated by myeloid Osr1 deletion. The results showed that the protein expressions of phosphorylated-JNK, NF-κB subunits p-p65 as well as p-p38 were significantly enhanced in $Osr1^{\Delta mac}$ mice (Fig.11E1 and E2). Collectively, these results indicate that macrophage Osr1 deletion induced more severe NASH phenotype and over-activated inflammatory response in the liver of MCD diet treatment.

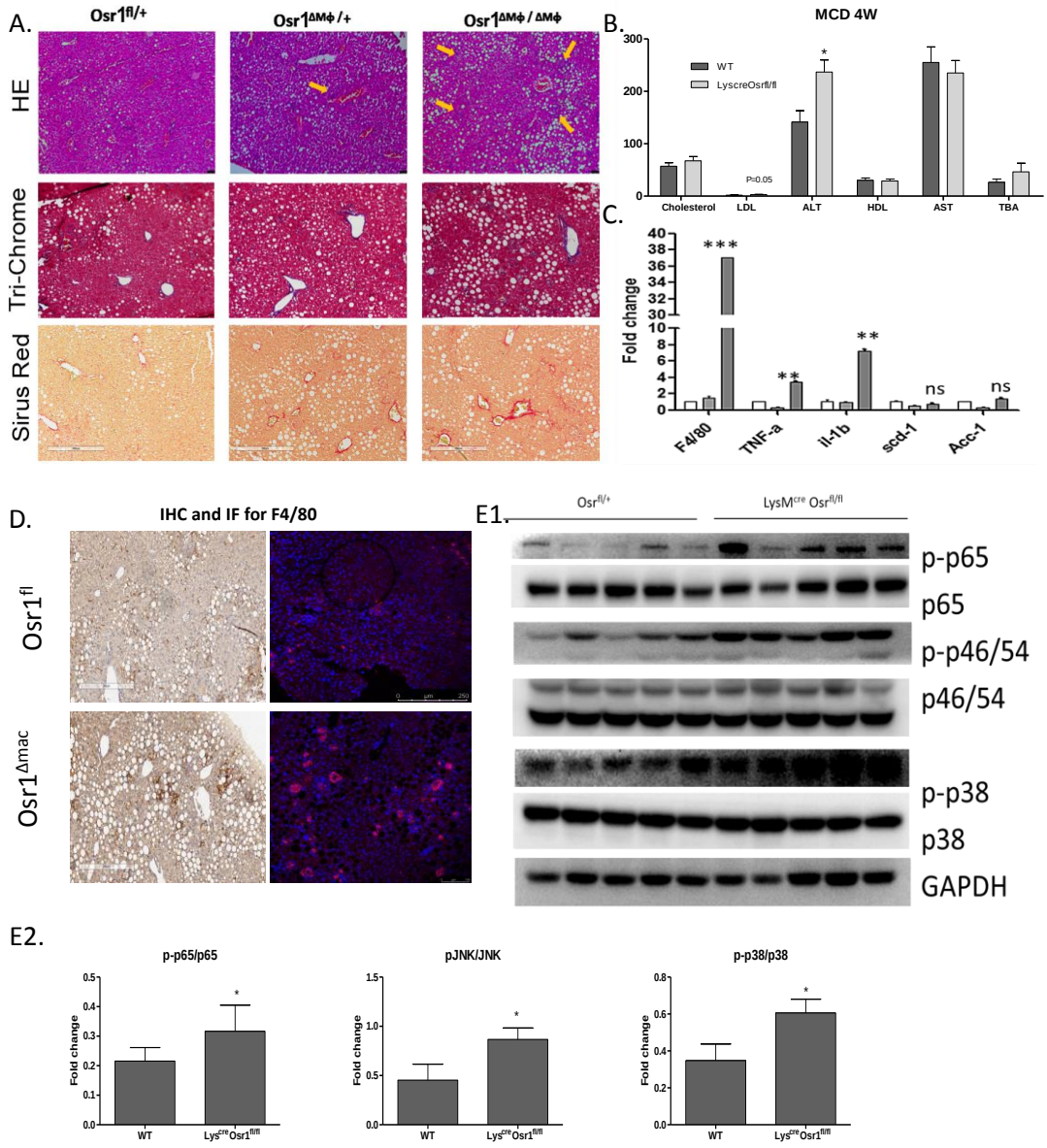

Figure 11. Deletion of macrophage Osr1 aggravated MCD diet-induced hepatic steatosis, early fibrosis and inflammation response

Male Osr1^{fl} and Osr1$^{\Delta mac}$ mice at 8 weeks of age, were fed with MCD diet for 4 weeks. (A) Representative images of H&E, Tri-Chrome Masson and Sirius red staining for liver sections. (B) Lipid metabolism and hepatocyte damage blood serum markers. (C) Inflammation and *de novo* lipogenesis related genes.

(D) Representative images of liver F4/80 immunohistochemistry (IHC) and immunofluorescence (IF) staining. (E) Liver proinflammatory signaling.

For B, serum levels were quantified by the biochemical analyzer (DxC 700 AU, Beckman Coulter). For C, gene expression was quantified by quantitative real time PCR (qRT-PCR). For E, liver lysates were subjected to Western blot analysis. Bar graphs, quantification of blots. For A – E, numeric data are means ± SE. n = 8 – 12. Numeric data are means ± SE. n = 6 – 8. Statistical difference between $Osr1^{fl}$ and $Osr1^{\Delta mac}$ mice in B, C, E : *, $P < 0.05$; **, $P < 0.01$; ***, $P < 0.001$.

3.3.4 Macrophage Osr1 inhibit liver fibrosis under a long-term MCD diet treatment.

Liver fibrosis is featured of abnormally large amount of collagen or other extracellular matrix (ECM) proteins disposition in the liver, making it a key character of NASH differing from simple steatosis. In mice exposed to MCD for 4 weeks, early onset of fibrosis was observed in the $Osr1^{\Delta mac}$ mice, evidenced by more collagen deposition in liver through Masson and Sirius red staining (Fig.11A). To confirm that the deletion of myeloid Osr1 could induce liver fibrosis, mice were fed with MCD for another 4 weeks (8 weeks of MCD diet feeding in total). The Tri-Chrome Masson and Sirius red staining did show severer fibrosis in the $Osr1^{\Delta mac}$ mice (Fig.12A). Consistently, the expression level of the fibrosis related genes was found significantly increased in the $Osr1^{\Delta mac}$ mice (Fig.12B).

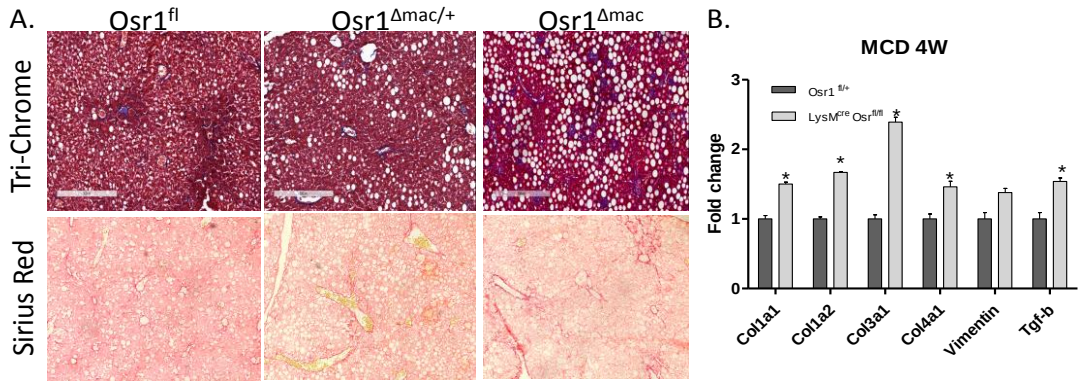

Figure 12. $Osr1^{\Delta mac}$ mice were induced more liver fibrosis under longer MCD diet treatment

Male $Osr1^{fl}$ and $Osr1^{\Delta mac}$ mice at 8 weeks of age, were fed with MCD diet for 8 weeks. (A) Tri-Chrome Masson and Sirius red staining for liver sections.(B) Fibrosis related genes. Numeric data are means ± SE. n = 6-8. *, $P < 0.05$.

CHAPTER IV

DELETING OSR1 IN MYELOID CELLS LED TO THE ABNORMAL BILE ACID SYNTHESIS AND CHOLESTEROL TRAP IN LIVER UPON MCD TREATMENT

In both HFD and MCD diet treatment mice, the myeloid Osr1 expression is negatively associated with the severity of the hepatic steatosis and inflammation. The *de novo* lipogenesis genes are significantly upregulated in HFD treated $Osr1^{\Delta mac}$ mice. Unlike the HFD model, we did not find the differences of *de novo* lipogenesis in MCD diet model between control and $Osr1^{\Delta mac}$ mice (Fig.10C), which could not explain the more severe steatosis in $Osr1^{\Delta mac}$ mice. To further explore the protecting mechanisms that are dependent on Osr1 for liver steatosis, we did RNA-seq analysis on the $Osr1^{fl}$ and $Osr1^{\Delta mac}$ livers treated with CD or MCD diet (4 weeks). Sequencing analysis from the liver sample of $Osr1^{\Delta mac}$ vs. $Osr1^{fl}$ identified differentially expressed genes (DEGs) including Cyp7a1 and Cyp8b1, and significant KEGG pathways including primary bile acid biosynthesis, bile secretion and cholesterol metabolism (Fig.13A). To investigate if there is altered metabolisms of cholesterol and other related lipids metabolisms in $Osr1^{\Delta mac}$ mice liver, we first assessed the level of cholesterol, triglyceride, and bile acid (which is synthesized from cholesterol) in both control and $Osr1^{\Delta mac}$ mice liver tissue. We did find relatively high triglyceride level in $Osr1^{\Delta mac}$ mice liver (Fig.13B). However, there were significantly higher level of cholesterol (Fig.13C) and lower level of total bile acid (Fig.13D) in the liver of $Osr1^{\Delta mac}$ mice. The result indicated cholesterol trap in the liver of $Osr1^{\Delta mac}$ mice

under MCD diet treatment. The hepatic free cholesterol accumulation in NAFLD is reported to correlate with the presence and severity of cytologic ballooning(*94*).In addition, inhibiting the cholesterol absorption has been shown to ameliorate non-alcoholic fatty liver disease (NAFLD) pathology (*95*). Therefore, the cholesterol accumulation in the $Osr1^{\Delta mac}$ mice liver might contribute to the aggregated steatosis in $Osr1^{\Delta mac}$ mice(*96*). Cyp7a1 is one of the two specific rate-limiting enzymes for bile acid synthesis and Cyp8b1 is required for synthesis of cholic acid(*97*). Interestingly, it has been reported that disruption Cyp7a1 expression in the liver could induce hepatic inflammation and fibrosis, which is consistent with our observations. And it has been shown that down regulating Cyp7a1 did not alter the total bile acid pool which was determined as the total amount of bile acids in liver, intestine, and gallbladder(*98*). Additionally, our data also showed that MCD diet itself could disrupt bile acid biosynthesis by reducing the protein level of Cyp7a1 (Fig.13E). We believe that it could serve as a potential new mechanism of MCD diet induced hepatic steatosis and NASH.

To establish the impact of macrophage Osr1 on liver cholesterol metabolism, we first confirmed the decreased protein level of Cyp7a1 in $Osr1^{\Delta mac}$ mice liver via western blot in Chow and MCD diet treated mice (Fig.13F and G). We also tested the hepatic levels of genes involved in bile acid synthesis including the Cyp7a1, Cyp8b1, Cyp27a1 and Cyp7b1, Cyp8b1, the low-density lipoprotein receptor (LDLr, which mediates the endocytosis of cholesterol-rich LDL), Hmgcr (rate-controlling enzyme of the mevalonate pathway, the metabolic pathway that produces cholesterol) and Srebp2(involved in cholesterol

synthesis and import) in the $Osr1^{fl}$ or $Osr1^{\Delta mac}$ liver. We could not find expression difference in these cholesterol synthesis and transportation controlling genes (Fig.13H). However, decreased expression of Cyp7a1, the key enzyme in primary bile acid synthesis was always detected in both Chow and MCD diet treated $Osr1^{\Delta mac}$ mice (Fig.13H). Collectively, these results indicated that macrophage Osr1 is involved in bile acid secretion and cholesterol metabolism.

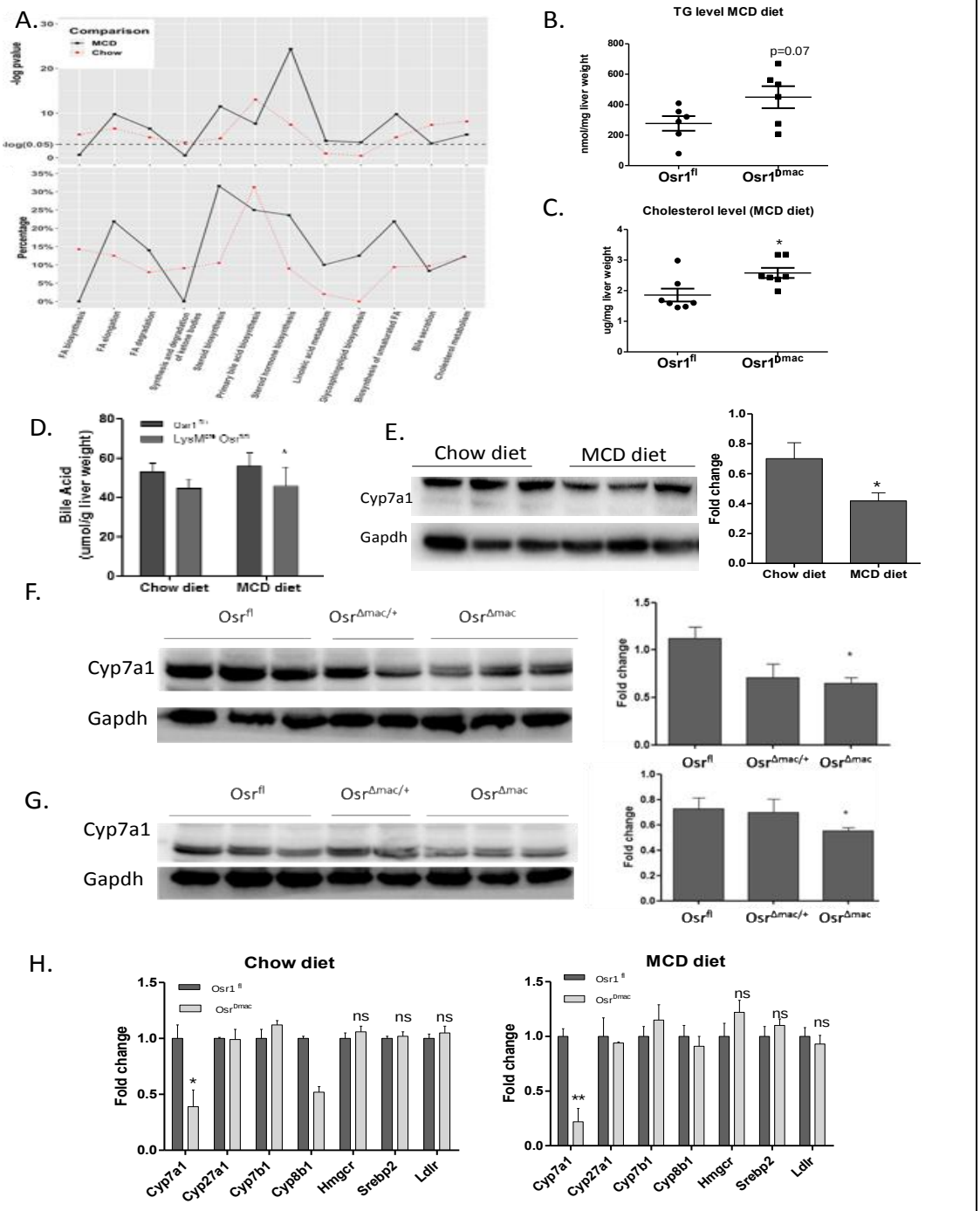

Figure 13. Deleting Osr1 leads to the disruption of bile acid synthesis and cholesterol trap in the liver upon MCD diet treatment

(A) The GO analysis identified distinct KEGG pathways for bile acid synthesis, secretion, and cholesterol metabolism associated with Osr1 level on CD or MCD. In upper panel, any –logP value higher than the dotted line was identified as significance (n=3, P<0.05). In the lower panel, the y-axis indicates the percentage of DEGs in this signaling pathway. (B) Total triglyceride level in liver tissue (C) Total cholesterol level in liver tissue. (D) Total bile acid level in liver tissue. (E)Cyp7a1 protein level in CD and comparative MCD treated WT mice liver and the quantification. (F) Cyp7a1 protein level during CD treatment and the quantification. (G) Cyp7a1 protein level during MCD diet treatment and the quantification. (H) Cholesterol and bile acid metabolic genes. For D, E, F, G, H, Numeric data are means ± SE. *, $P < 0.05$.

CHAPTER V

DELETING OSR1 IN MYELOID CELLS INDUCED HEPATIC PRO-INFLAMMATORY RESPONSE BY REGULATING MACROPHAGE M2 ALTERNATIVE POLARIZATION

5.1 Deleting Osr1 in myeloid cells induced hepatic pro-inflammatory response

5.1.1 Deleting Osr1 in myeloid cells induced more hepatic pro-inflammatory cytokine production *in vivo*

We have shown the significantly increased hepatic macrophage infiltration and overactivation of inflammation related signaling in $Osr1^{\Delta mac}$ mice liver, associated with increased expression level of inflammatory cytokines. As shown in Fig.9G and Fig.10C, pro-inflammatory cytokines such as IL-1b and TNF-a were significantly induced in HFD and MCD diet-fed $Osr1^{\Delta mac}$ mice compared to corresponding $Osr1^{fl}$ mice. Altogether, these results suggests that the deleting Osr1 in myeloid cells induced more hepatic pro-inflammatory cytokine production *in vivo*.

5.1.2 RNA sequencing and macrophage population analysis identified that Osr1 was required for macrophage alternative M2 polarization *in vivo*

The gene ontology (GO) analysis of the RNA-seq data from the $Osr1^{\Delta mac}$ liver vs the $Osr1^{fl}$ liver identified distinct KEGG (Kyoto Encyclopedia of Genes and Genomes) pathways associated with Osr1 level on CD or MCD (Fig. 14A). Specifically, we identified signaling pathways for macrophage differentiation and polarization, including PPAR signaling pathway, TGF-beta signaling pathway, JAK-STAT signaling pathway,

NF-κB signaling pathway and osteoclast differentiation pathway (Fig. 14A). These results suggested that Osr1 may be involved in maintaining macrophage plasticity and polarization.

To test if Osr1 regulates the macrophage polarization, we identified the macrophage subtypes in MCD-induced NASH liver of the $Osr1^{\Delta mac}$ and $Osr1^{fl}$ mice. Specifically, we analyzed M2 ($CD45^{+}F4/80^{+}CD11b^{+}$ $CD206^{+}$) macrophages from liver tissues of $Osr1^{fl}$ and $Osr1^{\Delta mac}$ mice by flow cytometry. Compared to $Osr1^{fl}$ mice fed with the MCD diet, $Osr1^{\Delta mac}$ mice fed with the same diet showed significantly decreased M2 macrophage ratios (Fig. 14B). The result also indicated that, upon Osr1 deletion, the macrophages alternative polarization ability is affected *in vivo* during MCD diet treatment.

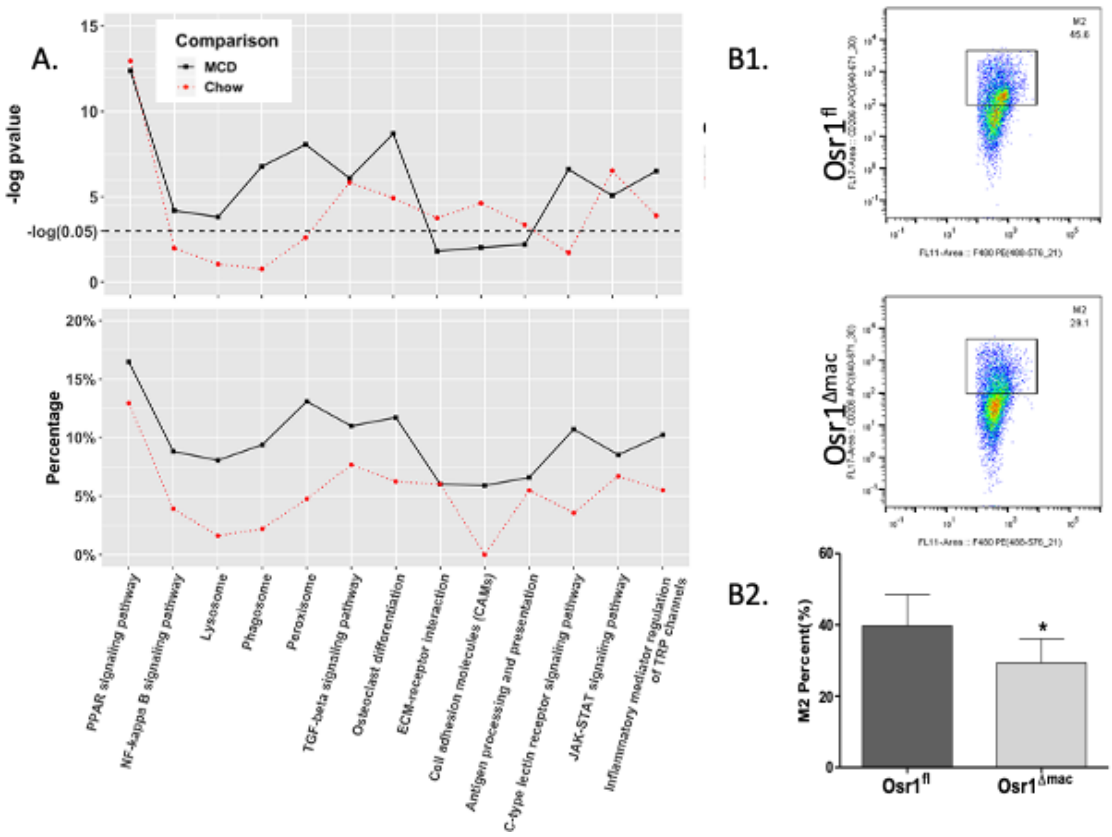

Figure 14. Osr1 was required for macrophage alternative M2 polarization *in vivo*

(A)The GO analysis identified distinct KEGG pathways for macrophage differentiation and polarization associated with Osr1 level on CD or MCD. In upper panel, any –logP value higher than the dotted line was identified as significance (n=3, P<0.05). In the lower panel, the y-axis indicates the percentage of DEGs in this signaling pathway. (B) Representative flow cytometry picture of M2 polarization distribution and the related quantification. Results are shown as means ± SE of n = 4 independent experiments. *, $P < 0.05$.

5.2 Macrophage specific Osr1 expression increased during macrophage M2 induction *in vitro*, while its deficiency blunted macrophage alternative polarization

To further investigate the underlying mechanisms how Osr1 is involved in the macrophage polarization, we performed polarization assay using isolated primary bone marrow-derived macrophages (BMDMs) from $Osr1^{fl}$ and $Osr1^{\Delta mac}$ mice. Western blot analysis indicated that BMDMs expressed relatively low levels of the Osr1 at M0 status. However, sustained induction of Osr1 was observed after exposure to IL-4 alternative induction (Fig.15A). Western blot analysis confirmed higher expression of the Osr1 protein in M2 cells compared with M0 (unstimulated) and M1 macrophages (Fig. 15A and B). In addition, Osr1 expression was reverted when polarized M2 cells are shifted to M1-polarizing conditions (Fig.15B). Similarly, Osr1 induction was restored by IL-4 after IFN-γ and LPS treatment. These results suggested that the Osr1-dependent transactivation might be part of the specific signature of alternative macrophage activation.

The functional relevance of Osr1 in alternative macrophage activation was investigated by comparing the expression of several M2 specific markers under IL-4 induction. During a total of 24h treatment, we set up a total of 5 time points and tested the gene expression level at each time point by quantitative real-time PCR. Interestingly, the results showed that Osr1 deletion decreased the ability of IL-4-induced M2 macrophage

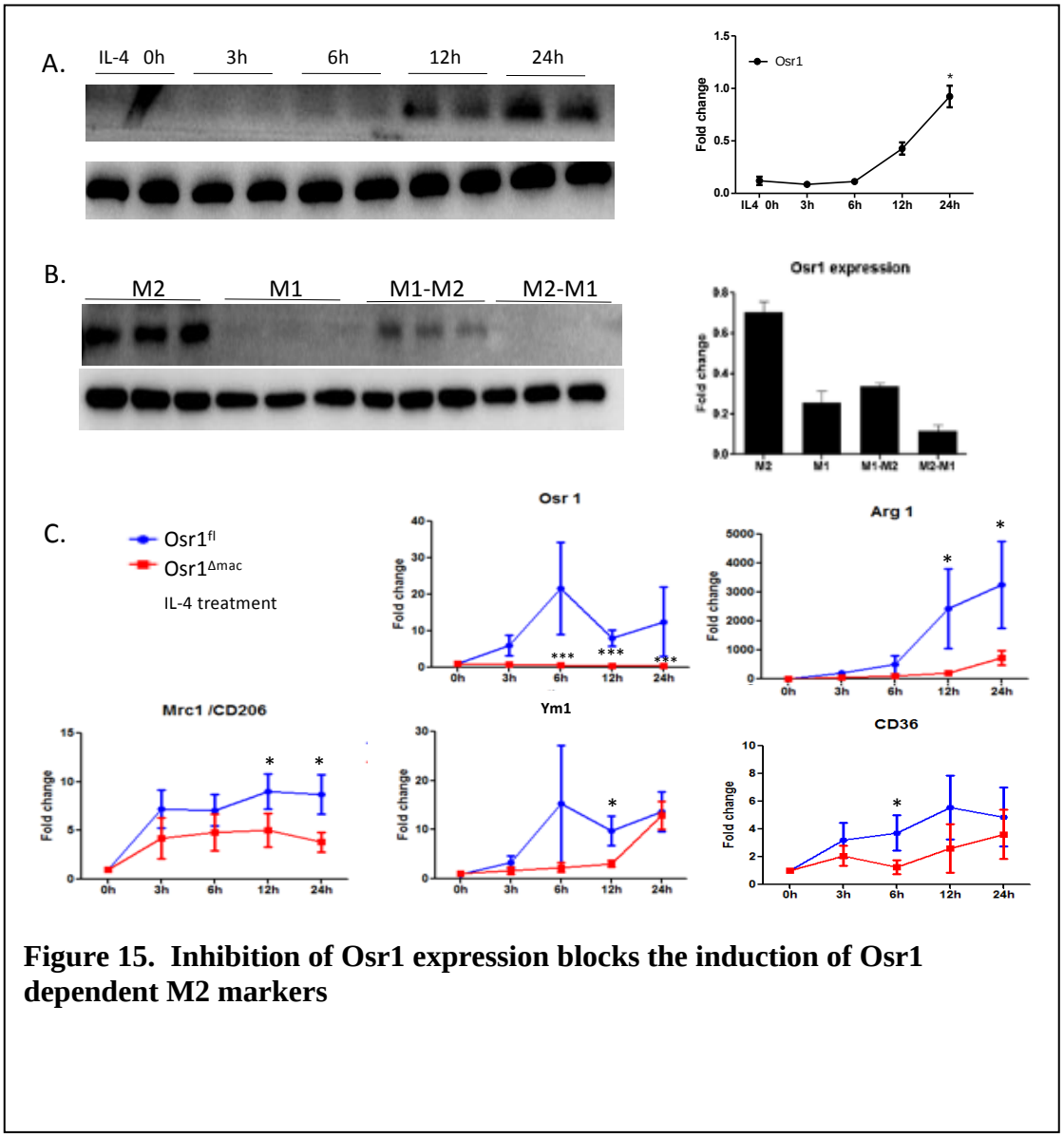

Figure 15. Inhibition of Osr1 expression blocks the induction of Osr1 dependent M2 markers

polarization, evidenced by down regulated M2 specific markers including *Arg1*, *Mrc1*, *Ym1*, and *CD36* (Fig. 15C).

(A) Expression levels of the Osr1 in resting macrophages (M0) and after exposure to 20 ng/mL of IL-4 at different time points.(B) Osr1 induction after exposure to 20 ng/mL of IL-4 is reverted when cells are shifted to M1-polarizing conditions (20 ng/mL of IFN-γ plus 10 ng/mL of LPS) for an additional 24 hours. (C) Expression levels relative to resting macrophages (M0) in macrophages exposed to 20 ng/mL of IL-4, in the presence of the presence or absence of *Osr1, of Arg1, Mrc1, Ym2, CD36*. Results are shown as means ± SE of n = 8 independent experiments. *, $P < 0.05$; **, $P < 0.01$; ***, $P < 0.001$.

5.3 PPAR-γ and c-Myc are direct targets of Osr1 for regulating macrophage alternative M2 polarization

PPAR-γ is known to skew monocytes toward an M2 phenotype and down-regulates inflammatory pathways in macrophages(*64*). Animal model also showed that macrophage specific PPAR-γ knockout mice have higher body mass and more severe insulin resistance. Transcription factors c-MYC was also reported to be required for the M2 macrophage polarization (*65, 99-106*). To be noted, c-Myc and *Pparγ* have relatively similar expression pattern with Osr1 under the specific M1 or M2 induction. (Figure 15B, Figure. 16A) Our RNA-Seq analysis identified several DEGs including *c-Myc* (CD treatment: 8.08 vs. 2.35, P=0.00005; MCD treatment: 14.08 vs. 7.89, P=0.001) and *Pparγ* (CD treatment: 4.53 vs. 2.32, P=0.0003; MCD treatment: 7.56 vs. 4.1, P=0.0056) and KEGG pathways including PPARγ signaling pathway are associated with Osr1 expression on CD or MCD diet treatment. We first determined if PPAR-γ and c-Myc were associate with Osr1 dosage. As shown in figure. 16A, both PPAR-γ and c-Myc

expressions positively responded to IL-4 stimulation, while negatively responded to LPS+INF- γ, regardless of its original status. Their expression pattern was similar as that of the Osr1 during macrophage phenotype switch. (Fig. 15B). To be noted, comparing to that the WT M0 BMDMs was sensitive to IL-4 treatment, the $Osr1^{\Delta mac}$ BMDMs no longer responded to it (Fig. 16B). On the contrast, Osr1 overexpression experiment in RAW264.7 cells resulted in increased expression of PPARγ and c-Myc(Fig. 16C). These results suggested that both expression of PPARγ and c-Myc depended on Osr1 in macrophages. To determine if they are direct targets of Osr1 transcription, we analyzed the genome potential promoter region of PPARγ and c-Myc by bioinformatically incorporative analysis and found several putative clustered Osr1 specific binding sites upstream of PPARγ and c-Myc transcriptional starting sites as indicated in Fig.16D. CHIP-Qpcr was performed to determine the Osr1 responsive genomic region of PPARγ and c-Myc. Three potential genomic regions of c-Myc and one potential genomic region of PPARγ were identified (Fig.16D), which were further tested by Luciferase reporter assay. Region 2 of c-Myc and region 2 of PPARγ were confirmed to be responsible to Osr1 transactivation by CHIP-Qpcr and Luciferase reporter assay (Fig. 16E). Taken together, our results demonstrated that c-Myc and PPARγ are direct downstream targets of Osr1.

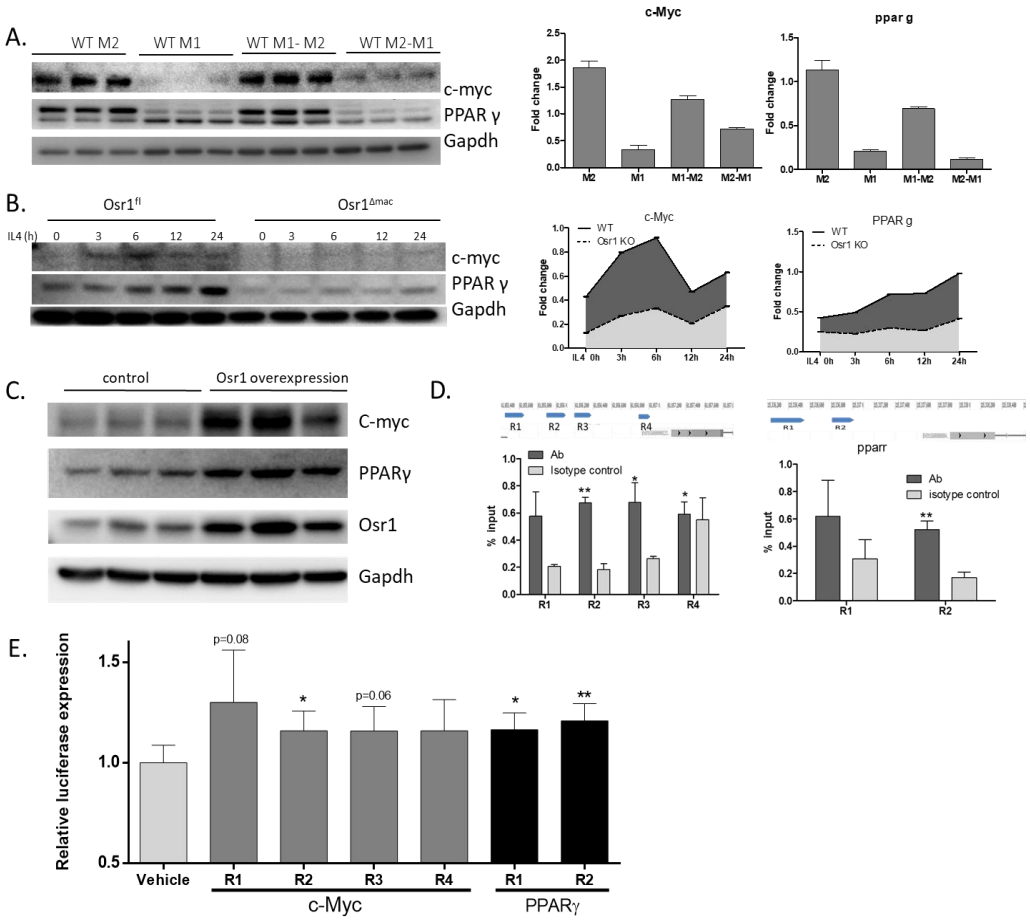

Figure 16. PPAR-γ and c-Myc are directly regulated by Osr1 in macrophages

(A)WT resident BMDMs (M0) were treated with either IL-4 or IFN- γ plus LPS for 24h to induce M2 or M1 phenotype, then the induced cells were restimulated to M1 or M2 like macrophages with IL-4 or LPS and IFN- γ respectively. The expression level of PPARγ and c-MYC were tested by western blot. (B) Expression levels of the PPARγ and c-MYC in resting macrophages (M0) and after exposure to 20 ng/mL of IL-4 at indicated time points in $Osr1^{fl}$ and $Osr1^{\Delta mac}$ BMDMs .(C) PPARγ and c-MYC expression level in control and Osr1 overexpression RAW264.7 cells.(D) CHIP-qPCR result indicated the directly binding motif of Osr1 in c-MYC and PPARγ promoter regin.(E) Luciferase reporter assay find the Osr1 transactivation responsible sequence.*, $P < 0.05$; **, $P < 0.01$.

To address the functional role of Osr1-PPARγ, we treated the BMDMs isolated from $Osr1^{fl}$ and $Osr1^{\Delta mac}$ mouse with IL-4 along with rosiglitazone. The result indicated that the addition of rosiglitazone recovered the ability of IL-4 to activate the expression of *Arg1, Ym1 and CD36 in* $Osr1^{\Delta mac}$ BMDMs (Fig.17A), indicating that these three M2 markers might be regulated by Osr1 dosage through PPARγ transactivation. Indeed, it has been previously reported that *Arg1* and *CD36* can be directly regulated by PPARγ in macrophages (*75*, *107*) . Rosiglitazone failed to recover the expression of c-Myc in the $Osr1^{\Delta mac}$ BMDMs (Fig.17A). This is within our expectation because c-Myc expression was not dependent on PPARγ. Collectively, these results demonstrated that Osr1 regulated macrophage alternative polarization largely through PPARγ.

To determine functional Osr1-PPARγ *in vivo,* we generated the compound heterozygotes of Osr1 and PPAR-γ by crossing the $Osr1^{fl/+}$, $LysoM\text{-}Cre^{fl/+}$ ($Osr1^{\Delta M\varphi/+}$) with $PPAR\text{-}\gamma^{fl/fl}$ mice. The $Osr1^{\Delta M\varphi/+}$, $PPAR\text{-}\gamma^{\Delta M\varphi/+}$ and the $PPAR\text{-}\gamma^{\Delta M\varphi/+}$ mice were treated with HFD for 14 weeks to induce NAFLD phenotype. The level of liver injury markers AST and ALT in blood serum were not significantly different (data not shown). However, more steatosis and fibrosis were detected by liver H&E staining and Sirus red staining in $Osr1^{\Delta M\varphi/+}$, $PPAR\text{-}\gamma^{\Delta M\varphi/+}$ mice comparing to the control (Fig.17B and C). This indicated that Osr1 and PPARγ interacted with each other *in vivo* during the NASH pathogenesis.

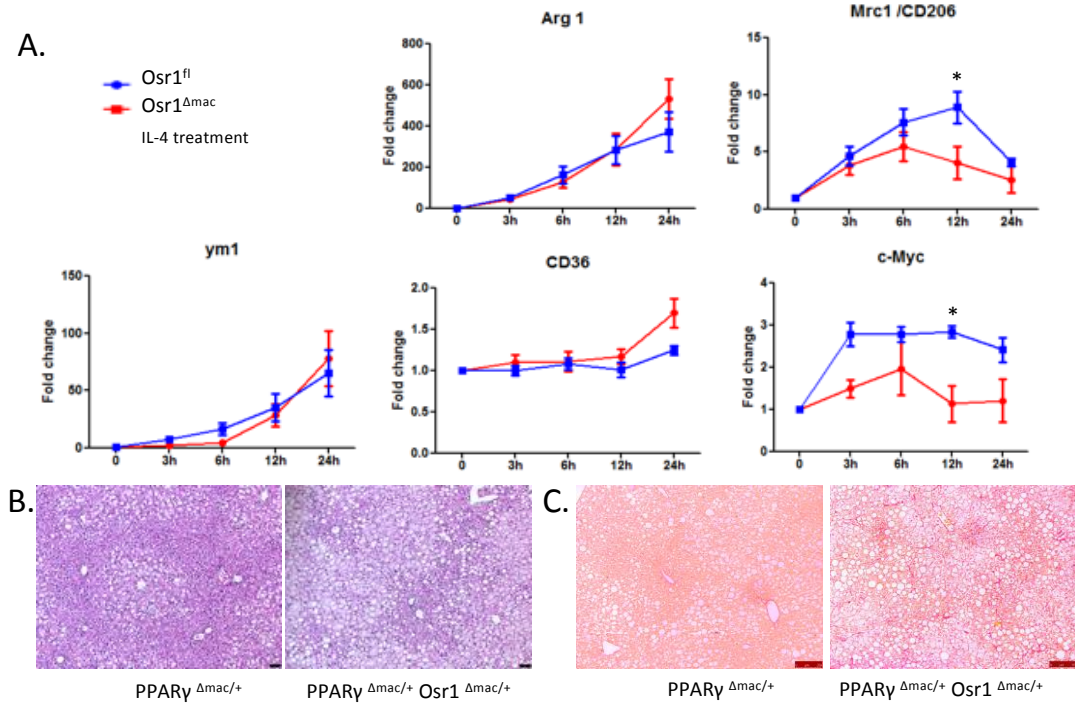

Figure 17. The PPARγ ligand, rosiglitazone, rescued the downregulated M2 markers in Osr1Δmac macrophages during M2 induction

(A) Expression levels relative to resting macrophages (M0) in macrophages exposed to 20 ng/mL of IL-4 in $Osr1^{fl}$ and $Osr1^{\Delta mac}$ macrophages in the presence of 1 µM rosiglitazone. The expression level of *Arg1, Mrc1, Ym2, CD36* and *c-Myc* were tested by quantitative real-time-PCR. (B) H&E staining and (C) Sirus red staining in $Osr1^{\Delta M\varphi/+}$ PPAR-γ $^{\Delta M\varphi/+}$ mice and control mice. For A, results are shown as means ± SE of n = 8 independent experiments. *, $P < 0.05$.

CHAPTER VI

OSR1 IN MACROPHAGES METABOLIC PROGRAMMING

6.1 Osr1 deletion shifted the macrophage towards the glycolysis dependent ATP production profile

It has been established that a switch to oxidative metabolism is an essential component of alternative macrophage polarization. Interestingly, PPARγ was reported to be required for IL-4 induced increase in β-oxidation of fatty acids. Deleting PPARγ would reduce ~70% in the rate of fatty acid oxidation under IL-4 treatment(*75*). Additionally, CD36 is a scavenger receptor expressed on macrophage membrane and plays an important role for fatty acid influx, which fuels β-oxidation(*108*). In this study, we have shown that PPARγ was a direct downstream target of Osr1 in macrophages and CD36 expression was significantly downregulated in $Osr1^{\Delta mac}$ macrophages. W hypothesis that Osr1 could modulate the macrophage metabolic change during the macrophage alternative polarization. We first treated primary BMDMs from $Osr1^{fl}$ and $Osr1^{\Delta mac}$ with LPS plus IFN-γ or Il-4 or for 24 h to induce the M1 or M2 phenotype respectively and assessed the ATP rate using a Seahorse extracellular flux analyzer. With glucose and pyruvate as substrates, the total ATP production rates were similar in control and $Osr1^{\Delta mac}$ macrophages. However, deleting Osr1 resulted in around 25% reduction in the rate of fatty acid oxidation (FAO) and upregulated about 50% of the ratio of glycolysis and oxidative phosphorylation (OXPHOS) during M1 induction (Fig. 18A). During M2 induction, deleting Osr1 resulted in around 7% reduction in the rate of FAO and about

29.5 % increase of the ratio of glycolysis and OXPHOS (Fig. 18B). Importantly, with the presence of rosiglitazone, the increased ratio of glycolysis and OXPHOS was rescued to a similar level of the WT (p=0.07, Fig. 18B). These experiments showed that Osr1 deletion inhibited glucose-fueled mitochondrial respiration, thereby trapping macrophages in a metabolic state with pro-inflammatory polarization.

6.2 Osr1 is required for the palmitate oxidation during macrophage alternative polarization

Lipids are oxidized primarily in the mitochondria in a multistep pathway called β-oxidation (or fatty acid oxidation, FAO) (*109*). This process begins by importing long-chain fatty acyl-CoAs into mitochondria, followed by a four-step reaction, generating an acyl-CoA shortened by two carbons. This shortened acyl-CoA continues through the reaction until the entire chain is oxidized into acetyl-CoA. A major result of metabolic shifts toward FAO is increased ATP production, and this is often associated with stress responses and survival (*110*). Long chain fatty acids (LCFAs) are the primary substrate fueling mitochondrial metabolism and has a profound impact on cell fate, function, and fitness(*111*). Based on this, to further figure out the underlying mechanism about how Osr1 deletion interrupt the ATP rate of the macrophages, we investigated if Osr1 deletion affected the long chain FAO process. NAFLD/NASH is a systematic metabolic disorder associated with glucose and lipid metabolism and insulin resistance. To begin with, we tested if Osr1 expression level was regulated by the glucose, insulin and palmitic acid (PA), which are elevated in patients with metabolic disease(*43*).Interestingly, we found that the transcription of Osr1 can be significantly

induced by palmitic acid (Fig. 18C). PA has long been reported to induce ER stress, inflammation, and lipotoxicity, which is crucial for the pathogenesis of NAFLD(*112*). Considering this, we tested the requirement for Osr1 in the palmitic acid oxidation activities. To have an oversight of the palmitate oxidation in macrophages, we first examined the palmitate oxidative profile of the WT BMDMs with resident M0, pro-inflammatory M1 or anti-inflammatory M2 phenotype with Seahorse XF Palmitate Oxidation Stress Test Kit. Oxygen consumption rate (OCR) was measured by XFe96 Seahorse bioanalyzer with palmitate (BSA conjugated) and be used to determine the basal, and maximum respiration. We found that pro-inflammatory M1 macrophages had the lowest basal and maximum respiration, and the M2 the highest by comparing to the resident M0 (Fig. 18D). When using Palmitate as a long-chain fatty acid substrate, both basal and maximal ($p=0.06$) OCR were significantly decreased in the $Osr1^{\Delta mac}$ M2 group (Fig. 18E). To be noted, the rosiglitazone rescued the OCR level in the $Osr1^{\Delta mac}$ BMDMs (Fig. 18E). This suggested that Osr1 is indeed involved in maintaining the palmitate long-chain fatty acid oxidation (FAO), and the process largely depends on PPARγ. Altogether, these also come to the schematic diagram about the role of Osr1 in cell metabolisms during the macrophage alternative polarization. (Fig. 19)

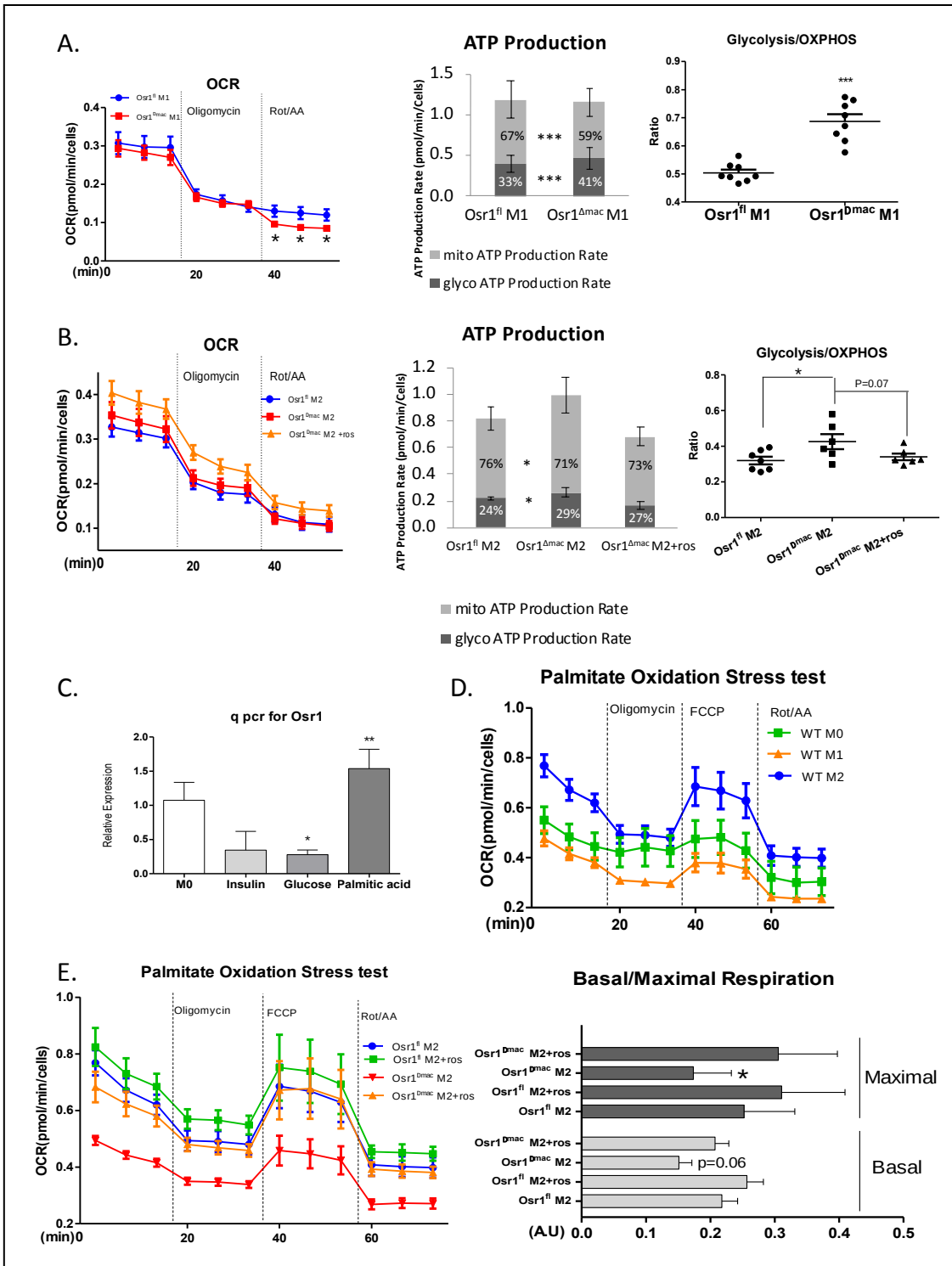

Figure 18. Osr1 deletion shift the macrophage to a glycolysis like metabolism profile and disrupt the mitochondrial palmitate oxidation during M2 polarization

(A, B) BMDMs from Osr1^{fl} or Osr1$^{\Delta mac}$ were cultured in Seahorse XF RPMI medium and seeded in Seahorse plates and stimulated with indicated drugs respectively for 24 hr. During real-time APT rate analysis, cells were sequentially treated with oligomycin (OM) and rotenone (ROT) plus antimycin A (AA), to assess the ATP production from glycolysis and mitochondria simultaneously using label- free technology in the BMDM cells. (C)Resident M0 BMDMs were treated with Glucose (30mM), insulin (10nM), or palmitate (0.4mM), the expression of Osr1 were detected by quantitative real-time PCR. (D, E) Mitochondrial respiration function in assessed by Seahorse Mito Stress test using palmitate (BSA-conjugated palmitate) as substrates. OXPHOS parameters were assessed by recording the OCR values after sequential injection of OM, FCCP, and Rot+ AA. Calculated basal respiration, ATP production, and maximal respiration were plotted in bar graphs. OCR: oxygen consumption rate. Oligomycin (OM): ATP synthase inhibitor. FCCP: mitochondrial uncoupler. Rot/AA: rotenone and antimycin A, specific inhibitors for ETC complex I and III respectively. Ros: rosiglitazone. *, $P < 0.05$; **, $P < 0.01$; ***, $P < 0.001$.

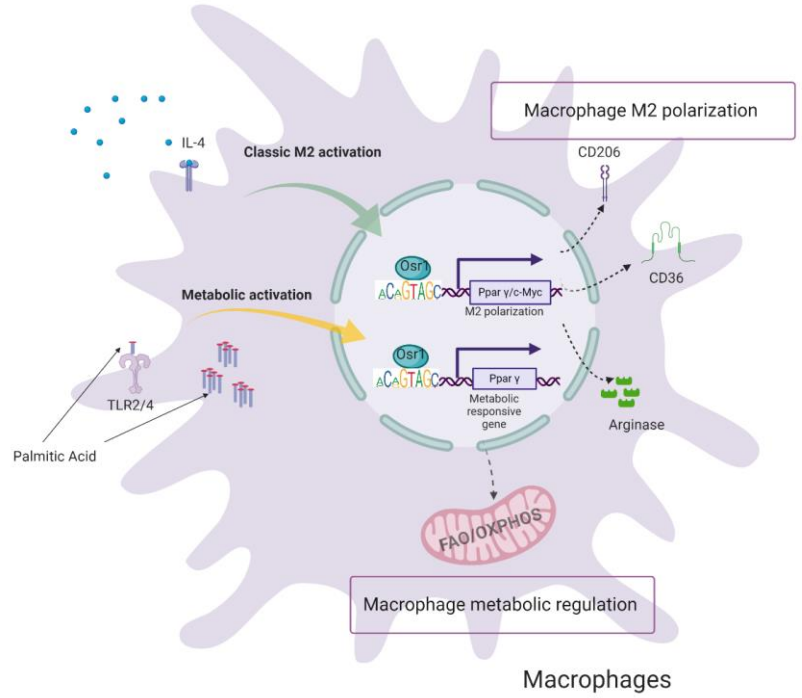

Figure 19. Schematic diagram of Osr1 in macrophage polarization and cell metabolic change(Created in BioRender.com)

6.3 The impairment of palmitate oxidation in Osr1 knockout macrophages is independent of the IL-4 and AKT signaling

Lastly, we tested if Osr1 response to IL-4 stimulation via upregulation of STAT6 signaling. Upon IL-4 treatment, the control and $Osr1^{\Delta mac}$ macrophages expressed equivalent levels of STAT6 phosphorylation, suggesting the impairment of FAO in $Osr1^{\Delta mac}$ macrophages was independent of IL-4-STAT6 signaling (Fig.20A). We also tested the AKT, as well as FOXO1 signaling, which are important for cellular lipid and glucose metabolisms. The FOXO1 signaling is also an indicator of AKT signaling activation status, considering AKT-TSC-mTOR signaling is highly involved in the macrophage polarization.(*113*) There were no different expression of FOXO1, p-FOXO1, Akt and p-Akt between the $Osr1^{fl}$ and $Osr1^{\Delta mac}$ macrophages (Fig.20B), suggesting the impairment of PA oxidation caused by Osr1 deletion was independent of AKT signaling.

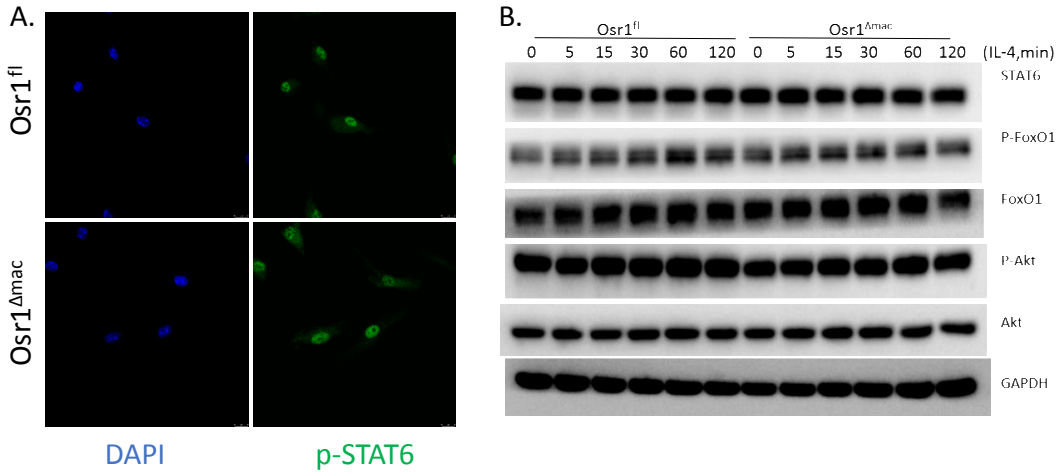

Figure 20. STAT6 and AKT activity are normal in Osr1$^{\Delta mac}$ macrophages and not involved in the macrophage metabolic profile change

(A) Immunoblot analysis of lysates from Osr1^{fl} and Osr1$^{\Delta mac}$ BMDMs stimulated with IL-4 for 5-120 min with the concentration of 10ng/ml.(B) Immunofluorescence staining of p-STAT6 in the BMDMs nuclei from Osr1^{fl} and Osr1$^{\Delta mac}$ with IL-4.

CHAPTER VII

DELETING MACROPHAGE OSR1 AGGRAVATED THE INFLAMMATION AND FAT DEPOSITION IN HEPATOCYTES

7.1 Osr1 deletion aggravated macrophage proinflammatory activation.

It has been established that, comparing to M1 macrophages, M2 macrophages are indeed highly plastic and easily adopt an M1-like inflammatory state (*114*). Considering that Osr1 expression was associated with a M2 phenotype, it is possible that blocking Osr1 may shift the cells to a M1 like pro-inflammatory macrophages, mediated by NF-κB, JNK or MAPK pathways. To test this possibility, we isolated bone marrow cells from $Osr1^{fl}$ and $Osr1^{\Delta mac}$ mice, differentiated the cells into macrophages (BMDMs), and analyzed the pro-inflammatory responses of BMDMs. Under lipopolysaccharide (LPS) treatment conditions, the phosphorylation states of MAPK p38, JNK p46 and NF-κB p65, expression level of IL-Iβ, IL-6 and iNOS, were significantly increased in $Osr1^{\Delta mac}$ BMDMs compared with the BMDMs. (Fig.21 A1-A4, 21B). Because alternatively activated macrophages can counteract pro-inflammatory cytokines excessive secretion, we examined whether IL-4 could appropriately attenuate LPS-induced IL-Iβ, TNF-α, and IL-6 secretion. The results indicated that IL-4 failed to suppress the expression of IL-Iβ and IL-6 in macrophages deficient of Osr1 (Fig.21D, E, F), indicating that a subset of IL-4 dependent anti-inflammatory responses were regulated by Osr1. Palmitic acid (PA) is a long chain saturated fatty acid with elevated blood concentration in obese patients. It has been indicated that PA could induce cellular inflammatory responses through toll-like receptors 2 and 4(TLR2 and TLR4) and PA-induced endoplasmic

reticulum (ER) stress(*115, 116*) Our results confirmed that PA could induce more phosphorylation of NF-κB, which is consistent with reported (Fig.21 C). In addition, we also found that PA could induce more phosphorylation of p38 MAPK (Fig.21 C). Then we also tested if alternatively activated macrophages can also counteract the pro-inflammatory responses PA. Similar with LPS, IL-4 failed to suppress the expression of Tnfα and IL-6 in macrophages deficient of Osr1(Fig.21D, E, F). To be noted, palmitic acid could induce the Osr1 expression in macrophages (Fig.21 C). This is consistent with the macrophage's mRNA level of Osr1 during PA treatment (Fig.18 C).

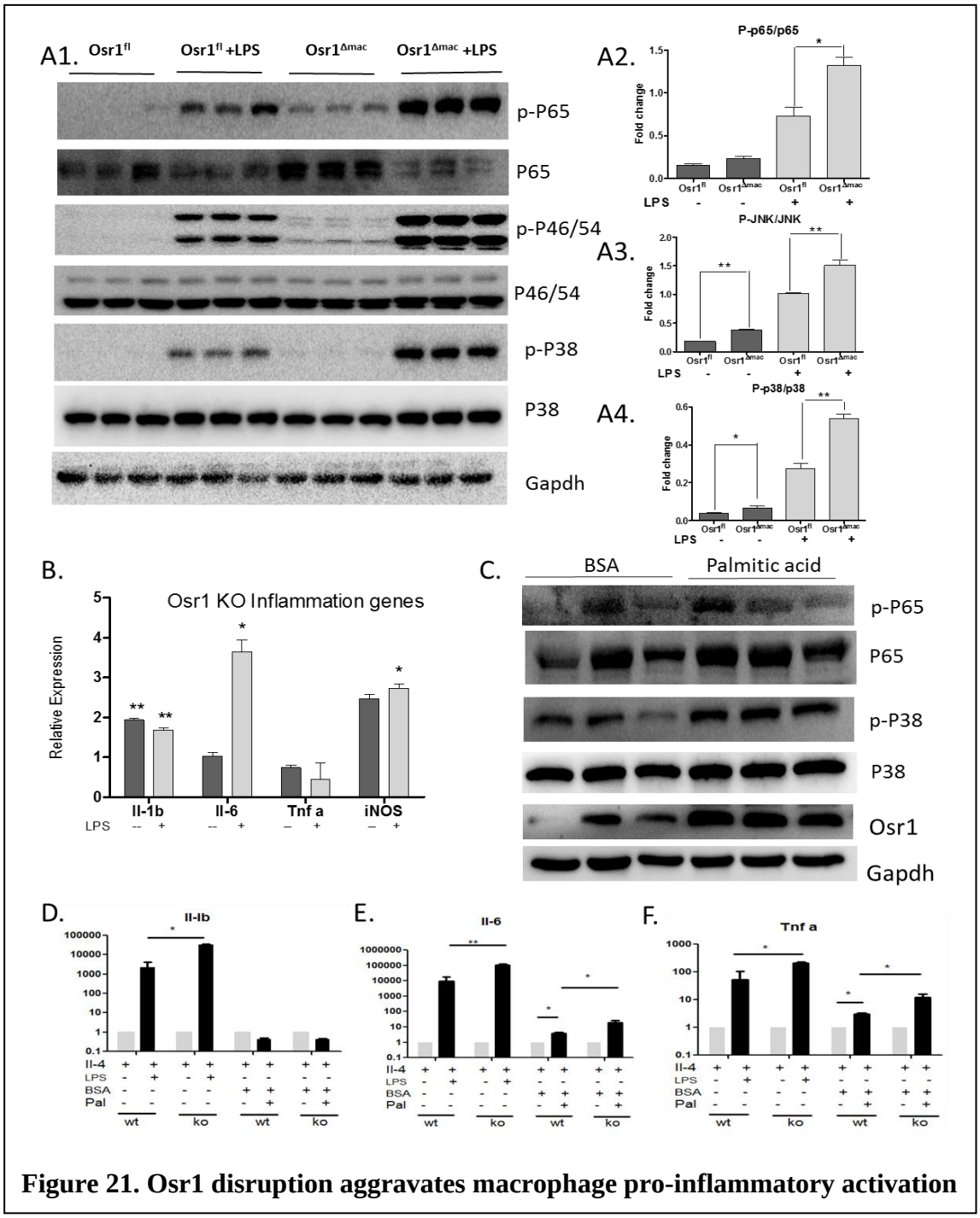

Figure 21. Osr1 disruption aggravates macrophage pro-inflammatory activation

BMDMs were prepared as described before. (A, B) Pro-inflammatory signaling (A) and cytokine production (B) BMDMS from $Osr1^{fl}$ and $Osr1^{\Delta mac}$ mice. For A, BMDM were treated with or without lipopolysaccharide (LPS, 100 ng/ml) for 30 min prior to harvest. Cell lysates were subjected to Western blot analysis. Bar graphs, quantification of blots. For B, $Osr1^{\Delta mac}$ macrophages gene expression levels were compared with $Osr1^{fl}$ macrophages with or with our LPS induction. (C) Immunoblot analysis of cell lysates from $Osr1^{fl}$ and $Osr1^{\Delta mac}$ BMDMs stimulated with BSA or BSA conjugated palmitic acid for 24h. (D, E, F) BMDMS from $Osr1^{fl}$ and $Osr1^{\Delta mac}$ mice were pretreated with IL-4 (10 ng/ml) for 24h were stimulated with LPS (10 ng/ml, with or without) or palmitic acid (with or without). The RNA was extracted and expression level of *Il-1β, Il-6* and *TNF-α* were quantified by qPCR. *Il-1 β* and *Il-6* were harvested after exposure to LPS for 12h, *TNF-α* for 6h. For all of the *Il-1β, Il-6* and *TNF-α*, expression level was detected after 24h exposure to palmitic acid. For B, D, E, F, cytokine expression was quantified by quantitative real-time PCR in the indicated BMDMs. Numeric data are means ± SE. n = 4 – 6. For A, D, E, F, statistical difference between the indicated and B, between $Osr1^{fl}$ and $Osr1^{\Delta mac}$, *, $P < 0.05$ and **, $P < 0.01$ in bar graphs.

7.2 Macrophage Osr1 deletion, via cytokine production, induced lipid accumulation and pro-inflammatory cytokine production in hepatocytes *in vitro*

7.2.1 Macrophage Osr1 deletion induced more pro-inflammatory response in hepatocytes

Considering $Osr1^{\Delta mac}$ mice had more severe NASH, we want to verify the direct role played by the Osr1 in macrophages in regulating lipid homeostasis and inflammation in hepatocytes. BMDMs were obtained from $Osr1^{fl}$ and $Osr1^{\Delta mac}$ mice and induced to M1 or M2 macrophages by LPS+IFN-γ or IL-4 respectively. The stimulated macrophages were co-cultured with primary hepatocytes isolated from $Osr1^{fl}$ mice, and the activation of NF-κB and MAPK p38 signaling in the mixed co-culture system was examined. The result indicated that $Osr1^{\Delta mac}$ M2 macrophages could induce more phosphorylation of NF-κB p65 and MAPK p38 signaling in the co-cultured macrophage-hepatocytes mixed system (Fig. 22A). To investigate if the macrophage induced inflammatory signaling was through directly cell-cell communication or cytokines secretion, we co-cultured primary $Osr1^{fl}$ hepatocytes with $Osr1^{fl}$ and $Osr1^{\Delta mac}$ BMDMs using a transwell system (Fig. 22B). Comparing to the hepatocytes co-cultured with $Osr1^{fl}$ BMDMs, the hepatocytes over phosphorylated NF- κB (P-p65/p65) when co-cultured with $Osr1^{\Delta mac}$ M1 BMDMs and overphosphorylated p38 signaling(P-p38/p38) when co-cultured with $Osr1^{\Delta mac}$ M2 BMDMs (Fig.22B and C). The results indicated that both $Osr1^{\Delta mac}$ M1 and $Osr1^{\Delta mac}$ M2 BMDMs induced more inflammation than the $Osr1^{fl}$ M1 or M2 did. Taken together, these results suggested that the Osr1 in macrophages protected macrophage

proinflammatory activation, which further acted on hepatocyte proinflammatory responses.

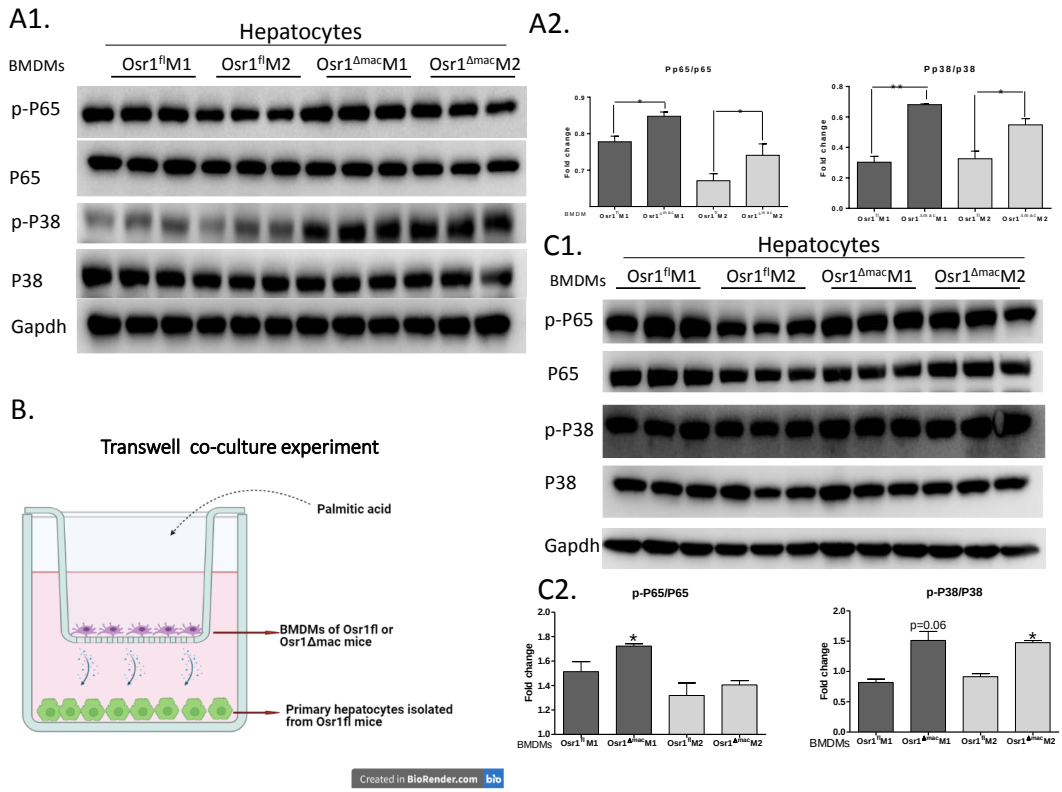

Figure 22. Osr1 disruption aggravate the effects of macrophages on increasing hepatocyte inflammation signaling through cytokine excretion

M1 or M2 BMDMs from Osr1^{fl} and Osr1$^{\Delta mac}$ mice were induced, and Macrophage-hepatocyte co-cultures were performed as described in Methods. (A)Macrophage-hepatocyte were co-cultured with the ratio 1:20 for 48h. Cell lysates were subjected to western blot analysis. Bar graphs, quantification of blots. (B, C) Macrophage-hepatocyte were co-cultured with the ratio 1:10 with the transwell (B) co-culture system (Corning) and the inflammation signaling were detected by western blot. The cells were treated with palmitate (Pal, 250 μM, conjugated in bovine serum albumin (BSA)) or BSA for the last 24 hr of the 48 hr incubation period.For A,C, bar graphs, quantification of the immune blot. *, $P < 0.05$.

7.2.2 Macrophage Osr1 deletion promoted hepatocyte steatohepatitic changes through the induction of cytokines

To identify if the cytokines secreted by macrophages were responsible for macrophage inflammation and hepatocyte steatohepatitic changes, the cytokine profiles of the culture medium of BMDMs isolated from $Osr1^{fl}$ and $Osr1^{\Delta mac}$ mice were analyzed. We used the transwell system to co-culture the primary $Osr1^{fl}$ hepatocytes with the $Osr1^{fl}$ or $Osr1^{\Delta mac}$ in the presence of palmitic acid. We found that the lipid accumulation (Oil Red O staining, Fig.23A and B) in the hepatocytes co-cultured with $Osr1^{\Delta mac}$ was significantly increased. In terms of inflammation and *de novo* lipogenesis, we found that the expression of the pro-inflammatory cytokines (Tnfa, Il6 and Il-1b) and the *de novo* lipogenesis genes were significantly increased in hepatocytes co-cultured with $Osr1^{\Delta mac}$

BMDMs in the presence of palmitic acid compared to those co-cultured with Osr1^{fl} BMDMs (Fig.23C).

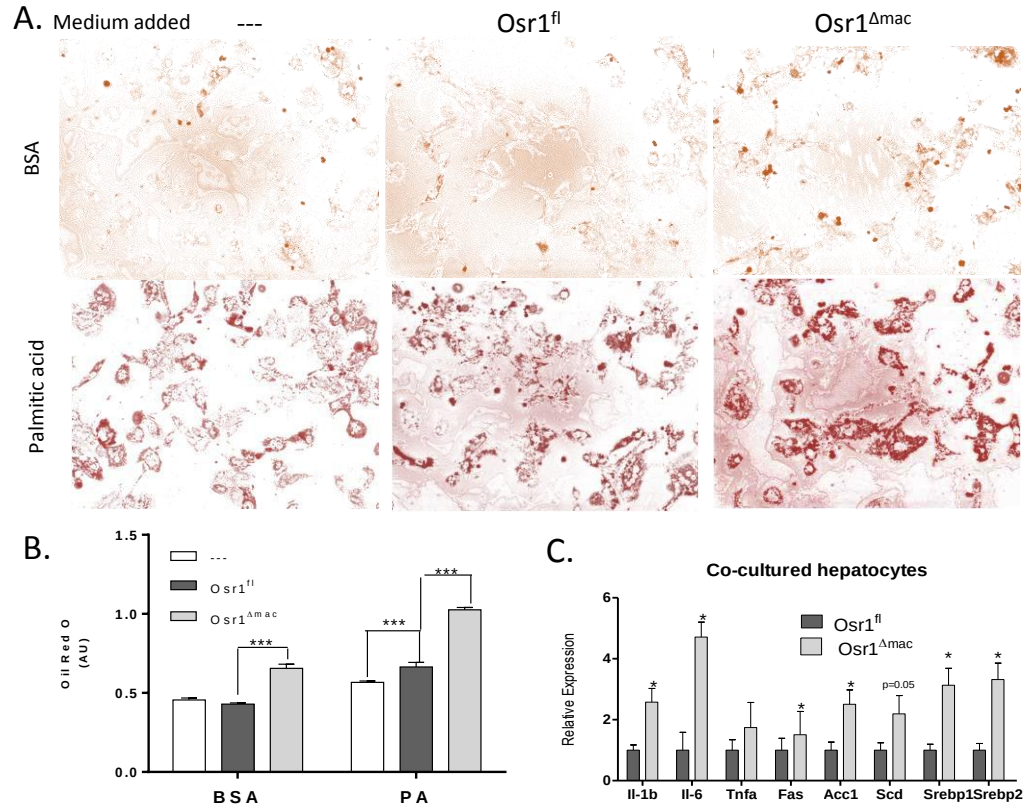

Figure 23. Osr1 disruption aggravate the effects of macrophages on increasing hepatocyte fat deposition and inflammation related gene expression through cytokine excretion

Primary hepatocytes were isolated from chow-diet-fed Osr1^{fl} mice at 10 – 12 weeks of age. BMDMs from Osr1^{fl} and Osr1$^{\Delta mac}$ mice were induced as described in the methods. (A)Representative pictures from Macrophage-hepatocyte co-culture with the ratio 1:10 for 48h. The cells were treated with palmitate (Pal, 250 μM, conjugated in bovine serum albumin (BSA)) or BSA for the last 24 hr of the 48 hr incubation period. (A) Hepatocyte fat deposition. The hepatocytes were stained with Oil Red O for 1 hr. (B) Bar graphs, quantification of fat content levels from the co-cultured hepatocytes. (C) The mRNA levels of genes related to fat metabolism and pro-inflammatory cytokines were examined in the hepatocytes using quantative real-time RT-PCR. For B , numeric data are means ± SE, n = 6. For C, numeric data are means ± SE, n = 3. *, $P < 0.05$, ***, $P < 0.001$.

CHAPTER VIII

PHARMACOLOGICAL PPAR-Γ AGONIST ROSIGLITAZONE PREVENTED HFD INDUCED STEATOHEPATITIS IN OSR1$^{\Delta MAC}$ MICE

Previous experiment has confirmed that PPARγ was the direct target of Osr1 in macrophages and the anti-inflammatory effect of Osr1 in macrophages were dependent on PPARγ. The *in vitro* study also demonstrated that the PPARγ agonist rosiglitazone rescued expression of M2 related genes including *Arg1, Ym1, CD36* and *CD206* in the Osr1$^{\Delta mac}$ BMDMs. Therefore, we examined the effects of the PPARγ agonist rosiglitazone on the steatohepatitis development in Osr1$^{\Delta mac}$ mice *in vivo*. The rosiglitazone was given to the Osr1^{fl} and Osr1$^{\Delta mac}$ mice during the last 4 weeks on HFD(started on week 10 and stopped on week 14).By the end of week14, the liver weight and liver-to-body weight ratio were not altered (data not show). However, the serum ALT levels (Fig.24A) were significantly down regulated in the Osr1$^{\Delta mac}$ mice receiving rosiglitazone comparing to those receiving DMSO. We also observed down regulated blood cholesterol and LDL level in rosiglitazone administrated Osr1$^{\Delta mac}$ mice comparing to the DMSO group (Fig.24A). In addition, liver steatosis was also improved as evidenced by liver histology revealed by H&E staining (Fig. 24B). Lipid accumulation was decreased in hepatocytes of HFD-fed Osr1$^{\Delta mac}$ mice treated with rosiglitazone as shown by Oil Red O staining (Fig.24C1, C2). Consistently, the hepatic triglyceride content was significantly lower in the Osr1$^{\Delta mac}$ group with rosiglitazone than

those with DMSO (Fig.24D). Taken together, these results suggested that the

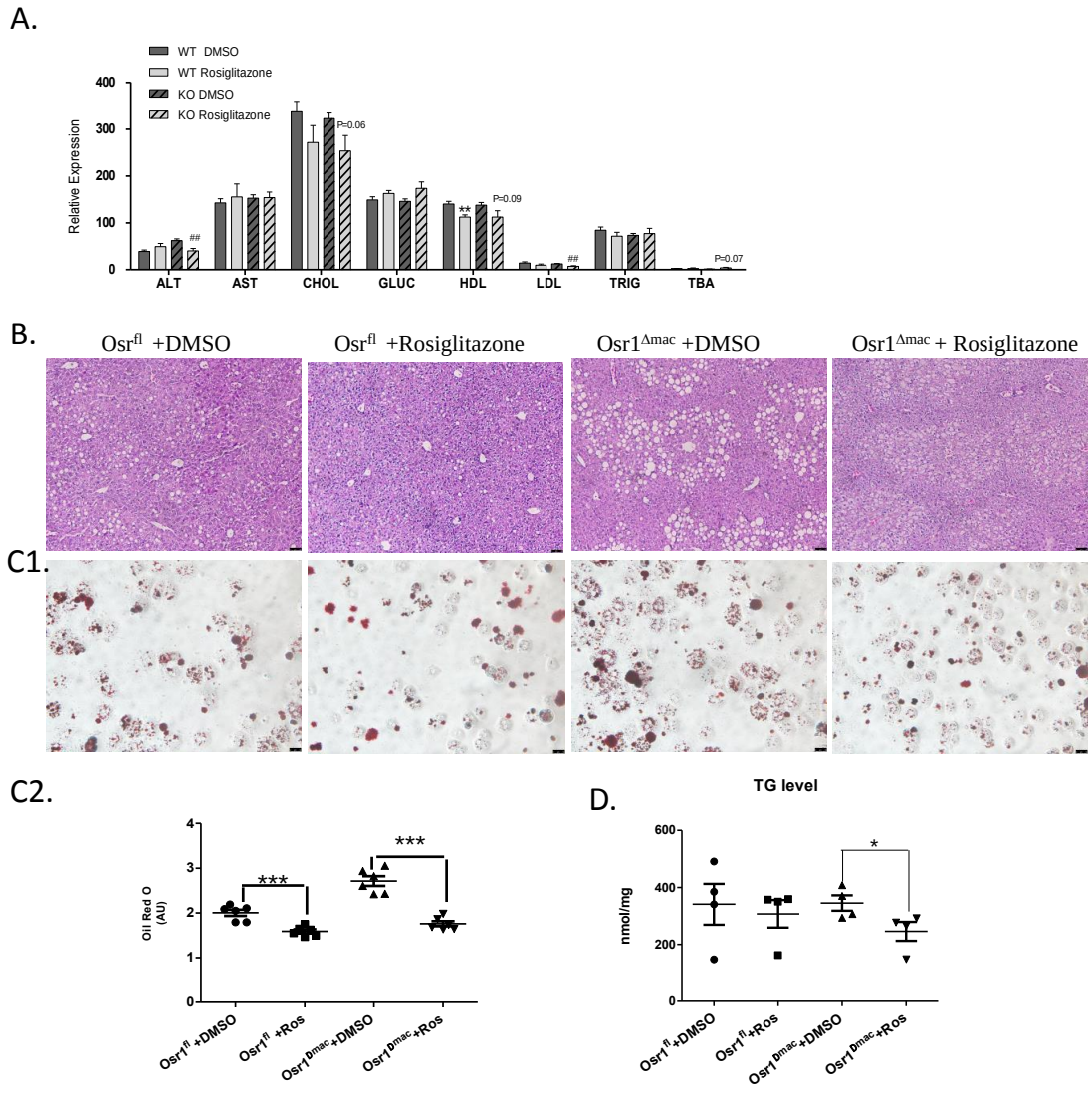

Figure 24. Pharmacological PPAR-γ agonist rosiglitazone prevent HFD induced liver injury in Osr1$^{\Delta mac}$ mice

Starting from the 10th week of HFD treatment, Osr1^{fl} and Osr1$^{\Delta mac}$ mice were injected with rosiglitazone (10mg/kg/day) or DMSO peritoneally for 4 weeks. (A) Lipid metabolism and hepatocyte damage blood serum markers. (B) Representative H&E staining of liver sections from HFD-fed mice treated with or without rosiglitazone. (C) Representative pictures and quantitation of Oil Red O staining in perfused hepatocytes from indicated groups. (D) Triglyceride level in the indicated mice liver.

rosiglitazone could prevent HFD-induced steatohepatitis in Osr1$^{\Delta mac}$ mice.

For B, serum levels were quantified by the biochemical analyzer (DxC 700 AU, Beckman Coulter). Statistical difference between Osr1^{fl} +DMSO and Osr1$^{\Delta mac}$+DMSO: *, P < 0.05 and **, P < 0.01. Statistical difference between Osr1$^{\Delta mac}$ +DMSO and Osr1$^{\Delta mac}$ +rosiglitazone: #, P < 0.05 and ##, P < 0.01. Marginal difference indicated p value were compared with Osr1^{fl} +rosiglitazone group. For A – B, numeric data are means ± SE. n = 6-8. For D and E, statistical difference between Osr1^{fl} and Osr1$^{\Delta mac}$ mice: *, P < 0.05 and ***, P < 0.001. H&E, hematoxylin & eosin; HFD, high-fat diet; Ros, rosiglitazone; DMSO, Dimethyl sulfoxide .

Rosiglitazone is a clinically used antidiabetic drug and works as an insulin sensitizer(*117*). Therefore, we investigated if rosiglitazone could improve the glucose intolerance of the Osr1$^{\Delta mac}$ mice. IPGTT was performed in each group before (10w HFD treatment) and after rosiglitazone administration (14w HFD treatment) and the fasting blood glucose was monitored once for each week. Before rosiglitazone administration, mice of both groups were glucose intolerance and responded similarly to glucose challenge (Fig. 25A). However, the glucose intolerance was significantly improved after the 4-week rosiglitazone treatment (Fig. 25B), despite of no changes of the fasting glucose (Fig. 25C). Interestingly, response to insulin challenge during IPITT remained similar between the two groups (Fig. 25D). Further analysis of the insulin signaling in liver lysates indicated that the phosphorylation of insulin receptor phosphorylation and Akt (S473) upon insulin stimulation were significantly higher in rosiglitazone treated mice compared with control mice under HFD (Fig. 25E). Collectively, these results suggested that rosiglitazone could partially rescue the glucose intolerance in the Osr1$^{\Delta mac}$ mice under HFD treatment and could sensitize the insulin signaling.

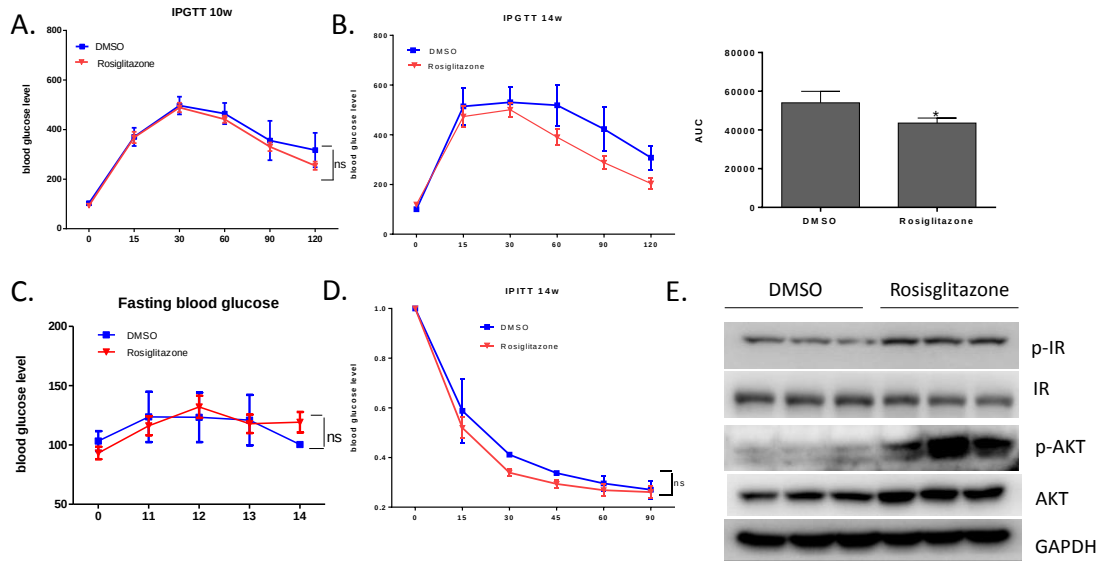

Figure 25. Rosiglitazone improves insulin sensitivity and glucose tolerance in Osr1$^{\Delta mac}$ mice under HFD treatment

(A) IPGTT result before rosiglitazone administration (HFD 10w) (B) IPGTT result and area under curve (AUC) bar graph after rosiglitazone and DMSO administration (HFD 14w) (C) Fasting blood glucose level during rosiglitazone and DMSO treatment in Osr1$^{\Delta mac}$ mice for each week. (D) IPITT result after rosiglitazone administration (HFD 14w) (E) Insulin signaling in indicated liver lysates. Prior harvest, mice were injected with insulin peritoneally.

For A – D, numeric data are means ± SE. Statistical difference among indicated groups were performed with t-test , n=6-8. For B, *, P<0.05; and compared with DMSO group. HFD, high-fat diet; Ros, rosiglitazone; DMSO, Dimethyl sulfoxide; IPGTT, intraperitoneal glucose tolerance test; IPITT, intraperitoneal insulin tolerance test; AUC, area under curve.

Furthermore, rosiglitazone treatment suppressed liver inflammation in the Osr1$^{\Delta mac}$ mice liver as shown by reduced number of macrophage infiltration (Fig.26A) and decreased phospho-p65, and MAPK c-Jun N-terminal kinase (JNK) and p38 protein levels and reduced *Il-6* mRNA expression (Fig.26B). Notably, rosiglitazone also restored the ATP production rate in peritoneal macrophages (PMs, Fig.26C) and liver non-parenchymal cells (NPCs, Fig.26D) with anti-inflammatory macrophage polarization profile evidenced by reduced glycolysis and increased FAO rate (marginal significance, $p=0.08$). These results suggested that pharmacological PPARγ agonist might prevent HFD-induced steatohepatitis in Osr1$^{\Delta mac}$ mice by inducing PPARγ activation and suppressing inflammation. These results also suggested the protective role of Osr1-PPARγ axis in the macrophages during the NAFLD pathogenesis.

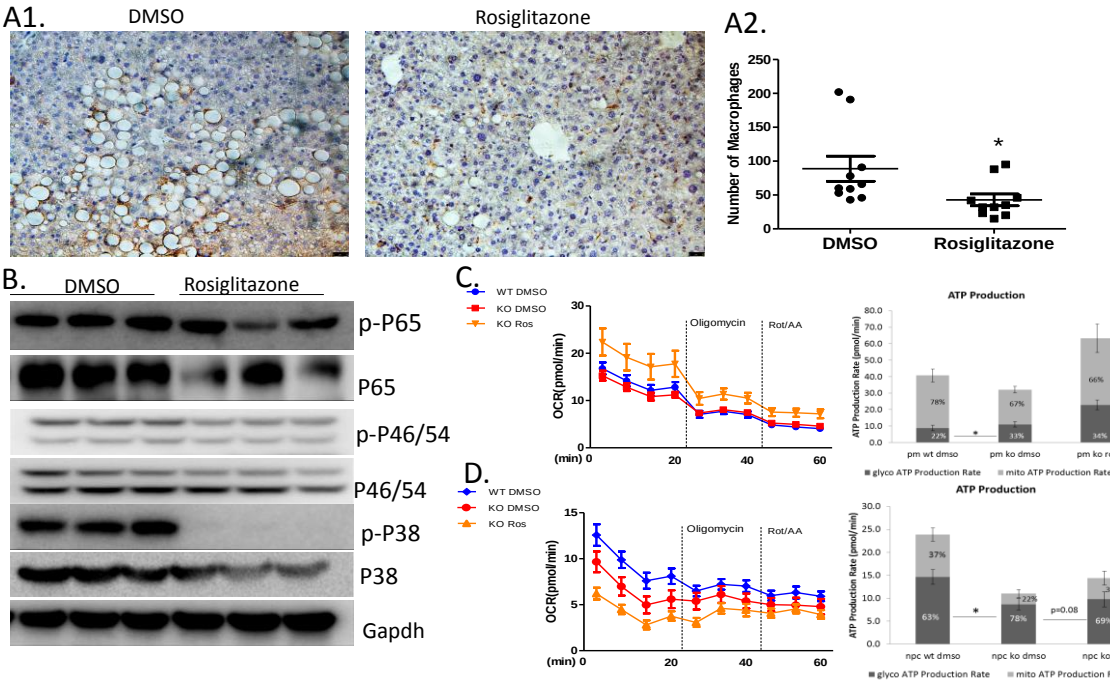

Figure 26. Pharmacological PPARγ agonist rosiglitazone prevents HFD-induced liver inflammation in Osr1$^{\Delta mac}$ mice

(A) Representative IHC staining of F4/80 and quantitation of macrophage numbers in liver sections from HFD-fed Osr1$^{\Delta mac}$ mice with or without rosiglitazone. (B) Phosphorylated NF-κB p65 and MAPK c-Jun N-terminal kinase (JNK) and p38 protein levels in liver of HFD-fed Osr1$^{\Delta mac}$ mice with or without rosiglitazone. (C) Peritoneal macrophages (PM) and (D) non-parenchymal cells(NPC) from Osr1^{fl} or Osr1$^{\Delta mac}$ were cultured in Seahorse XF RPMI medium and seeded in Seahorse plates and subject to real-time APT rate analysis to assess the ATP production rate from glycolysis and mitochondria fatty acid oxidation. OCR: oxygen consumption rate. Oligomycin (OM): ATP synthase inhibitor. Rot/AA: rotenone and antimycin A, specific inhibitors for ETC complex I and III respectively. Ros: rosiglitazone. *, $P < 0.05$

CHAPTER IX

DISCUSSION

In this study, we established the role of Osr1 in the polarization of macrophages and the associated function of the inflammation-induced pathogenesis of NASH. We found the enhanced macrophage Osr1 expression in liver tissues of both clinical NASH patients and murine models. Osr1 is expressed in both macrophages and hepatocytes in mouse liver, while nuclear Osr1 expression was only found in macrophages. Using *in vitro* and *in vivo* study, we established the role of Osr1 in maintaining the macrophage alternative polarization. In HFD and MCD induced murine NAFLD/NASH model, specifically deleting myeloid Osr1 resulted in more severe steatohepatitis via activating the pro-inflammatory signaling and enhancing the production of pro-inflammatory cytokines. Thus, we established the molecular mechanism underlying NASH onset and progression promoted by enhanced inflammation due to macrophage Osr1 deletion.

Osr1 has been previously widely studied in organ development, however, its role in regulating macrophage polarization has never been reported. From a view of evolution, a conserved function for promoting prohemocyte differentiation and cell fate choice of *odd* in *Drosophila* lymph gland has been reported(*82*). Our RNA-seq results identified several KEGG signaling pathways for macrophage polarization depending on Osr1 dosage, including PPAR signaling, TGF-beta signaling, JAK-STAT signaling, NF-κB signaling and osteoclast differentiation signaling pathways, suggesting a role Osr1 in the

macrophage polarization. Indeed, M2 macrophages from liver tissues of $Osr1^{\Delta mac}$ mice were significantly reduced comparing to that of the $Osr1^{fl}$ mice. Induced by IL-4 in BMDMs, the expression of Osr1 were enhanced, which correlated with the expression of specific M2 markers (Arg1, Ym1, CD36 and Mrc1/CD206). Consistently, expression of the M2 marker genes in macrophages were repressed in primary BMDMs isolated from $Osr1^{\Delta mac}$ mice, while Osr1 overexpression induced expression of c-Myc and PPAR-γ, two important TFs regulating phenotype switch of macrophages.(*75, 99*) We further determined that Osr1 directly regulating the expression of *PPAR-γ* and *c-Myc*, whose upstream regulators are not fully identified. The functional role of Osr1-PPARγ axis in controlling the polarization of macrophages was confirmed by the fact that treating rosiglitazone, a PPARγ agonist, rescued the population of M2 macrophage in the $Osr1^{\Delta mac}$ liver exposed to MCD diet. Collectively, our data support Osr1's role in maintaining M2 polarization and identify Osr1 as a novel TF targeting on PPAR-γ and c-Myc for macrophage plasticity.

Macrophage polarization is always associate with the cell metabolic change. The signature difference between M1 and M2 polarization is the energy production, in which M2 cells are more dependent on oxidative phosphorylation (OXPHOS) and fatty acid oxidation (FAO) for their energy production comparing to the M1 pro-inflammatory macrophages (*45*). Among the various regulators in the cell metabolism, PPARγ is a master regulator in the macrophage metabolism and was reported to be required for IL-4 induced increase in β-oxidation of fatty acids. CD36, as scavenger receptor, also plays the central role in the

fatty acid transportation which fuels β-oxidation(*108*). Upon establishing that PPARγ is a direct downstream target of Osr1 in macrophages and CD36 expression was significantly downregulated in Osr1$^{\Delta mac}$ BMDMs, it is necessary to investigate if Osr1 could modulate the macrophage metabolic change during the macrophage alternative polarization. With glucose and pyruvate as substrates, we found that deleting Osr1 resulted in around 25% reduction in the rate of FAO and upregulated about 50% of the ratio of OXPHOS and rosiglitazone could partially rescue the skewed ratio of glycolysis and OXPHOS. PA is a primary substrate fueling mitochondrial metabolism and has a profound impact on cell fate, function, and fitness(*111*). It has also been reported to be elevated in patients with NAFLD. Interestingly, PA significantly induced the Osr1 expression in the macrophages. Considering we have identified PPARγ as a direct target of Osr1, this consistent result explained the increasing level of macrophage PPARγ in the presence of palmitic acid. (*43*)When using Palmitate as a long-chain fatty acid substrate, both basal and maximal (p=0.06) OCR were significantly decreased in the Osr1$^{\Delta mac}$ BMDMs with increased ratio of Glycolysis/ FAO, possibly due to the reduced FAO. Collectively, the above results indicated that Osr1 plays an important role in the macrophage metabolism, especially OXPHOS and FAO.

Upon activation, macrophage inflammation induced pro-inflammatory signaling pathways in the liver such as NF-κB and MAPK were also reported to play important role in the pathogenesis of NASH and related liver injury, accompanied with diabetes and glucose intolerance(*20, 31*). When treated with HFD or MCD diet, there were more

macrophages infiltrated to the Osr1$^{\Delta mac}$ liver tissue. Overactivated inflammatory signaling pathways such as NF-κB and MAPK, and increased mRNA levels of inflammatory genes were observed in the Osr1$^{\Delta mac}$ liver. These results indicated that specifically deleting Osr1 in the myeloid cells would greatly inflame the liver. According to the two-hit hypothesis, enhanced inflammation initiates the second hit that promotes the progression of hepatic steatosis to hepatic fibrosis in NASH(*8*). In our model, the Osr1$^{\Delta mac}$ liver did exhibit an advanced phenotype of NASH with more collagen deposition in the liver and higher expression of fibrotic genes.

Liver macrophages exhibit relatively high heterogeneity, especially under pathological conditions such as diet induced steatohepatitis(*42*). The intervention of macrophage polarization switching may cause a different effect on the crosstalk between macrophages and hepatocytes during steatohepatitis progression. And this is mainly mediated by the differences of inflammatory cytokine secretion of macrophages. We have shown significantly more LPS stimulated pro-inflammation with elevated *Tnf-a* and *Il-1b* expression in the macrophages when deleting Osr1, suggesting a higher pendency for proinflammatory cytokine secretion. When primary hepatocytes were co-cultured with primary Osr1$^{\Delta mac}$ macrophages, there were increased hepatocyte lipid accumulation and inflammatory injury in the presence of palmitic acid. This might be due to more inflammatory cytokine secretion of the macrophages because more fat deposition and DNL gene expression were observed in primary hepatocytes cultured in Osr1$^{\Delta mac}$ macrophages conditioned medium. Thus, these results suggested that macrophage Osr1

deletion induced steatohepatitis by inducing a more inflamed microenvironment. Future study will be performed to identify the responsible cytokines for the liver injury and inflammation.

It has been established that Inflammation could induce the *de novo* lipogenesis (DNL) gene expression in the liver as well as insulin resistance. In our study, we found significantly increased DNL gene expression and more severe insulin resistance in HFD induced Osr1$^{\Delta mac}$ mice. However, in a more severe NASH model induced by MCD diet, we did not see the same expression changes in Osr1$^{\Delta mac}$ mice, suggesting other mechanisms rather than DNL contribute to steatosis. RNA-seq analysis identified that the primary bile acid synthesis signaling was significantly disrupted in Osr1$^{\Delta mac}$ mice comparing to the control. Down regulated expression of Cyp7a1 were observed at both mRNA and protein levels in Osr1$^{\Delta mac}$ mice liver. Cholesterols serves as precursors for critical regulators of lipid homeostasis such as bile acids and Cyp7a1 is the key rate limit enzyme for the bile acid synthesis(*97*). In MCD diet treated Osr1$^{\Delta mac}$ mice deletion of Osr1 in macrophages induced a cholesterol trap, which might be due to the lower expression of Cyp7a1 and its associated bile acid synthesis.

Cholesterol is one of the important determinants in NAFLD pathogenesis and it is already established that cholesterol plays more important role in the pathogenesis of liver lesions than liver triglyceride(*118, 119*). The widely accepted mechanisms about MCD diet induced steatosis and NASH relies on its lack of methionine and choline, which are

indispensable for hepatic mitochondrial β-oxidation and VLDL(*120*). This means the main lipid excretion and oxidation pathways are blunted in MCD diet treated liver, which makes MCD diet a good model to test if other lipid accumulation and cytotoxicity pathways in the hepatic steatosis. However, the underling mechanisms about how MCD diet induce NASH is not fully understood. We found that the MCD diet could disrupt the bile acid synthesis and further induce the cholesterol trap in the liver by reducing Cyp7a1 expression. In the myeloid Osr1-null model, disrupted Cyp7a1 and bile acid synthesis signaling could be due to overactivated NF-κB and JNK signaling, because both are reported to disrupt the expression of Cyp7a1(*121, 122*). Future study focusing on bile acid and cholesterol metabolism and liver inflammation would provide more evidence to support this mechanistic possibility.

Pharmacological agonist of PPARγ has been proven to be effective in treating or alleviating diabetes and increasing insulin sensitivity(*123*). Elegant studies also found that rosiglitazone could improve the liver NASH even though sometimes the result seems controversial (*124, 125*). The debate of using rosiglitazone to treat NAFLD/NASH mainly focuses on the following two issues: i) rosiglitazone is positively associated with an increased expression of genes responsible for lipid accumulation in the liver such as Mgat1, Cd36, and Fabp4. ii) the relatively wide expression of PPARγ in different tissues and cell types such as adipose tissue and adipocytes. Thus, we cannot rule out the possibility that the rescue effects of rosiglitazone were via relived lipotoxicity and improved insulin sensitivity in adipocytes. However, the specific effect of rosiglitazone on the macrophage

PPARγ in the liver inflammation has not been determined. We found that rosiglitazone could partially rescue the Osr1 activity in macrophages by significantly reducing the macrophages number and the activation states of inflammatory signaling in the liver tissue, resulting in ameliorated experimental steatohepatitis and inflammation in $Osr1^{\Delta mac}$ mice. Additionally, the separated NPC from liver tissue exhibit more FAO ATP production profile under rosiglitazone treatment, which is the signature of the anti-inflammatory macrophage polarization. Consistent with previously reported, we also found that rosiglitazone could help improve the glucose intolerance in the $Osr1^{\Delta mac}$ mice. Thus, our study provides a potential cellular therapy via modifying the macrophage plasticity, which further improve the innate immunity of the body and thus treat or stop the progression of NASH.

To be noted, we majorly used the male rodents for our *in vivo* studies considering that the male mice are more susceptible to the pathogenesis of NAFLD/NASH under special diet induction, which replicates the situation in humans that the incidence of NAFLD is higher in men than in women(*126, 127*). In terms of this, our *in vivo* study cannot rule out the possibility that female may exhibit different phenotypes from male mice. Thus, future studies will be performed with sex as a biological variance fully considered.

In conclusion, this study identified a specific role of Osr1 in overload nutrition induced steatohepatitis. Macrophage Osr1 may play a preventive role in the pathogenesis of steatohepatitis by maintaining M2 macrophage polarization. Specifically deleting Osr1 in

myeloid cells impairs macrophage alternative activation and predisposes the mice to the development of diet-induced obesity and NASH. Further analysis indicated that the role of Osr1 was dependent on the PPARγ function. The Osr1-PPARγ axis activation in macrophages by PPARγ agonist rosiglitazone could rescue the overactivated inflammation and fat deposition during the *in vitro* experiment as well as in the Osr1 myeloid knockout mice *in vivo*. Altogether, this study may provide a new approach targeting Osr1 for the treatment of steatohepatitis in the future and targeting Osr1 in the macrophages to suppress inflammation and lipogenesis is a potential and promising therapeutic strategy for the treatment of NASH in human liver diseases.

REFERENCES

1. Z. M. Younossi *et al.*, Global epidemiology of nonalcoholic fatty liver disease-Meta-analytic assessment of prevalence, incidence, and outcomes. *Hepatology* **64**, 73-84 (2016).

2. J. M. Clark, The epidemiology of nonalcoholic fatty liver disease in adults. *J Clin Gastroenterol* **40 Suppl 1**, S5-10 (2006).

3. A. B. Siegel, A. X. Zhu, Metabolic syndrome and hepatocellular carcinoma: two growing epidemics with a potential link. *Cancer* **115**, 5651-5661 (2009).

4. G. S. Hotamisligil, Inflammation and metabolic disorders. *Nature* **444**, 860-867 (2006).

5. H. Liu, H. Y. Lu, Nonalcoholic fatty liver disease and cardiovascular disease. *World J Gastroenterol* **20**, 8407-8415 (2014).

6. J. G. Fan, S. U. Kim, V. W. Wong, New trends on obesity and NAFLD in Asia. *J Hepatol* **67**, 862-873 (2017).

7. S. W. Wong, Y. W. Ting, W. K. Chan, Epidemiology of non-alcoholic fatty liver disease-related hepatocellular carcinoma and its implications. *JGH Open* **2**, 235-241 (2018).

8. Y. L. Fang, H. Chen, C. L. Wang, L. Liang, Pathogenesis of non-alcoholic fatty liver disease in children and adolescence: From "two hit theory" to "multiple hit model". *World J Gastroenterol* **24**, 2974-2983 (2018).

9. E. Buzzetti, M. Pinzani, E. A. Tsochatzis, The multiple-hit pathogenesis of non-alcoholic fatty liver disease (NAFLD). *Metabolism* **65**, 1038-1048 (2016).

10. J. Yu, S. Marsh, J. Hu, W. Feng, C. Wu, The Pathogenesis of Nonalcoholic Fatty Liver Disease: Interplay between Diet, Gut Microbiota, and Genetic Background. *Gastroenterology research and practice* **2016**, 2862173 (2016).

11. J. A. Del Campo, P. Gallego, L. Grande, Role of inflammatory response in liver diseases: Therapeutic strategies. *World J Hepatol* **10**, 1-7 (2018).

12. M. Ganz, G. Szabo, Immune and inflammatory pathways in NASH. *Hepatol Int* **7 Suppl 2**, 771-781 (2013).

13. C. A. Janeway, Jr., R. Medzhitov, Innate immune recognition. *Annu Rev Immunol* **20**, 197-216 (2002).

14. T. Kawai, S. Akira, The role of pattern-recognition receptors in innate immunity: update on Toll-like receptors. *Nat Immunol* **11**, 373-384 (2010).

15. A. Katsarou *et al.*, Metabolic inflammation as an instigator of fibrosis during non-alcoholic fatty liver disease. *World Journal of Gastroenterology* **26**, 1993 (2020).

16. E. Liaskou, D. V. Wilson, Y. H. Oo, Innate immune cells in liver inflammation. *Mediators of inflammation* **2012**, (2012).

17. M. Arrese, D. Cabrera, A. M. Kalergis, A. E. Feldstein, Innate immunity and inflammation in NAFLD/NASH. *Digestive diseases and sciences* **61**, 1294-1303 (2016).

18. S. L. Friedman, B. A. Neuschwander-Tetri, M. Rinella, A. J. Sanyal, Mechanisms of NAFLD development and therapeutic strategies. *Nature medicine* **24**, 908-922 (2018).

19. L. Zeng, W. J. Tang, J. J. Yin, B. J. Zhou, Signal transductions and nonalcoholic fatty liver: a mini-review. *International journal of clinical and experimental medicine* **7**, 1624 (2014).

20. Y. Cai *et al.*, Disruption of adenosine 2A receptor exacerbates NAFLD through increasing inflammatory responses and SREBP1c activity. *Hepatology* **68**, 48-61 (2018).

21. X. Luo *et al.*, Expression of STING Is Increased in Liver Tissues From Patients With NAFLD and Promotes Macrophage-Mediated Hepatic Inflammation and Fibrosis in Mice. *Gastroenterology* **155**, 1971-1984 e1974 (2018).

22. T. Sharifnia *et al.*, Hepatic TLR4 signaling in obese NAFLD. *American Journal of Physiology-Gastrointestinal and Liver Physiology* **309**, G270-G278 (2015).

23. E. Seki, D. A. Brenner, M. Karin, A liver full of JNK: signaling in regulation of cell function and disease pathogenesis, and clinical approaches. *Gastroenterology* **143**, 307-320 (2012).

24. S. Win *et al.*, New insights into the role and mechanism of c‐Jun‐N‐terminal kinase signaling in the pathobiology of liver diseases. *Hepatology* **67**, 2013-2024 (2018).

25. J. Hirosumi *et al.*, A central role for JNK in obesity and insulin resistance. *Nature* **420**, 333-336 (2002).

26. G. Sabio *et al.*, A stress signaling pathway in adipose tissue regulates hepatic insulin resistance. *Science* **322**, 1539-1543 (2008).

27. R. J. Davis, Signal transduction by the JNK group of MAP kinases. *Cell* **103**, 239-252 (2000).

28. A. Lawan, A. M. Bennett, Mitogen-Activated Protein Kinase Regulation in Hepatic Metabolism. *Trends in endocrinology and metabolism: TEM* **28**, 868-878 (2017).

29. M. Cargnello, P. P. Roux, Activation and function of the MAPKs and their substrates, the MAPK-activated protein kinases. *Microbiology and molecular biology reviews* **75**, 50-83 (2011).

30. K. P. Chooi *et al.*, Synthetic phosphorylation of p38alpha recapitulates protein kinase activity. *Journal of the American Chemical Society* **136**, 1698-1701 (2014).

31. X. Zhang *et al.*, Macrophage p38alpha promotes nutritional steatohepatitis through M1 polarization. *J Hepatol* **71**, 163-174 (2019).

32. M. Otsuka *et al.*, Distinct effects of p38alpha deletion in myeloid lineage and gut epithelia in mouse models of inflammatory bowel disease. *Gastroenterology* **138**, 1255-1265, 1265 e1251-1259 (2010).

33. L. R. Coulthard, D. E. White, D. L. Jones, M. F. McDermott, S. A. Burchill, p38(MAPK): stress responses from molecular mechanisms to therapeutics. *Trends Mol Med* **15**, 369-379 (2009).

34. J. A. Van Ginderachter *et al.*, Classical and alternative activation of mononuclear phagocytes: picking the best of both worlds for tumor promotion. *Immunobiology* **211**, 487-501 (2006).

35. M. S. Han *et al.*, JNK expression by macrophages promotes obesity-induced insulin resistance and inflammation. *Science* **339**, 218-222 (2013).

36. M. Orecchioni, Y. Ghosheh, A. B. Pramod, K. Ley, Macrophage Polarization: Different Gene Signatures in M1(LPS+) vs. Classically and M2(LPS-) vs. Alternatively Activated Macrophages. *Front Immunol* **10**, 1084 (2019).

37. Y. Yao, X. H. Xu, L. Jin, Macrophage Polarization in Physiological and Pathological Pregnancy. *Front Immunol* **10**, 792 (2019).

38. L. X. Wang, S. X. Zhang, H. J. Wu, X. L. Rong, J. Guo, M2b macrophage polarization and its roles in diseases. *J Leukoc Biol* **106**, 345-358 (2019).

39. G. Zizzo, B. A. Hilliard, M. Monestier, P. L. Cohen, Efficient clearance of early apoptotic cells by human macrophages requires M2c polarization and MerTK induction. *J Immunol* **189**, 3508-3520 (2012).

40. A. Viola, F. Munari, R. Sánchez-Rodríguez, T. Scolaro, A. Castegna, The Metabolic Signature of Macrophage Responses. *Frontiers in Immunology* **10**, (2019).

41. R. A. Isidro, C. B. Appleyard, Colonic macrophage polarization in homeostasis, inflammation, and cancer. *Am J Physiol Gastrointest Liver Physiol* **311**, G59-73 (2016).

42. A. Sica, P. Invernizzi, A. Mantovani, Macrophage plasticity and polarization in liver homeostasis and pathology. *Hepatology* **59**, 2034-2042 (2014).

43. M. Kratz *et al.*, Metabolic dysfunction drives a mechanistically distinct proinflammatory phenotype in adipose tissue macrophages. *Cell Metab* **20**, 614-625 (2014).

44. S. Epelman, K. J. Lavine, G. J. Randolph, Origin and functions of tissue macrophages. *Immunity* **41**, 21-35 (2014).

45. A. Batista-Gonzalez, R. Vidal, A. Criollo, L. J. Carreño, New Insights on the Role of Lipid Metabolism in the Metabolic Reprogramming of Macrophages. *Frontiers in Immunology* **10**, (2020).

46. P. van Uden, N. S. Kenneth, S. Rocha, Regulation of hypoxia-inducible factor-1alpha by NF-kappaB. *Biochem J* **412**, 477-484 (2008).

47. S. Joshi, A. R. Singh, M. Zulcic, D. L. Durden, A macrophage-dominant PI3K isoform controls hypoxia-induced HIF1alpha and HIF2alpha stability and tumor growth, angiogenesis, and metastasis. *Molecular cancer research : MCR* **12**, 1520-1531 (2014).

48. S. C. Cheng *et al.*, mTOR- and HIF-1alpha-mediated aerobic glycolysis as metabolic basis for trained immunity. *Science* **345**, 1250684 (2014).

49. A. Arranz *et al.*, Akt1 and Akt2 protein kinases differentially contribute to macrophage polarization. *Proc Natl Acad Sci U S A* **109**, 9517-9522 (2012).

50. D. van der Heide, R. Weiskirchen, R. Bansal, Therapeutic Targeting of Hepatic Macrophages for the Treatment of Liver Diseases. *Front Immunol* **10**, 2852 (2019).

51. F. Heymann, F. Tacke, Immunology in the liver--from homeostasis to disease. *Nat Rev Gastroenterol Hepatol* **13**, 88-110 (2016).

52. V. L. Gadd *et al.*, The portal inflammatory infiltrate and ductular reaction in human nonalcoholic fatty liver disease. *Hepatology* **59**, 1393-1405 (2014).

53. P. Ramachandran *et al.*, Differential Ly-6C expression identifies the recruited macrophage phenotype, which orchestrates the regression of murine liver fibrosis. *Proc Natl Acad Sci U S A* **109**, E3186-3195 (2012).

54. A. Pellicoro, P. Ramachandran, J. P. Iredale, J. A. Fallowfield, Liver fibrosis and repair: immune regulation of wound healing in a solid organ. *Nat Rev Immunol* **14**, 181-194 (2014).

55. K. R. Karlmark *et al.*, Hepatic recruitment of the inflammatory Gr1+ monocyte subset upon liver injury promotes hepatic fibrosis. *Hepatology* **50**, 261-274 (2009).

56. T. Zeng, C. L. Zhang, M. Xiao, R. Yang, K. Q. Xie, Critical Roles of Kupffer Cells in the Pathogenesis of Alcoholic Liver Disease: From Basic Science to Clinical Trials. *Front Immunol* **7**, 538 (2016).

57. G. Kolios, V. Valatas, E. Kouroumalis, Role of Kupffer cells in the pathogenesis of liver disease. *World J Gastroenterol* **12**, 7413-7420 (2006).

58. W. Z. Mehal, D. Schuppan, Antifibrotic therapies in the liver. *Semin Liver Dis* **35**, 184-198 (2015).

59. A. Jindal *et al.*, Fat-laden macrophages modulate lobular inflammation in nonalcoholic steatohepatitis (NASH). *Exp Mol Pathol* **99**, 155-162 (2015).

60. J. Wan *et al.*, M2 Kupffer cells promote M1 Kupffer cell apoptosis: a protective mechanism against alcoholic and nonalcoholic fatty liver disease. *Hepatology* **59**, 130-142 (2014).

61. J. I. Odegaard *et al.*, Alternative M2 activation of Kupffer cells by PPARdelta ameliorates obesity-induced insulin resistance. *Cell Metab* **7**, 496-507 (2008).

62. Z. Papackova *et al.*, Kupffer cells ameliorate hepatic insulin resistance induced by high-fat diet rich in monounsaturated fatty acids: the evidence for the involvement of alternatively activated macrophages. *Nutr Metab (Lond)* **9**, 22 (2012).

63. M. W. Robinson, C. Harmon, C. O'Farrelly, Liver immunology and its role in inflammation and homeostasis. *Cellular & molecular immunology* **13**, 267-276 (2016).

64. M. A. Bouhlel *et al.*, PPARgamma activation primes human monocytes into alternative M2 macrophages with anti-inflammatory properties. *Cell Metab* **6**, 137-143 (2007).

65. W. Luo, Q. Xu, Q. Wang, H. Wu, J. Hua, Effect of modulation of PPAR-gamma activity on Kupffer cells M1/M2 polarization in the development of non-alcoholic fatty liver disease. *Sci Rep* **7**, 44612 (2017).

66. B. Daniel *et al.*, The Nuclear Receptor PPARγ Controls Progressive Macrophage Polarization as a Ligand-Insensitive Epigenomic Ratchet of Transcriptional Memory. *Immunity* **49**, 615-626.e616 (2018).

67. C. Janani, B. D. Ranjitha Kumari, PPAR gamma gene--a review. *Diabetes Metab Syndr* **9**, 46-50 (2015).

68. D. Moseti, A. Regassa, W. K. Kim, Molecular Regulation of Adipogenesis and Potential Anti-Adipogenic Bioactive Molecules. *Int J Mol Sci* **17**, (2016).

69. U. Kintscher, R. E. Law, PPARgamma-mediated insulin sensitization: the importance of fat versus muscle. *Am J Physiol Endocrinol Metab* **288**, E287-291 (2005).

70. J. Skat-Rordam, D. Hojland Ipsen, J. Lykkesfeldt, P. Tveden-Nyborg, A role of peroxisome proliferator-activated receptor gamma in non-alcoholic fatty liver disease. *Basic Clin Pharmacol Toxicol* **124**, 528-537 (2019).

71. A. Wolf Greenstein *et al.*, Hepatocyte-specific, PPARgamma-regulated mechanisms to promote steatosis in adult mice. *The Journal of endocrinology* **232**, 107-121 (2017).

72. G. Chinetti, S. Lestavel, J. C. Fruchart, V. Clavey, B. Staels, Peroxisome proliferator-activated receptor alpha reduces cholesterol esterification in macrophages. *Circ Res* **92**, 212-217 (2003).

73. G. Chinetti *et al.*, Activation of proliferator-activated receptors alpha and gamma induces apoptosis of human monocyte-derived macrophages. *J Biol Chem* **273**, 25573-25580 (1998).

74. G. Chinetti, J. C. Fruchart, B. Staels, Peroxisome proliferator-activated receptors (PPARs): nuclear receptors at the crossroads between lipid metabolism and inflammation. *Inflamm Res* **49**, 497-505 (2000).

75. J. I. Odegaard *et al.*, Macrophage-specific PPARgamma controls alternative activation and improves insulin resistance. *Nature* **447**, 1116-1120 (2007).

76. L. Yang *et al.*, Regulation of peroxisome proliferator-activated receptor-gamma in liver fibrosis. *Am J Physiol Gastrointest Liver Physiol* **291**, G902-911 (2006).

77. E. Moran-Salvador *et al.*, Cell-specific PPARgamma deficiency establishes anti-inflammatory and anti-fibrogenic properties for this nuclear receptor in non-parenchymal liver cells. *J Hepatol* **59**, 1045-1053 (2013).

78. D. E. Coulter *et al.*, Molecular analysis of odd-skipped, a zinc finger encoding segmentation gene with a novel pair-rule expression pattern. *Embo J* **9**, 3795-3804 (1990).

79. D. E. Coulter, E. Wieschaus, Gene activities and segmental patterning in Drosophila: analysis of odd-skipped and pair-rule double mutants. *Genes Dev* **2**, 1812-1823 (1988).

80. C. Nusslein-Volhard, E. Wieschaus, Mutations affecting segment number and polarity in Drosophila. *Nature* **287**, 795-801 (1980).

81. S. Yu, F. Luo, L. H. Jin, The Drosophila lymph gland is an ideal model for studying hematopoiesis. *Dev Comp Immunol* **83**, 60-69 (2018).

82. H. Gao, X. Wu, N. Fossett, Odd-skipped maintains prohemocyte potency and blocks blood cell development in Drosophila. *Genesis* **49**, 105-116 (2011).

83. K. K. Zhang *et al.*, Gene network and familial analyses uncover a gene network involving Tbx5/Osr1/Pcsk6 interaction in the second heart field for atrial septation. *Hum Mol Genet* **25**, 1140-1151 (2016).

84. L. Zhou *et al.*, Tbx5 and Osr1 interact to regulate posterior second heart field cell cycle progression for cardiac septation. *J Mol Cell Cardiol* **85**, 1-12 (2015).

85. W. Chen *et al.*, Odd-skipped related transcription factor 1 (OSR1) suppresses tongue squamous cell carcinoma migration and invasion through inhibiting NF-kappaB pathway. *Eur J Pharmacol* **839**, 33-39 (2018).

86. M. Yamauchi, S. Kawai, T. Kato, T. Ooshima, A. Amano, Odd-skipped related 1 gene expression is regulated by Runx2 and Ikzf1 transcription factors. *Gene* **426**, 81-90 (2008).

87. L. Verlinden *et al.*, The odd-skipped related genes Osr1 and Osr2 are induced by 1,25-dihydroxyvitamin D3. *J Steroid Biochem Mol Biol* **136**, 94-97 (2013).

88. K. Otani *et al.*, Odd-skipped related 1 is a novel tumour suppressor gene and a potential prognostic biomarker in gastric cancer. *The Journal of pathology* **234**, 302-315 (2014).

89. Y. Zhang *et al.*, OSR1 is a novel epigenetic silenced tumor suppressor regulating invasion and proliferation in renal cell carcinoma. *Oncotarget* **8**, 30008-30018 (2017).

90. Y. Li, J. Qin, J. Wu, X. Dai, J. Xu, High expression of OSR1 as a predictive biomarker for poor prognosis and lymph node metastasis in breast cancer. *Breast cancer research and treatment* **182**, 35-46 (2020).

91. Y. Li *et al.*, OSR1 phosphorylates the Smad2/3 linker region and induces TGF-beta1 autocrine to promote EMT and metastasis in breast cancer. *Oncogene* **40**, 68-84 (2021).

92. Y. Zhou *et al.*, Osr1 regulates hepatic inflammation and cell survival in the progression of non-alcoholic fatty liver disease. *Laboratory Investigation*, (2020).

93. T. D. Schmittgen, K. J. Livak, Analyzing real-time PCR data by the comparative C(T) method. *Nat Protoc* **3**, 1101-1108 (2008).

94. F. Caballero *et al.*, Enhanced free cholesterol, SREBP-2 and StAR expression in human NASH. *J Hepatol* **50**, 789-796 (2009).

95. Y. Takeshita *et al.*, The effects of ezetimibe on non-alcoholic fatty liver disease and glucose metabolism: a randomised controlled trial. *Diabetologia* **57**, 878-890 (2014).

96. A. Arvind, S. A. Osganian, D. E. Cohen, K. E. Corey, in *Endotext*, K. R. Feingold *et al.*, Eds. (South Dartmouth (MA), 2000).

97. I. Kim *et al.*, Differential regulation of bile acid homeostasis by the farnesoid X receptor in liver and intestine. *J Lipid Res* **48**, 2664-2672 (2007).

98. H. Liu, P. Pathak, S. Boehme, J. Y. Chiang, Cholesterol 7alpha-hydroxylase protects the liver from inflammation and fibrosis by maintaining cholesterol homeostasis. *J Lipid Res* **57**, 1831-1844 (2016).

99. O. M. Pello *et al.*, Role of c-MYC in alternative activation of human macrophages and tumor-associated macrophage biology. *Blood* **119**, 411-421 (2012).

100. O. M. Pello, V. Andres, Role of c-MYC in tumor-associated macrophages and cancer progression. *Oncoimmunology* **2**, e22984 (2013).

101. O. M. Pello, Macrophages and c-Myc cross paths. *Oncoimmunology* **5**, e1151991 (2016).

102. T. Zhang, B. Shao, G. A. Liu, Rosuvastatin promotes the differentiation of peripheral blood monocytes into M2 macrophages in patients with atherosclerosis by activating PPAR-gamma. *Eur Rev Med Pharmacol Sci* **21**, 4464-4471 (2017).

103. M. Zhang, Z. Zhou, J. Wang, S. Li, MiR-130b promotes obesity associated adipose tissue inflammation and insulin resistance in diabetes mice through alleviating M2 macrophage polarization via repression of PPAR-gamma. *Immunol Lett* **180**, 1-8 (2016).

104. M. C. Herwig, C. Bergstrom, J. R. Wells, T. Holler, H. E. Grossniklaus, M2/M1 ratio of tumor associated macrophages and PPAR-gamma expression in uveal melanomas with class 1 and class 2 molecular profiles. *Exp Eye Res* **107**, 52-58 (2013).

105. D. Zhou, L. Ji, Y. Chen, TSPO Modulates IL-4-Induced Microglia/Macrophage M2 Polarization via PPAR-gamma Pathway. *J Mol Neurosci* **70**, 542-549 (2020).

106. I. Linares *et al.*, PPAR-gamma activation is associated with reduced liver ischemia-reperfusion injury and altered tissue-resident macrophages polarization in a mouse model. *PLoS One* **13**, e0195212 (2018).

107. P. Tontonoz, L. Nagy, J. G. Alvarez, V. A. Thomazy, R. M. Evans, PPARgamma promotes monocyte/macrophage differentiation and uptake of oxidized LDL. *Cell* **93**, 241-252 (1998).

108. L. D. Ly *et al.*, Oxidative stress and calcium dysregulation by palmitate in type 2 diabetes. *Exp Mol Med* **49**, e291 (2017).

109. J. D. McGarry, D. W. Foster, Regulation of hepatic fatty acid oxidation and ketone body production. *Annu Rev Biochem* **49**, 395-420 (1980).

110. F. K. Huynh, M. F. Green, T. R. Koves, M. D. Hirschey, Measurement of fatty acid oxidation rates in animal tissues and cell lines. *Methods Enzymol* **542**, 391-405 (2014).

111. P. Schonfeld, L. Wojtczak, Short- and medium-chain fatty acids in energy metabolism: the cellular perspective. *J Lipid Res* **57**, 943-954 (2016).

112. P. Rada, A. Gonzalez-Rodriguez, C. Garcia-Monzon, A. M. Valverde, Understanding lipotoxicity in NAFLD pathogenesis: is CD36 a key driver? *Cell death & disease* **11**, 802 (2020).

113. V. Byles *et al.*, The TSC-mTOR pathway regulates macrophage polarization. *Nat Commun* **4**, 2834 (2013).

114. J. Van den Bossche *et al.*, Mitochondrial Dysfunction Prevents Repolarization of Inflammatory Macrophages. *Cell Rep* **17**, 684-696 (2016).

115. G. I. Lancaster *et al.*, Evidence that TLR4 Is Not a Receptor for Saturated Fatty Acids but Mediates Lipid-Induced Inflammation by Reprogramming Macrophage Metabolism. *Cell Metab* **27**, 1096-1110 e1095 (2018).

116. J. Korbecki, K. Bajdak-Rusinek, The effect of palmitic acid on inflammatory response in macrophages: an overview of molecular mechanisms. *Inflamm Res* **68**, 915-932 (2019).

117. A. B. Mayerson *et al.*, The effects of rosiglitazone on insulin sensitivity, lipolysis, and hepatic and skeletal muscle triglyceride content in patients with type 2 diabetes. *Diabetes* **51**, 797-802 (2002).

118. T. A. Kerr, N. O. Davidson, Cholesterol and nonalcoholic fatty liver disease: renewed focus on an old villain. *Hepatology* **56**, 1995-1998 (2012).

119. H. K. Min *et al.*, Increased hepatic synthesis and dysregulation of cholesterol metabolism is associated with the severity of nonalcoholic fatty liver disease. *Cell Metab* **15**, 665-674 (2012).

120. Q. M. Anstee, R. D. Goldin, Mouse models in non-alcoholic fatty liver disease and steatohepatitis research. *Int J Exp Pathol* **87**, 1-16 (2006).

121. S. Gupta, R. T. Stravitz, P. Dent, P. B. Hylemon, Down-regulation of cholesterol 7alpha-hydroxylase (CYP7A1) gene expression by bile acids in primary rat hepatocytes is mediated by the c-Jun N-terminal kinase pathway. *J Biol Chem* **276**, 15816-15822 (2001).

122. D. Okin, R. Medzhitov, The Effect of Sustained Inflammation on Hepatic Mevalonate Pathway Results in Hyperglycemia. *Cell* **165**, 343-356 (2016).

123. M. Saryusz-Wolska *et al.*, Rosiglitazone treatment in nondiabetic subjects with nonalcoholic fatty liver disease. *Pol Arch Med Wewn* **121**, 61-66 (2011).

124. P. Mulder *et al.*, Reduction of obesity-associated white adipose tissue inflammation by rosiglitazone is associated with reduced non-alcoholic fatty liver disease in LDLr-deficient mice. *Sci Rep* **6**, 31542 (2016).

125. V. Ratziu *et al.*, Long-term efficacy of rosiglitazone in nonalcoholic steatohepatitis: results of the fatty liver improvement by rosiglitazone therapy (FLIRT 2) extension trial. *Hepatology* **51**, 445-453 (2010).

126. M. Ganz, T. Csak, G. Szabo, High fat diet feeding results in gender specific steatohepatitis and inflammasome activation. *World J Gastroenterol* **20**, 8525-8534 (2014).

127. S. Stoppeler *et al.*, Gender and strain-specific differences in the development of steatosis in rats. *Lab Anim* **47**, 43-52 (2013).

APPENDIX

Table 1 Primers used for RT-qPCR

Gene	Forward primer (5' to 3')	Reverse primer (5' to 3')
Osr1	CCATCCCTGCAGCTTACCAA	GCATGAAGAGCGCTGAAACC
c-Myc	CCCTATTTCATCTGCGACGAG	GAGAAGGACGTAGCGACCG
Arg1	CAGAAGAATGGAAGAGTCAG	CAGATATGCAGGGAGTCACC
Mrc1	GCAAATGGAGCCGTCTGTGC	CTCGTGGATCTCCGTGACAC
Ym1	GATCTCAATATACACAGTGC	GAGCTTAGCCAAAGCTGAC
CD36	TGGAGGCATTCTCATGCCAG	TTGCTGCTGTTCTTTGCCAC
Srebp1	AGCAGTCACCAGCTTCAGTC	GGTCATGTTGGAAACCACGC
Srebp2	TGAAGGACTTAGTCATGGGGAC	CGCAGCTTGTGATTGACCT
Tnf-α	CCCTCACACTCAGATCATCTTCT	GCTACGACGTGGGCTACAG
Il-1β	CCTTCCAGGATGAGGACATGA	TGAGTCACAGAGGATGGGCTC
Il-6	GAGGATACCACTCCCAACAGACC	AAGTGCATCATCGTTGTTCATACA
Nos2	GGCAGCCTGTGAGACCTTTG	GCATTGGAAGTGAAGCGTTTC
Adgre1	CTTTGGCTATGGGCTTCCAGTC	GCAAGGAGGACAGAGTTTATCGTG
Fasn	TTGCTGGCACTACAGAATGC	AACAGCCTCAGAGCGACAAT
Acc1	CCTCCGTCAGCTCAGATACA	TTTACTAGGTGCAAGCCAGACA
Scd1	CTGTACGGGATCATACTGGTTC	GCCGTGCCTTGTAAGTTCTG
Col1a1	ATGTGCCACTCTGACTGGAA	TCCATCGGTCATGCTCTCTC
Col1a2	TAGAAAGAACCCTGCTCGCA	CGGCTGTATGAGTTCTTCGC
Col3a1	GGTGGTTTTCAGTTCAGCTATGG	CTGGAAAGAAGTCTGAGGAATG
Col4a1	ACAACATCCGGCCCTTCATT	CTGTGTACCGCCATCACCAT
Vimentin	ATGCTTCTCTGGCACGTCTT	AGCCACGCTTTCATACTGCT
Tgf-β	TCGCTTTGTACAACAGCACC	ACTGCTTCCCGAATGTCTGA

Cyp7a1	CTGGGGGATTGCTGTGGTAG	GCACAGCCCAGGTATGGAAT
Cyp7b1	AGCTGCTTACTGATGACGACC	AGTGAGCCACAGAATGCAAAT
Cyp27a1	AAGGACCACCGAGACCACAA	TTAAGGCATCCGTGTAGAGCG
Cyp8b1	CGGAACTTCCTGAACAGCTC	TGGCCTCTTTCACTTCTGCT
Hmgcr	CAAGGAACGTGCACCAAGAA	AACACAGCACGGAAAGAACC
Ldlr	CCAATCGACTCACGGGTTCA	CTCACACCAGTTCACCCCTC

Table 2 Primers used for ChIP-qPCR

Amplicon	Forward primer (5' to 3')	Reverse primer (5' to 3')
c-Myc -R1	CAATGAGCTCGATGAAGGAAG	CTCTCACTGCTACCCGGTTT
c-Myc -R2	ATCTGATCAGGGCCGACTTT	AAAGGGGGAGGAGTGAATTG
c-Myc -R3	CTGCAAACTGGCTCCACAG	CTGCGCAGTCCAGTAAAGTG
c-Myc -R4	AACAACCGTACAGAAAGGGAAA	GCTCCGGGGTGTAAACAGTA
Pparγ -R1	GGGCTGGCCTTAGGAGAATA	ACTCCATTTCCATGCCTGTC
Pparγ -R2	TGTCTGGTGAGGATGGTTTG	CACCAAAGGCCGTTCTTTTA